Evaluation of corrosion in different parts of an oil refinery using corrosion coupons

Thesis by Thomas Olsson, December 2012

19841202-4815

TABLE OF CONTENTS

Table of figures

Table of Tables

1.1 Background

Preem refinery Gothenburg Sweden is operating a fuels refinery in Gothenburg. The refinery contains vast volumes of flammable gases and liquids. Loss of containment is therefore a major safety threat. Corrosion is the most probable cause of unintentional loss of product at the refinery. The refinery uses a variety of methods for corrosion control. As one of these methods a number of corrosion control coupons have been installed. The coupons have been installed at locations where either high corrosion rates are expected or corrosion rates are unknown.

The corrosion coupons can only be removed and investigated during an inspection shutdown of the refinery. Such shut downs have up to now been occurring every fourth year. The interval will now be prolonged to six years.

1.2 Purpose

The **main purpose** of the study is to establish corrosion rates and to evaluate probable corrosion mechanisms for each coupon.

The purpose of study is also to:

- Evaluate the method of using corrosion coupons in relation to other corrosion control methods. If relevant, comparison with inspection results from corresponding locations will be made.
- Suggest improvements in the existing corrosion coupon method and documentation.
- Estimate lifetime for associated piping and equipment based on measured corrosion rates and relevant corrosion allowances. Highlight locations with increased risks due to the prolonged inspection interval from four to six years.
- Update the 2007 literature study regarding organic acid corrosion in the inlet and upper part of the Green Hydrotreater reactor, 16C-2.

1.3 Study limitations

The 22 corrosion coupons are located in different process units with various liquid and gas compositions at different pressures and temperatures. The contaminants also vary from process stream to process stream. There are a number of possible corrosion mechanisms for each corrosion coupon. Given the system complexity it is not possible to include recommendations regarding process parameters or material selection within the scope of this study.

2. Methodology

2.1 Background

The Preem Gothenburg refinery is a fuels refinery producing LPG, gasoline, jet-fuel, diesel, heating oil and fuel oil from predominantly North Sea crude oils. The refinery was commissioned in 1967 and expanded, with units necessary to produce Swedish environmental diesel, in 1996. The refinery contains at any set time vast amounts of highly flammable liquids. A major oil spill will cause severe pollution. The refinery is operated at high pressures and temperatures. Loss of containment is therefore the dominating process safety hazard. There is a wide range of systems, such as work practices, design practices, and emergency systems, in place to reduce the risk of loss of containment. However, the most important way to avoid loss of containment is corrosion control.

The crude oils contain, apart from hydrocarbons, water, sulphur, chlorides, transition metals and a number of other contaminants. Hydrogen is produced and additives are injected. The crude oil and other feedstock can contain organic acids. It is obvious that these components can cause rapid corrosion at certain flow regimes, temperatures and pressures. There is also a risk of corrosion of external surfaces due to the climate where the refinery is located. A special such risk is corrosion under insulation. To manage the corrosion control activities the refinery has a dedicated Inspection department. Third party inspectors are used for mandatory inspections. The inspections are done systematically based on estimated risks and historical data. A wide variety of methods are used. The inspection of the refinery piping and pressure vessels is subjected to mandatory regulation, which governs inspection intervals. As the refinery is configured with most units in series and in continuous operation the whole refinery has to be shut down in order to do the mandated inspections. An inspection shutdown is a major undertaking for the refinery. All pressurised equipment, such as heaters, exchangers, distillation towers, have to be emptied, dismantled and cleaned in order to enable the inspection.

2.2 Corrosion coupons

The use of corrosion coupons is an effective way to provide a quantitative estimation of corrosion rates occurring in an operating system. They also provide a qualitative visual indication of the type of degradation occurring in the monitored system. Corrosion coupons are metal samples with known composition, appearance, density, size and weight. The corrosion coupons are exposed to a certain environment for a known period of time after which it is recovered. The method is guided by the standard ASTM G4-01 "Conducting Corrosion Tests in Field Applications" [1].

In the present study, observations and data derived from the retrieved coupons are subjected to a Weight loss analysis and an Optical inspection to determine rate, type and degree of corrosion damage. A Background study is included in order to estimate sample environment, predict the range of corrosion damage and to propose a hypothesis concerning degradation modes. X-ray diffraction (XRD) together with results from the weight loss analysis and the optical inspection are used to evaluate the proposed hypothesis.

2.2.1 Sample set-up

In total 22 coupons have been installed in five different process units. Because the coupons are positioned in the areas where corrosion is a concern, the distribution of coupons among the process units differ. The units are identified as Amine Recovery Unit (ARU), Synsat unit, Green Hydrotreater (GHT), Common unit and Sulphur Recovery Unit (SRU). A more detailed explanation of these units can be found in *chapters 4.2* to *4.6*. In addition to the unit name each relevant process unit has a number which recur in the Coupon sample name.

Table 1. *Coupon sample name and Unit name.*

Unit Nr.	Unit name	Coupon sample name
9	Amine regeneration unit (ARU)	9CC-1
15	Synsat	15CC-2 A&B 15CC-8 A&B
16	Green Hydrotreater (GHT)	16CC-2 A&B 16CC-8 A&B 16CC-10 A-F
17	Common	17CC-1 A&B 17CC-2 17CC-3 17CC-6 17CC-10
27	Sulphur recovery unit (SRU)	27CC-2

Coupons designated A, B etc. are individual coupons installed at the same position in the process flow. For example 15CC-2 A&B designate two individual coupons and 16CC-10 A-F designate six individual coupons. Each coupon has a unique serial number stamped into it and is mounted on an individual coupon holder.

2.2.1.1 Coupon categories

There are three categories of coupons installed in the process, see Figure 1 for schematic illustrations; (a) Disc coupons, (c) Strip coupons and (e) Green Hydrotreater (GHT) coupons. Which of these coupon categories is mounted into the process flow depends on the conditions at the position, see descriptions below.

Figure 1. *Coupon categories.*

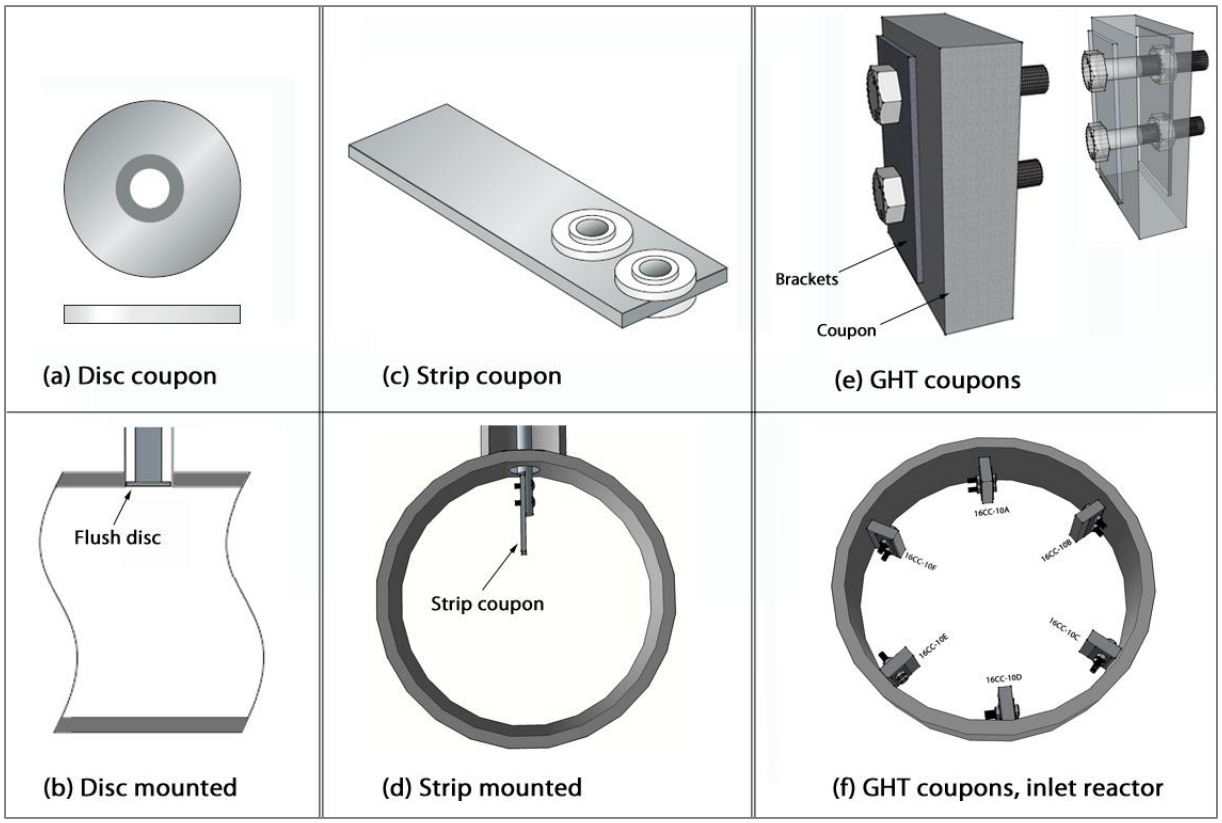

Disc coupons are thin circular coupons fitted to the coupon holder with a single screw. The screw is insulated with nylon insulators to avoid galvanic corrosion. The disc coupon holder is a stainless steel rod with a threaded hole on top, the rod is welded to a flange. The disc coupon holder is inserted into a 2'' dummy leg pipe and secured by pinning the holder between a larger blind flange with multiple bolts. See Appendix C for photograph of a disc coupon holder as well as on scene photos. Disc coupons are mounted to be in "flush"; thus, they line up with the wall of the process flow pipe to imitate the conditions experienced at the process interface, see Figure 1 (b). Besides closely simulating the conditions occurring at the pipe wall they are mounted at plane right angles to the holder stem, thereby avoiding any necessity to orientate them with the system flow. In total 12 disc coupons are installed in the process flow.

Strip coupons are thin rectangular coupons fitted to the coupon holder with two screws. The screws are insulated with nylon insulators to avoid galvanic corrosion. The strip coupon holder is a stainless steel rod with two threaded horizontal holes on the top part, the rod is welded to a flange. See Appendix C for photograph of a strip coupon holder and on scene photos. The strip coupons are fitted in a similar way to a disc coupon, into a 2'' dummy leg pipe and secured by pinning the holder between a larger blind flange. The strip coupons are fitted so that they are parallel to the process flow; see Figure 1 (d). Strip coupons will be slightly less accurate at imitating the process interface at the pipe wall but they are larger than the disc coupons, thus provides a larger area on which corrosion can develop and be readily observed. Accordingly, the strip coupon gives more accurate weight loss results because of its larger surface area. In total 4 strip coupons are installed in the process flow.

The GHT coupons are adapted to fit the corrosion considerations and corrosion monitoring objective inside the GHT-reactor, located in the Green Hydrotreater unit (16CC-10 A-F). The GHT coupons are thick rectangular metal blocks with larger mass and surface area than the strip- and disc coupons. The large surface area of the coupons results in higher accuracy of weight loss determinations. The GHT-coupon holders are basically two ceramic brackets with two holes on each side. The coupon is fitted to the holder with two ceramic bolts through two unthreaded holes in the coupon; see Figure 1 (e). The GHT-brackets are secured in a circular fashion to the inside of the inlet pipe to the GHT reactor; see Figure 1 (f). In total 6 GHT coupons are installed in the inlet. Given that the holders are stationary, the coupons are recovered by releasing the bolts. See Appendix C for photograph of a GHT-coupon and on-scene photos.

2.2.1.2 Coupon materials

The material of the coupon is analogous to the material of the process pipe or equipment where it is installed. Accordingly, the coupon steel quality varies according to the different construction materials used in the equipment.

- 12 **Disc coupons**: 10 coupons are made of carbon steel (C1018), the remaining 2 coupons are made of stainless steel (grade classified)
- 4 **Strip coupons**, all consisted of carbon steel (C1018)

All of the disc and strip coupons together with insulators are provided by *Cormon corrosion monitoring limited.* Prior to installation they were stored in hermetically sealed envelopes and weighed to four decimal places. All the 16 coupons had a ground polish finish.

The 6 **GHT-coupons** are specialized coupons and require a bit more consideration. As mentioned they are located in the GHT-reactor with the intention of mimicking the corrosion environment of the reactor. *The GHT-coupon material grades are considered classified and will not be published in this report.*

The GHT-coupons are provided by *Haldor Topsoe* [3]. The GHT-coupons were weighed to one decimal point prior to installation.

There will be no attempt to motivate the choice of coupon type or coupon material in this study.

The coupons have different exposed areas and installation dates. The exposed area was calculated from drawings of the coupons, provided from *Cormon* and *Haldor Topsoe*. Table 2 below specifies the serial number, coupon category, coupon material, installation date, installation weight and the calculated exposed area for each of the sampled coupons in this study.

Table 2. *Corrosion coupon details.*

Name	**Serial No.**	**Category**	**Material [grade]**	**Installation date** [yyyy-mm-dd]	**Installation Weight** [g]	**Exposed Area** [cm^2]
9 CC-1	S 0193	Disc coupon	C 1018	2007-05-08	17,7952	15,86
15 CC-2A	S 0186	Disc coupon	C 1018	2007-05-08	17,5906	15,86
15 CC-2B	S 0185	Disc coupon	C 1018	2007-05-08	17,568	15,86
15 CC-9A	S 0187	Disc coupon	C 1018	2007-05-08	17,751	15,86
15 CC-9B	S 0188	Disc coupon	C 1018	2007-05-08	17,6127	15,86
16 CC-2A	181	Disc coupon	*	2010-05-03	18,204	15,86
16 CC-2B	182	Disc coupon	*	2010-05-03	18,284	15,86

16 CC-8A	S 0189	Disc coupon	C 1018	2007-05-08	17,8073	15,86
16 CC-8B	S 0184	Disc coupon	C 1018	2007-05-08	17,5689	15,86
16CC-10A	1	GHT coupon	*	2010-11-23	250,4	53,54
16CC-10B	2	GHT coupon	*	2010-11-23	250,6	53,54
16CC-10C	3	GHT coupon	*	2010-11-23	230,9	53,54
16CC-10D	4	GHT coupon	*	2010-11-23	228,8	53,54
16CC-10E	5	GHT coupon	*	2010-11-23	400,8	100,93
16CC-10F	Not stamped (6)	GHT coupon	*	2010-11-23	239,9	62,02
17 CC-1A	S 0192	Disc coupon	C 1018	2007-05-08	17,692	15,86
17 CC-1B	S 0194	Disc coupon	C 1018	2007-05-08	17,8236	15,86
17 CC-2	H 0052	Strip Coupon	C 1018	2007-05-08	36,9854	32,46
17 CC-3	H 0059	Strip Coupon	C 1018	2007-05-08	37,6833	32,46
17 CC-6	H 0051	Strip Coupon	C 1018	2007-05-08	37,0406	32,46
17 CC-10	H 0055	Strip Coupon	C 1018	2007-05-08	37,4718	32,46
27CC-2	S 0190	Disc coupon	C 1018	2007-05-08	17,6797	15,86

**Considered classified and will not be published in this report*

2.2.2 Weight loss analysis

The weight loss analysis refers to the quantitative method of establishing the corrosion losses at the coupon position by weight loss. The corrosion coupon has been exposed to an environment for a known exposure time after which it is recovered. The recovered coupon is cleaned from all corrosion products and weighed. The weight loss difference between before and after exposure is used to calculate the volume of metal lost. The volume of metal lost relative to the surface area is converted to the average penetration depth in mm per year (mm). The average penetration depth, determined from coupon weight loss, can be expressed as eq.1 below [2].

$$Average\ penetration\ (mm) = \frac{Weight\ loss\ (g)\cdot 10}{Alloy\ density\left(\frac{g}{cm^3}\right)\cdot Exposed\ area\ (cm^2)} \qquad \text{(eq.1)}$$

The depth of material loss relative to the exposure time can be used to calculate the corrosion rate, expressed in millimetres per year (mm/y). This can be expressed in an equation, see eq.2 below [2].

$$v_{average}(mm/y) = \frac{Weight\ loss\ (g)\cdot 8.76\cdot 10^4}{Alloy\ density\left(\frac{g}{cm^3}\right)\cdot Exposed\ area\ (cm^2)\cdot Exposure\ time\ (hr)} \qquad \text{(eq.2)}$$

Weight loss refers to the difference in mass between before and after exposure without corrosion products, Alloy density is the estimated density of the coupon and Exposed area is the shell area of the coupon. The constant is only there to convert the corrosion rate into desired unit, for mm/y: 8.76×10^4 [hr·mm/(cm·year)]. The exposed area is difficult to evaluate with precision, especially throughout the exposure time, since the surface is uneven. The alloy density will also differ over time and between coupons. However a sensitivity analysis of eq.2 indicates that the corrosion rate is not sensitive to small changes in Alloy density, but fairly sensitive to changes in Mass loss, Exposure time and Exposure area. The relative change in Exposure area with and without corrosion products present can be predicted to be very small. Thus, if initial estimated exposed surface area is used as Exposed area and the initial typical coupon alloy density is used as Alloy density, then the corrosion rate acquired from eq. 2 will be sufficiently accurate for the purpose of this study. The penetration depth calculated from eq.1 corresponds to a situation with uniform corrosion and does not quantify the depth of material loss if the corrosion is localised, for example in the case of pit corrosion or galvanic corrosion. This will be resolved by optical analysis of the coupons. The densities and calculated exposed areas used in the weight loss analysis are presented in table 24, *Appendix D*.

2.2.3 Optical inspection and XRD analysis

The aim of the optical inspection is to establish the type of degradation and to investigate localized attacks on the coupon. As mentioned the petrochemical industry is a high risk process and it's important to not underestimate the corrosion damage. If the coupon has suffered non-uniform localized attacks the weight loss analysis will not be sufficient to estimate the material degradation and depth of penetration. For example if the degradation is predominantly caused by severe pitting, the material loss might be small while the depth of penetration can be very large. Further, determining whether the corrosion is non-uniform and describing the non-uniform attacks gives useful information concerning the type of corrosion. The X-ray diffraction analysis is used as a complementary investigation by identifying the corrosion products formed on the coupons.

After the corrosion coupon has been exposed to an environment and recovered, it is cleaned from all residues of the process liquid. The corrosion product present on the coupon is investigated visually and photographed for documentation purposes. The information gained from the visual analysis of the corrosion product will be used to investigate: What corrosion mechanism causes the present products, why does the mechanism occur and are the corrosion products localized or uniform. On selected samples the corrosion products are stripped from the coupon. The salvaged corrosion products are used in X-ray diffraction (XRD) analysis to establish the phase composition. The results from the visual analysis and the XRD analysis may help to establish the composition of the corrosion products qualitatively. Through the composition the most likely mechanisms may be established.

Once the corrosion products have been removed two actions are performed on the coupons: Visually, it is determined whether corrosion is uniform and with optical microscopy the maximum pitting depth, pit shape and pit density are determined. The measured maximum pitting depth is used in eq.3 below to calculate the maximum annual corrosion rate due to pitting, $v_{pitting}$ [21].

$$v_{pitting}\left(\frac{mm}{y}\right) = \frac{Max.measured\ depth\ (mm)\cdot 8.76\cdot 10^3}{Exposure\ time\ (hr)} \qquad \text{(eq.3)}$$

By dividing the maximum measured depth difference with the exposure time the annual pitting depth can be calculated. The constant is to convert the corrosion rate into desired unit, mm/y: 8.76×10^3 [hr/year]. The maximum measured depth is used since the most important information will be to make accurate lifetime assessments and predict the penetration depth before it reaches a critical depth. The margin of error will be large since the occurrence of pitting is a statistical phenomenon and its incidence is related to the area of metal exposed. As the coupon area is small the phenomenon can be underestimated or even missed. The corrosion rate due to pitting corrosion can be used as a compliment to the uniform corrosion rate calculated in eq.2.

To evaluate the significance of the localized attacks a Pitting factor can be calculated. This is the ratio of the deepest metal penetration to the average metal penetration. Where the deepest metal penetration is the measured maximum pitting depth and the average metal penetration is calculated from the weight loss in eq.1. The relationship is expressed in eq.4 [21].

$$Pitting\ factor = \frac{Max.measured\ depth\ (mm)}{Average\ prenetration\ (mm)} \qquad \text{(eq.4)}$$

A pitting factor of unity represents uniform corrosion. A larger number means greater significance of localized attacks. The factor does not apply if pitting depth or average depth is very small, as the

pitting factor will vary from zero or infinity. The pitting factor can be used as a simplified method to predict where the probability of localized attacks is large. If the pitting factor is high the average corrosion rate calculated from eq.2 is not useful for calculating penetration rate.

To determine type and severity of attack the shape and density of the localized attacks should be specified. This is evaluated visually and using an optical microscope. The pit density is expressed as high, moderate or low while the shape is expressed as narrow, elliptical or shallow. The expressions are visualized in Figure 2 [5]. Note that no cross-section analysis is performed, only vertical optical analysis.

Figure 2. *Shape and density of localised attacks.*

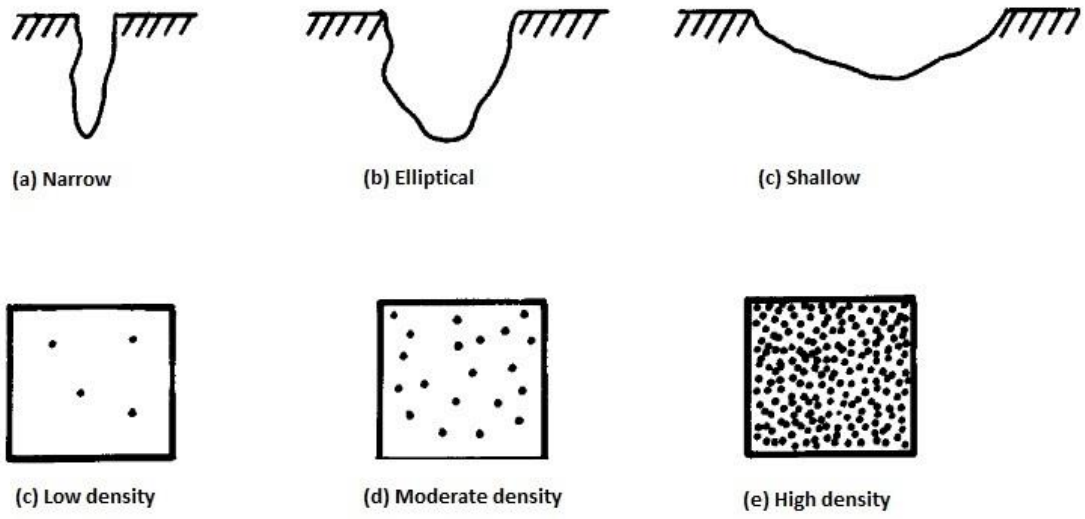

As the shape and pit density is very subjective and observer dependent, the information is only used as a visual estimation. The estimated shape and pit density is used to investigate the degradation mode. Pit shape and pit density is useful in an evaluation of the pitting factor. If the penetration depth is low, the pit density is high and the pits shallow, then one can expect a pitting factor fairly close to one.

2.2.4 Background study

The background study is done in order to propose a hypothesis concerning coupon degradation modes and to predict the range of corrosion damage. The background study is done in four coupled steps:

1. Find and describe potential corrosion mechanisms and degradation modes in relevant applications in the petrochemical industry (*chapter 3*).
2. Describe the process units where coupons are installed and estimate the environment that the coupons are exposed to (*chapter 4*).
3. Use the corrosion/degradation descriptions to propose a hypothesis of possible degradation modes for each coupon environment (*chapter 4*).
4. Use the process descriptions to correlate the data from each coupon position to an extended area by dividing sections of the process unit into so called "corrosion loops" (*chapter 4*).

The **first step** is achieved by carrying out a literature study of possible corrosion mechanisms and degradation modes in the petrochemical industry. The literature study is coupled with step two in order to exclude irrelevant mechanisms and modes. During the study it should become clear which parameters that have a major impact on corrosion behaviour in the petrochemical industry. The literature study is presented in *chapter 3*.

The **second step** is attained through internal information obtained at Preem Gothenburg. Initially an overview of the relevant process units is made in order to illustrate the coupon positions in the process flow. The process unit descriptions should contain description of: process unit function, type of equipment in process unit and a record of relevant equipment material. The description of the environment that the coupon is exposed to should contain estimates for: phase, rate, pH, temperature and pressure of the corrosive medium as well as an estimated composition of water, oxidizing agents and reducing agents. Process descriptions and coupon environment descriptions can be found in *chapter 4*.

The **third step** is achieved by comparing the estimated coupon exposure environment in step 2 with the potential degradation modes in step 1. A degradation mode is proposed based on the likeliness of it occurring in the environment present at the coupon position. A list of proposed degradation modes for each coupon is presented in *chapters 4.2* to *4.7*.

The **fourth step** is based on the concept of corrosion loops. A corrosion loop is basically sections of process units where the conditions are considered to be similar. If one assumes that the degradation mode remains the same as long as the material and conditions does not change, then a coupon in the loop experiences similar material degradation as the rest of the material in the corresponding corrosion loop. For a more detailed description of corrosion loops see *chapter 2.2.4.1* further down in this chapter. Sections of the process units, around the coupons, are divided accordingly into corrosion loops. By comparing the list of proposed degradation modes developed in step 3 the coupons can be incorporated into loops. The corrosion loops are presented in *chapters 4.2* to *4.8.*

2.2.4.1 Corrosion loops

Degradation of a specific material as an effect of corrosion depends on the conditions at which it is subjected to. Therefore it can be assumed that as long as the material and conditions does not change the degradation mode should remain unchanged [6]. Based on this assumption the areas of the process units in question are divided into corrosion loops. The corrosion loops will represent areas where conditions are similar, and consequently the degradation mode can be expected to be similar. This is done for three reasons. Reason one; to correlate the degradation of the coupons to the degradation of surrounding equipment. Thus be able to speculate about the condition of equipment and piping in the entire loop, making the coupon represent a larger area and not just a single-point test. Reason two; be able to compare results from coupons that are located in different process units. This allows comparing of coupons in corresponding loops. Reason three; be able to make reasonable statements about the amount of corrosion or the degradation mode in matching loops without any installed coupons.

A corrosion loop represents a range of equipment where conditions are similar, so some process units may have more than one corrosion loop, also some corrosion loops can include more than one process unit. To be able to keep track of the different loops each corrosion loop is colour coded. To motivate a loop the approach is to first acquire stream data for each coupon position (step 2). If two

streams have similar stream data they are considered one loop designated by one colour (step 4). The extent of the loop coincides with the region where the stream data is valid.

A hypothesised list of degradation modes for each loop is compiled from corresponding stream data (step 3) - presented and motivated in *chapter 4.8*. The validity of the proposed hypothesis is evaluated through coupon quality and quantity measurements and comparing coupon measurements between similar loops.

2.3 Methodology summary

The potential degradation modes (*chapter 3*) are used together with the estimated coupon conditions (*chapter 4*) to propose a hypothesis of potential degradation modes for each coupon. The proposed degradation modes together with the interpretation of the process descriptions are used to approximate the corrosion loops (*chapter 4*). Separately, the corrosion coupons are removed from each position and transported to a laboratory environment. The organic products are removed from the coupons, a visual analysis is preformed and photographs are taken for documentation. The corrosion products are removed from the coupons and kept for XRD analysis. The base material of the coupons are photographed and compared with coupon appearance prior to exposure. A weight loss analysis and optical analysis is performed where weight loss, penetration depth and other observations are documented. Corrosion rates, average penetration depth and pitting factors are calculated and XRD results are interoperated.

The pitting factors and penetration depth are used to evaluate the method and provide information for determining the coupons degradation modes. The corrosion rates are the most important part of the corrosion damage evaluation, they can be used to predict lifetimes of equipment in the future. The measured corrosion rates can also be used together with past corrosion values and pitting factors to evaluate the reliability of the method. The measured pit shape, pit depth and pit density from the optical inspection can be used to evaluate the severity of the corrosion attack. The XRD results, measured pit shape, measured pit density and calculated pit factors can be valuable information in determining the most probable degradation modes. The approximated corrosion loops are intended to expand the results of the individual coupons to equipment in a larger area. This makes it possible to make predictions of equipment lifetime and material degradation modes within the loop. They also make it possible to compare coupon results between different process units and highlight areas where corrosion damage is of importance.

Corrosion rates, penetration depth, pitting factors will be considered results and will be presented in *chapter 5.* Data required for weight loss analysis and optical inspection will be presented in a*ppendix D.*

3. Corrosion in the Refining Industry

Corrosion in a refinery is a very complex and extensive subject. The refinery process handles hydrocarbons, water, salts, solid impurities and chemicals at both low and high temperatures. The materials involved are carbon steel, stainless steel and special alloys. It is not possible, within the scope of this study, to cover all possible corrosion mechanisms.

The corrosion mechanisms detailed below are those that, based on installed materials and existing process conditions, have been deemed to be the most important for the corrosion loops where the corrosion coupons are located. [9] [10][15]

3.1 Aqueous corrosion

Aqueous corrosion refers to corrosion in conditions where water is in liquid or vapour/liquid mixed state.

3.1.1 NH_4HS corrosion

Ammonium bisulphide (NH4HS) causes aggressive corrosion occurring in reactor effluent streams and in units handling alkaline sour water. Sour water is the waste water produced in the refinery, typically containing hydrogen sulphide and other contaminants that must be removed. Corrosion increases with increasing NH_4HS concentration and increasing velocity. Below 2 wt %, solutions generally have low corrosion rates. Above 2 wt % NH_4HS, solutions are increasingly corrosive [15].

The selection of materials of construction to resist NH_4HS corrosion was primarily based on empirical findings that relied heavily on evaluations of operational experience. In the period 2000-2007 two joint industry programs titled —"*Prediction and Assessment of Ammonium Bisulfide Corrosion Under Refinery Sour Water Service Conditions*" were initiated to develop a quantitative engineering database and provide guidelines to predict corrosion in hydrogen sulphide (H_2S)-dominated alkaline sour water systems typically found in refinery services, such as the reactor effluent air cooler systems of hydroprocessing units described in *chapter 4*[13]. Several major failures have occurred in hydroprocessing reactor effluent systems due to localized corrosion [15].

The following main conclusions were drawn based on the results of these programs:

i. P_{NH3}, especially in the 100 to 620 kPa absolute range, had a significant effect on the corrosion of carbon steel, stainless steels and nickel-based alloys in refinery alkaline sour water environments.

ii. Carbon steel corrosion rates under conditions of high P_{NH3} at 55 °C were generally less than approximately 0.64 mm/y. Carbon steel corrosion rates increased with increasing test velocity (wall shear stress) but were relatively insensitive to P_{NH3} and NH_4HS concentration.

iii. Stainless steel corrosion rates under conditions of high P_{NH3} at 55 °C were low at low NH_4HS concentration and velocity and steadily increased with increasing NH_4HS concentration and velocity. The stainless steel alloys corroded at much higher rates than carbon steel at the most severe conditions tested.

iv. Nickel-based alloys evaluated under conditions of high P_{NH3} at 55 °C showed the same trend of increased corrosion with increasing NH_4HS concentration and velocity but exhibited very good corrosion resistance even at the most severe conditions tested.

v. For all materials evaluated at all three levels of P_{NH3}, corrosion rates increased with increasing temperature from 43 °C to 55 °C, but the magnitude of the increase varied considerably among the different materials. The extreme magnitude of the stainless steel corrosion rate increase for a small change in temperature was quite surprising.

vi. Free cyanide will increase corrosion rates since cyanides may react stoichiometrically with iron sulphide. The resulting removal of the protective film exposes fresh steel surface. But since Preem Refinery Gothenburg has no catalytic cracker unit the amount of free cyanides are very low or non-existent.

3.1.2 NH_4Cl corrosion

Wet ammonium chloride (NH_4Cl) causes general or localized corrosion - often pitting. It is normally occurring under ammonium chloride or amine salt deposits, often in the absence of an aqueous phase. NH_4Cl corrosion is one of the main causes of equipment and piping failures in today's refining industry [14]. Ammonium chloride corrosion has affected equipment and piping in areas such as hydroprocessing effluent systems, overhead systems of crude distillation and fractionation columns of thermal and catalytic conversion units.

The typical construction material of most of the equipment in the above-mentioned processes is carbon steel. When wet ammonium chloride salt is present, the corrosion rate of carbon steel is generally considered unacceptably high. Unfortunately, many common alloys (such as common austenitic stainless steels) are not suitable replacements because they are susceptible to chloride stress corrosion cracking (Cl-SCC) in these environments. Use of duplex stainless steels has given mixed success with some reports of pitting corrosion and stress corrosion cracking under the combined effect of chlorides and sulphides. Thus far, only nickel alloys have demonstrated satisfactory performance in these services.

Despite these significant concerns, the industry's understanding of wet ammonium chloride corrosion is still very limited. Ammonium chloride is considered an acid salt because it is formed from a strong acid (HCl) and a weak base (NH_3). Dilute solutions of stoichiometric NH_4Cl salt (e.g. less than 0.1wt %) are generally not considered to be very corrosive. However, corrosion is most severe at or near the aqueous dew point, where NH_4Cl concentration can be very high.

Critical factors for NH_4Cl corrosion as suggested by [15]:

i. Concentration (NH_3, HCl, H_2O or amine salts), temperature and water availability are the critical factors.

ii. Ammonium chloride salts may precipitate from high temperature streams as they are cooled, depending upon the concentration of NH_3 and HCl, and may corrode piping and equipment at temperatures well above the water dew point (> 149°C).

iii. Ammonium chloride salts are hygroscopic, and readily absorb water. A small amount of water can lead to very aggressive corrosion (>2.5 mm/y).

iv. Ammonium chloride and amine hydrochloride salts are highly water soluble, highly corrosive and form an acidic solution when mixed with water.

3.1.3 Wet H2S corrosion

Wet H_2S corrosion refers to the corrosion of carbon steel in the presence of aqueous hydrogen sulphide (H_2S). Hydrogen sulphide is an acid gas at room temperature that is easily soluble in water.

$$H_2S\ (g) \leftrightarrow H_2S\ (aq) \qquad (K_H \approx 0.1M/atm \text{ at } 25°C) \qquad \text{(R1)}$$

The corrosion reaction between steel and hydrogen sulphide forms the characteristic black sulphide scale commonly seen in the petrochemical industry. Wet H_2S corrosion normally results in uniform thinning although localised thinning can be experienced when the metal sulphide scale is disturbed. The formed ferrous sulphide scale is a reasonably adherent film that is generally considered protective in most petroleum refinery environments. Wet H_2S corrosion has however an additional characteristic; it promotes hydrogen diffusion into the base metal which leads to hydrogen damage, also known as "Wet H_2S cracking" , see chapter *3.5.2*. This characteristic is a serious concern since the sulphide scale is somewhat protective and usually leads to uniform thinning while hydrogen damage is harder to detect and manage. Most of the aqueous H_2S at the studied positions are dissolved in the sour water running to the water treating unit. In an aqueous H_2S environment many different types of ferrous sulphides may form. The ferrous sulphides may form a cubic crystal systems such as troilite (FeS), greigite (Fe_3S_4) and pyrite (FeS_2) or amorphous ferrous sulphides such as mackinawite (FeS). The surface scale formation is an important factor governing the corrosion rate since the scale growth depends primarily on the kinetics of formation. The wet H_2S corrosion reaction with steel in a sour environment is proposed by [8] to proceed by reactions R2 through R4. The aqueous H_2S first dissociates into ions according to reaction R1:

Dissociation of H_2S: $$H_2S(aq) \leftrightarrow H^+ + HS^- \qquad \text{(R2)}$$

At higher pH (>6) HS^- will dissociate further into H^+ and S^{2-}.

Second dissociation: $$HS^- \leftrightarrow H^+ + S^{2-} \qquad \text{(R3)}$$

The corrosion reaction is electrochemical; the acidity of the electrolyte will oxidize iron (R4) while hydrogen will be reduced according to R13 and R14 respectively [8]:

Oxidation: $$Fe \rightarrow Fe^{2+} + 2e^- \qquad \text{(R4)}$$

Reduction: $$2H^+ + 2e^- \rightarrow H_2 \quad \text{or} \quad HS^- + e^- \rightarrow H^\circ + S^{2-} \qquad \text{(R5, R6)}$$

The proposed overall reaction can be may be written as reaction R7:

Overall reaction: $$xFe^{2+} + yHS^- \rightarrow Fe_xS_y + yH^+ \qquad \text{(R7)}$$

In most cases the main iron sulphide formed is FeS. If the FeS is dense and adherent to the metal surface the diffusion rate to the metal will decrease and act as a protective solid-state diffusion barrier. The diffusion barrier will act as a protective film on the surface of the metal and will decrease potential corrosion rates.

The main parameters affecting wet H_2S corrosion rates at the studied positions are pH, H_2S concentration and temperature. Both an increase in cathodic proton reduction or higher concentration of bisulphide will increase corrosion rates. Higher temperature will increase corrosion rates by increasing diffusion and reaction rates. Generally, the lowest rates in steels typically results from corrosion in near natural pH solutions (pH 5.5-7.5). In very low pH (<2) iron is dissolved and iron sulphide is not precipitated on the surface of the metal due to a very high solubility of iron sulphide phases [7, 8, 9].

As mentioned wet H_2S corrosion promotes hydrogen damage through diffusion of atomic hydrogen (H°) into the base metal, for more information see *chapter 3.5.2.* If the wet H_2S corrosion is managed correctly the cathodic (R6) reaction can be minimized and the hydrogen damage halted. Thus the wet corrosion controls the severity of the hydrogen damage.

Above acknowledged critical factors:

i. Partial Pressure of H_2S.

ii. Concentration of Dissolved H_2S and pH.

iii. Fluid Temperature.

iv. Fluid Velocity/Turbulent Flow.

3.1.4 Wet CO_2 corrosion

Carbon dioxide gas $(CO_2)_g$ is soluble in water. Dissolved carbon dioxide $(CO_2)_{aq}$ will hydrate in water and form carbonic acid (H_2CO_3) in a relatively slow reaction. The aqueous carbonic acid will cause corrosion on low alloy steels, producing carbonates ($FeCO_3$). The reaction path may be written as R8 to R12 below [18]:

Gas dissolution: $CO_2(g) \leftrightarrow CO_2(aq)$ (K_H≈0.1M/atm at 25°C) (R8)

Formation of carbonic acid: $CO_2(aq) + H_2O \rightarrow H_2CO_3(aq)$ (R9)

First dissociation: $H_2CO_3 \rightarrow HCO_3^- + H^+$ (R10)

Second dissociation $HCO_3^- \rightarrow CO_3^{2-} + H^+$ (R11)

Formation of iron carbonate: $Fe^{2+} + CO_3^{2-} \rightarrow FeCO_3$ (R12)

Solubility of CO_2 in water is directly proportional to the partial pressure. The produced corrosion product, iron carbonate, could be protective or non-protective depending on acting conditions. Generally for low alloyed steels the corrosion deposit film is considered protective at high temperature, high pH and low flow rates. The corrosion reaction is electrochemical; the acidity of the electrolyte will oxidize iron (R12) while hydrogen will be reduced according to R13 and R15 respectively [18]:

Oxidation: $Fe \rightarrow Fe^{2+} + 2e^-$ (R13)

Reduction: $2H^+ + 2e^- \rightarrow H_2$ *Or:* $2H_2CO_3 + 2e^- \rightarrow H_2 + 2HCO_3^-$ (R14, R15)

Higher pH leads to decreased solubility of iron carbonate ($FeCO_3$) and thus increases the precipitation rate of corrosion product, which leads to faster formation of protective film and lower corrosion rate. Typically at very low pH the solubility of iron carbonate increases and no protective film will be formed. Temperature accelerates all processes involved in wet CO_2 corrosion [15]. At very low pH where no protective film is formed, corrosion rate will increase with increasing temperature. At higher pH where a protective film is formed, higher temperature will increase the rate of precipitation and decrease the corrosion rate, why corrosion resistance for low alloyed steels and carbon steels show an improved corrosion resistance at temperatures over 175°C [20].

Corrosion resistance is improved with increasing chromium level of steels. Wet carbon dioxide corrosion of stainless steels generally show little dependence on carbon dioxide level and temperature if no chlorides or other contaminants are present [14]. Higher alloyed steels will experience higher corrosion rates with increased chloride concentration and temperature. Type 316 stainless steels and duplex steels may experience local corrosion attacks (pitting or crevice corrosion) in the presence of chlorides, due to local depletion of chromium [13].

The addition of hydrogen sulfide (H_2S) increases the acidic activity, and thus the partial pressure of H_2S must also be considered when estimating the pH level. In a CO_2/H_2S system, wet CO_2 corrosion is usually regarded to be more severe than wet H_2S corrosion and give higher corrosion rates. When H_2S is present in a CO_2 environment, the formation of FeS (see chapter 3.2.3) interferes with the formation of $FeCO_3$. To determine which corrosion mechanism predominates (wet H_2S- or wet CO_2 corrosion) the ratio of partial pressure CO_2/H_2S could be contemplated. CO_2 corrosion should be considered whenever the ratio of CO_2 to H_2S partial pressure is higher than 100 [10].

Above acknowledged critical factors:

i. Partial Pressure of CO_2.

ii. Concentration of Dissolved CO_2 and pH.

iii. Fluid Temperature.

iv. Fluid Velocity/Turbulent Flow.

v. Chloride concentration

3.1.5 HCl corrosion and chloride induced pitting corrosion

Hydrochloric acid (aqueous HCl) causes both general and localized corrosion and is very aggressive to most common materials of construction across a wide range of concentrations. Damage in refineries is most often associated with dew point corrosion in which vapours containing water and hydrogen chloride condense from the overhead stream of a distillation, fractionation or stripping tower. The first water droplets that condense can be highly acidic (low pH) and can promote high corrosion rates. High temperature HCl corrosion (dry gaseous HCl) has low to minuscule corrosion rates for carbon steels. If the temperature decreases in the presence of moisture corrosion rates increase due to the dew point effect. The corrosion process is usually electrochemical, thus the mass loss and hydrogen evolution is produced by the same reaction proposed previously in this chapter:

$$Fe(s) + 2H^+ \rightarrow Fe^{2+} + H_2(g) \qquad \text{(R16)}$$

Hydrochloric acid is soluble in water. In aqueous form it is completely dissociated then separated into ions, making it a source of chlorides (Cl^-) and hydrogen (H^+), which are highly aggressive towards metals. Halide ions such as chloride often stimulate pitting corrosion. As the pit grows accumulation of positive Fe^{2+} attracts negatively charged chloride ions, creating ferrous chloride. The resulting ferrous chloride hydrolyses according to proposed reaction R17 below [20]:

$$Fe^{++}(Cl^-)_2 + 2H_2O \leftrightarrow Fe(OH)_2 + 2Cl^- + 2H^+ \quad \text{(R17)}$$

As illustrated by reaction R17 access chloride ions and hydrogen ions are created, both of which accelerates corrosion at the bottom of the pit. Chlorides also have the ability to penetrate and destroy the protective oxide film of stainless steels. The oxide film on stainless steel is responsible for the corrosion resistance (passivity). This means that stainless Cr-Ni steels may even be unsuitable for use in very dilute HCl concentrations and in cold conditions [19]. Austenitic stainless steels such as 306- and 316 series are generally considered unsuitable for use in HCl containing environments [18].

Critical factors for HCl corrosion as suggested by [15]:

i. HCl acid concentration, temperature and alloy composition.

ii. The severity of corrosion increases with increasing aqueous HCl concentration and increasing temperature.

iii. Aqueous HCl can form beneath deposits of ammonium chloride or amine hydrochloride salts in exchangers and piping. The deposits readily absorb water from the process stream or from injected wash water.

iv. Carbon steel and low alloy steels are subject to excessive corrosion when exposed to any concentration of HCl acid solution at with pH below about 4.5

3.1.6 Amine Corrosion

Amine corrosion refers to the general and/or localized corrosion that occurs principally on carbon steel in amine treating processes. Corrosion is not caused by the amine itself, but results from dissolved acid gases (CO_2 and H_2S), amine degradation products, Heat Stable Amine Salts (HSAS) and other contaminants.

Stress corrosion cracking of carbon steel in amine services is discussed in *chapter 3.4.2*.

Critical factors for Amine corrosion as suggested by [15]:

i. Corrosion depends on design and operating practices, the type of amine, amine concentration, contaminants, temperature and velocity.

ii. Corrosion is also dependent on the type of amine used. In general, alkanolamine systems can be rated in order of aggressiveness from most to least as follows: monoethanolamine (MEA), diglycolamine (DGA), diisopropylamine (DIPA), diethanolamine (DEA), and methyldiamine (MDEA).

iii. Lean amine solutions are generally not corrosive because they have either low conductivity and or high pH.

iv. Lean amine solutions contain a small amount of H_2S which helps to maintain a stable iron sulfide film.

v. Ammonia, H_2S and HCN accelerate corrosion in the regenerator overhead condenser and outlet piping as well as reflux piping, valves and pumps.

vi. Corrosion rates increase with increasing temperature, particularly in rich amine service. Temperatures above about 104°C can result in acid gas flashing and severe localized corrosion due to 2-phase flow, if the pressure drop is high enough.

vii. Process stream velocity will influence the amine corrosion rate and nature of attack. Corrosion is generally uniform however high velocities and turbulence will cause localized thickness losses.

3.2 High temperature corrosion

High temperature corrosion refers to corrosion at conditions where water is in gaseous state.

3.2.1 Sulphidic corrosion

Sulphidic corrosion consumes a metal by reaction between the metal surface and liquid or gaseous hydrocarbon streams containing sulphur compounds at elevated temperatures. In a petroleum refinery the active corrosive agent is H_2S. Almost all of the H_2S at Preem Refinery is produced in the hydrotreating units Synsat and GHT (see *chapter 4*) by catalytic decomposition of sulphur compounds (e.g. mercaptans, sulphides, disulphides or polysulphides).

The corrosion reaction produces a sulphide scale or a layer of metal sulphides on the surface of the metal. In the case of carbon steel, an iron sulphide (FeS) scale is produced on the metal surface. For carbon steel equipment the sulphide scale tends to be protective and under less aggressive corrosive conditions it usually decreases the corrosion rates significantly. Low alloy chromium and chromium-nickel steels produce more tenacious, protective sulphide scales than regular carbon steels. This means that the low alloy steels provides enhanced resistance to sulphidic corrosion at higher temperatures, where the resistance of regular carbon steels are limited. Sulphidic corrosion normally results in uniform thinning, although localised thinning can be experienced when the parabolic growth of the metal sulphide scale is disturbed. Carbon steels are considered more or less resistant to sulphidic corrosion at temperatures up to about 230°C. Depending on the sulphur content of the oil, carbon steel can exhibit useful corrosion resistance up to about 330°C. The increasing chromium contents of Cr-Mo steels and austenitic stainless steels provide proportionately greater resistance to sulphidic corrosion at higher temperatures. The corrosion rates for all these steels reach a maximum at approximately 450°C. Above 450°C the corrosion rate decreases rapidly to very low rates. This behaviour is generally attributed to the formation of a protective coke layer on the hot metal surface. Further, adding silicon to carbon steels enhances its sulphidic corrosion resistance.

Temperature, the concentration of H_2S and the metal composition are the major factors affecting the rate of sulphidic corrosion. Also, conditions that remove the metal sulphide scale (such as erosion or abrasion) can drastically increase the sulphidic corrosion rate, thus flow rate of corrosive medium is a factor, increasing flow rate increases corrosion rate. In the above mentioned, temperature is the most important factor in determining the corrosion rate. The presence of hydrogen in operations

such as hydrotreating in the Synsat or GHT unit, may increase the severity of the sulphidic corrosion by converting organic sulphur compounds in feed stock to the active corrosive agent H_2S.

The modified "McConomy curves" in Figure 3a provide industry-accepted estimates of the corrosion rates of various steels as a function of temperature and sulphur content of the oil, in the absence of hydrogen. The curves clearly demonstrate the corrosion rate reduction that results from alloying the steel with chromium. The modified McConomy curve apply only to liquid hydrocarbon streams containing 0.6 wt% of sulphur unless a correction factor for sulphur content is applied. Furthermore, it does not take into account the effects of vaporization or other dynamic and chemical flow properties.

Figure 3. a) *Modified McConomy curve; showing temperature effect on corrosion rate of sulphidic corrosion on various steels* **b)** *Modified Couper-Gorman curve; showing the effect of temperature and H_2S concentration on sulphidic corrosion rate [9].*

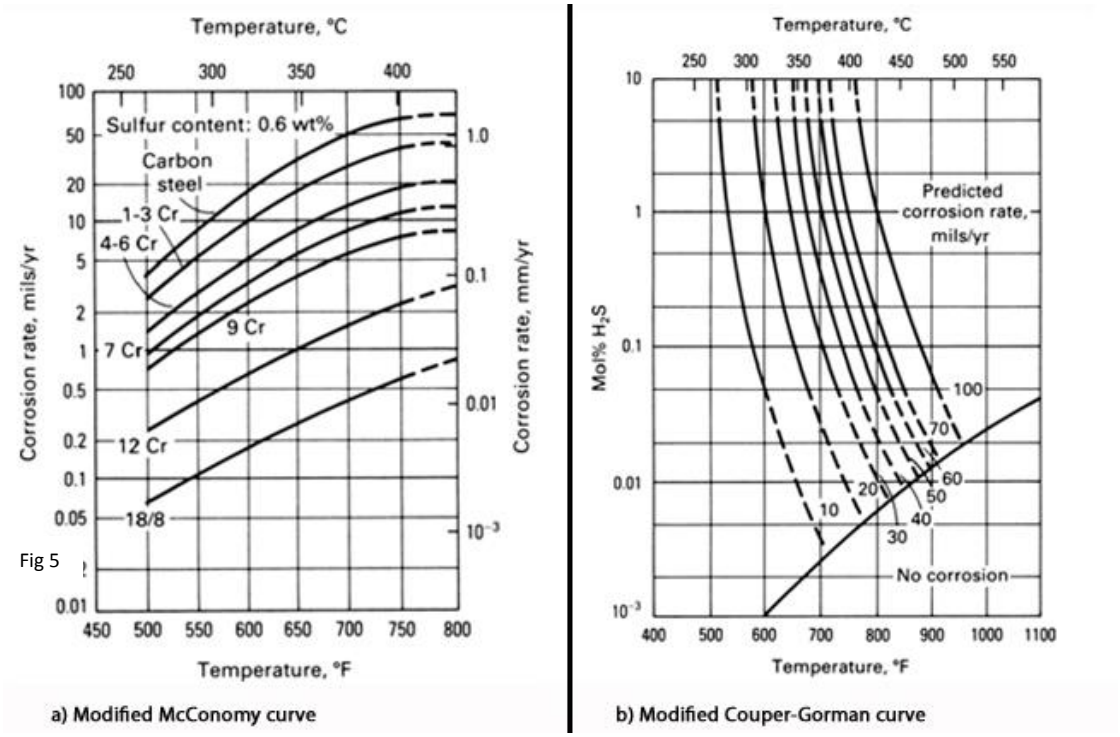

Fig 5

The Couper-Gorman curves in figure 3b are primarily based on corrosion rate data for an all-vapor system, partial condensation will most likely increase corrosion rates. At low H_2S concentrations and temperatures above 315 °C the formation of iron sulphide (FeS) becomes thermodynamically impossible, as shown by the part denoted "no corrosion" in the modified Couper-Gorman curve. With the presence of hydrogen there is a possibility of high-temperature hydrogen attack, which should be considered [9, 10].

3.2.2 High Temperature Hydrogen Attack (HTHA)

High temperature hydrogen attack refers to loss in tensile strength and ductility due to the ingress of hydrogen in steel which can conclude in catastrophic failures. It occurs in carbon steels exposed for to hydrogen under high pressure and at high temperature [4]. Atomic hydrogen formed in a reduction reaction on a metal or by dissociative chemical adsorption of H_2 (similar to hydrogen embrittlement and low temperature hydrogen blistering) diffuses into the metal surface. The atomic

hydrogen reacts with dissolved carbons (R1) or carbides in steel (R2) to form methane gas in accordance with the proposed chemical reactions R5 or R6

$$4\mathrm{H} + \mathrm{C} \rightarrow \mathrm{CH}_4\ (\mathrm{g}) \qquad \text{Or} \qquad 4\mathrm{H} + \mathrm{MC} \rightarrow \mathrm{CH}_4\ (\mathrm{g}) + 3\mathrm{M} \qquad \text{(R17, R18)}$$

Where H is atomic hydrogen and M refers to bulk metal atoms [6]. This gaseous methane forms voids on grain boundaries, inclusions or other defects. The increase of gaseous methane pressure inside the voids will produce high local stresses at the void circumference, comparable to low temperature hydrogen blistering. The high stresses may result in the formation of micro fissure, blistering or cracking. Further the decarburization process (carbon loss) of parent steel reduces tensile strength and increases ductility and creep rate [5].

Critical factors for HTHA corrosion as suggested by [15]:

i. For a specific material, HTHA is dependent on temperature, hydrogen partial pressure, time and stress. Service exposure time is cumulative.

ii. The hydrogen/carbon reaction can cause surface decarburization of steel. If the diffusion of carbon to the surface is limiting, the reaction can result in internal decarburization, methane formation and cracking.

iii. Figure 4 below contains curves that show a temperature/hydrogen partial pressure safe operating envelope for carbon and low alloy steels.

iv. 300 Series SS, as well as 5Cr, 9Cr and 12 Cr alloys, are not susceptible to HTHA at conditions normally seen in refinery units.

3.3 Fatty acid corrosion

Fatty acids can be defined as an organic acid with more than six carbons in length with the general formula ROOC, where R is a hydrocarbon chain. Fatty acids are classified as weak acids as the hydrogen (H^+) dissociation is slight in aqueous solutions. Factors affecting fatty acid corrosion are:

i. Fatty acid concentration and nature of acid. As a general rule the corrosivity increases when the alkyl group, attached to the acid, decreases in size [23, 26]. Vegetable oils and animal fats are less corrosive than tall oil acids [25].

ii. Temperature; higher temperatures increase corrosion rate [25]. At temperatures over 300 °C stainless steel series 300 is questionable [23].

iii. The oxidizing effect of water seems to reduce corrosion rates on stainless steels [23, 25].

iv. Fluid flow conditions [23].

The RTD reactor operates at high temperatures (>300 °C) and pressures (>25 bar). Uniform corrosion can be expected, however pitting and crevice corrosion can occur on essentially all alloys under these operating conditions [23].

This chapter will only deal with longer chain organic acids present in Raw Tall Diesel (RTD). Raw Tall Diesel is not a pure compound, but a mixture of several compounds meeting a certain specification. The corrosive action of RTD is complicated since the mixture contains different organic acids and impurities such as chlorides. To make matters worse, when the RTD is processed it is mixed with a diesel component containing moisture and other contaminants. Therefore this chapter will be limited to the corrosion effects of isolated straight long-chained fatty acids, whilst discussing potential process effects.

The RTD reactor operates in a H_2 environment which will act as a weak reducing agent, and most likely act to decrease the corrosivity. As mentioned the RTD reactor operates at high temperatures and pressures and it has been suggested by [23, 24] that low alloyed carbon steels have insufficient resistance to fatty acid corrosion. Carbon steel samples exposed to concentrations, temperatures and pressures similar to the RTD operating conditions have been completely consumed [23, 24]. It seems that more highly alloyed stainless steels are required. According to [24, 25] type 316L is widely used, but as temperatures increase towards the operating of the RTD reactor higher molybdenum grades must be used. Highly alloyed 904L, alloy C-276 and alloy 625 has been used successfully.

In a laboratory test reported in [23] samples were exposed tall oil acids at 300 °C for 3 days. The cast iron showed a corrosion rate of 11.1 mm/y, while stainless steel 304 series showed a corrosion rate of 4.7 mm/y.

3.4 Stress-Corrosion Cracking

Stress-corrosion cracking (SCC) can be described as environmentally induced crack propagation. The crack propagation is a result of combined interaction between the anodic corrosion reactions and the mechanical stress. In other words, the SCC phenomena results in crack propagation during combined simultaneous interaction of mechanical and chemical forces. Both factors acting independently or alternately would not result in the same effect. The SCC phenomena is usually a very complex issue that depends on type of loading, materials involved, environment and the interaction between them.

Many models have been proposed to describe the SCC mechanism for crack propagation. None of these models will be discussed in this study [7, 10]. However, a few arguments reoccur in the crack propagation models [10]:

v. Typically, SCC of an alloy is the result of the presence of a specific chemical species.

vi. In general, SCC is observed in alloys that form a scale on the metal surface. Therefore, SCC is of greatest concern in the corrosion-resistant alloys exposed to a aggressive liquid solutions. The liquid can be condensed layers of moisture or the bulk solution.

vii. The stresses required to cause SCC are small, usually below the macroscopic yield stress, and are tensile in nature.

At the studied coupon positions the SCC phenomena may occur as a consequence from exposure to chlorides, caustic, amines or polythionic acid

3.4.1. Chloride stress corrosion cracking (Cl-SCC)

Chloride stress corrosion cracking (Cl-SCC) is very common in austenitic stainless steels and nickel alloys that usually results in transgranular, highly branched cracking. Typically, high applied or tensile stresses and high dissolved oxygen content produce higher risk for Cl-SCC at lower chloride concentrations. In a refinery environment where there is no dissolved oxygen Cl-SCC is only possible with high H2S concentrations. In very special cases, with high oxygen and tensile stresses, a concentration of 1 ppm chlorides can result in cracking however higher concentrations are usually required. Factors that affect rate and severity of Cl-SCC in aqueous solutions are chloride content, oxygen content, temperature, stress level, and pH value. In the absence of H_2S, oxygen is usually required for Cl-SCC to occur because when the oxygen content decreases the critical chloride content for cracking to occur. Therefore Cl-SCC in refineries often occurs during production stops when air and moisture enters equipment that has been opened for inspection. The likelihood of Cl-SCC In alkaline solutions is very low. Consequently, austenitic stainless steel can be used in equipment exposed to amine solutions in the Amine recovery unit (ARU), Common unit and sulfur recovery unit (SRU). The ARU, SRU and Common unit are explained in chapter 4. Since alkaline conditions are favorable it has been found that when 5 to 40% aqueous caustic solution is added as a precautionary measure during stoppages for the prevention of cracking by polythionic acids, it also helps in preventing cracking by chlorides (if not excessive concentrations of polythionic acid is formed). The severity of cracking increases with temperature and Cl-SCC of process equipment generally only occur at temperatures above 60°C [10].

3.4.2 Amine stress corrosion cracking (ASCC)

Amine stress corrosion cracking (ASCC) is cracking of carbon steel by aqueous amine solutions, which is primarily used to remove H_2S and CO_2 in the Amine recovery unit (ARU). ASCC is a form of alkaline stress corrosion cracking. The cracking is intergranular in otherwise ductile materials, without formation of large amounts of corrosion products. Amine stress corrosion cracks are usually found in carbon steel welds. The cracks typically run parallel to the weld (in the weld metal) roughly 5 mm from weld center in the heat affected zone. The best measure to prevent ASCC in carbon steel welds is through post-weld heat treating [10].

3.4.3 Polythionic acid cracking (PA-SCC)

Polythionic acid cracking (PA-SCC) is stress corrosion cracking that affects austenitic stainless steels by polythionic acids. Polythionic acids are straight chains of sulphur atoms with the chemical formula $H_2S_xO_y$. The acids are formed from the reaction between water/oxygen and the alloy sulphide scale. PA-SCC only occurs in austenitic stainless steels and Ni-Cr-Fe alloys that have been thermally sensitized. The sensitization normally arises when the alloy is slowly cooled between 400-815°C, for example during welding. During the sensitization the chromium reacts with the alloys carbon to form carbides. The carbides form adjacent to the grain boundaries, depleting areas close to the grain boundary of chromium. The depleted areas will no longer offer full corrosion resistance in aggressive environments and will act as initiation sites for PA-SCC. At the studied positions at Preem; austenitic stainless steels and Ni-Cr-Fe alloys are commonly used in equipment where there is a high risk for sulphide corrosion. For instance in the hydrotreating units Synsat and GHT, especially since the risk for sulphide corrosion increases in the presence of hydrogen. In the Synsat and GHT unit, as well as most units at Preem, there is neither oxygen nor excessive amounts of water present. Thus the acid

formation which causes PA-SCC is formed during stoppages when oxygen and water is provided through equipment cleaning. To prevent PA-SCC caustic solutions can be added during stoppages to neutralize the created acids [10].

3.5 Hydrogen Assisted Cracking (HAC)

Hydrogen has the ability to influence the mechanical integrity of a metal and making it more susceptible to cracking. In the petrochemical industry there are several environments which hydrogen can be introduced into the alloy, for example by gaseous hydrogen, water (vapour or liquid) or other hydrogen containing substances. Hydrogen assisted cracks are typically not very branched and can be either transgranular or intergranular. Fractures in materials where hydrogen propagates the crack generally doesn't experience much plastic deformation, and are thus considered brittle fractures.

The phase Hydrogen assisted cracking (HAC) is a loosely defined term and for the purpose of this report only include hydrogen damage relevant to the studied positions. The relevant hydrogen damage is believed to be hydrogen embrittlement (HE), wet H_2S cracking, hydrogen induced blistering and high temperature hydrogen attack (HTHA). There are several cracking phenomena's where hydrogen may play a role in the material degradation but corrosion processes are absent, these will not be considered in this report [12].

3.5.1 Hydrogen embrittlement

Hydrogen embrittlement can be considered the process where hydrogen degrades the fracture behavior of an alloy and makes it more brittle. Under certain conditions most structural alloys can be degraded by hydrogen. Hydrogen embrittlement occurs as a result of hydrogen introduced into the bulk of the alloy. During the application of a load the hydrogen migrates to regions of high stress in the alloy. Thus, the hydrogen is drawn to regions ahead of cracks and notches. The lattice becomes locally distorted by atomic hydrogen which restricts dislocation movement and lattice mobility causing embrittlement. The hydrogen embrittlement seriously reduce ductility (loss of tensile ductility), causes cracking (Hydrogen stress cracking) and catastrophic brittle failures at stresses below the normal yield stress of the exposed material. There are two ways, relevant to this study, in which atomic hydrogen can migrate to regions of high stress in an alloy where it does damage during loading:

a) Chemical absorption of the H_2
b) The cathodic side of a corrosion reaction

The two processes are described in figure 4a and 4b below.

Figure 4. ***a)*** *Cathodic corrosion and* ***b)*** *chemical absorption of* H_2

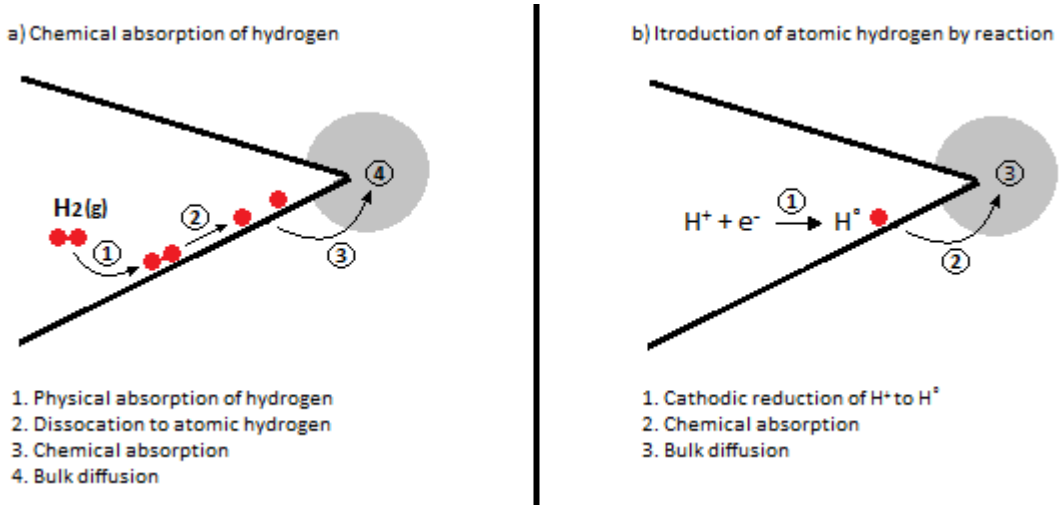

Generally speaking embrittlement increases with decreased strain rate and it decreases with increasing temperature. High-strength metals and alloys are more susceptible to embrittlement and it is likely to become a serious issue at yield strengths above 600-1000 MPa. Hydrogen embrittlement prevention techniques may for example include: minimizing hydrogen source in production or the use of lower strength type of materials at ambient conditions [11, 12].

3.5.2 Wet H_2S cracking

Corrosion of carbon and low alloy steels by aqueous hydrogen sulphide (H_2S), also known as wet H_2S corrosion in chapter 3.2.3, can result in hydrogen damage. Wet H_2S cracking is the result of hydrogen embrittlement caused by the corrosion reaction with H_2S in a aqueous environment. The types of hydrogen damage that can occur as a result of wet H_2S corrosion include sulphide stress cracking (SSC), hydrogen Induced cracking (HIC) and stress-oriented hydrogen induced cracking (SOHIC). Wet H_2S cracking is the interaction between mechanical forces and the cathodic corrosion reaction and should not be confused with stress-corrosion cracking which is related to the anodic reactions [10].

The wet H_2S corrosion reaction with steel in an aqueous H_2S environment is proposed in chapter 3.1.3. Besides consuming metal in the wet H_2S corrosion mechanism, the H_2S alters the hydrogen recombination process and forces hydrogen into the metal surface; causing hydrogen damage. The hydrogen damage is caused by atomic hydrogen evolving from the cathodic reaction on the metal surface (R19).

$$HS^- + e^- \rightarrow H^\circ + S^{2-} \qquad \text{(Cathodic reaction)} \qquad \text{(R19)}$$

When the corrosion rates of the wet H_2S reaction is high enough the concentration of atomic hydrogen (H°) builds up on the metal surface. The atomic hydrogen usually form H_2 at the metal surface, but sulphur alters the hydrogen recombination process and the amount of atomic hydrogen which recombines to form H_2 is greatly reduced, thereby increasing the amount of diffusion of atomic hydrogen into the metal matrix. The hydrogen atoms are small enough to penetrate the metal lattice and position themselves interstitially between metal atoms. There are two possibilities of H_2S induced hydrogen damage commonly recognized.

The lattice becomes locally distorted by atomic hydrogen which restricts dislocation movement and lattice mobility causing embrittlement. The embrittlement caused by atomic hydrogen leads to cracking, also known as Sulphide Stress Cracking (SSC).

The other possibility is that the atomic hydrogen atoms combine into molecular hydrogen (H_2) inside the metal creating voids inside the metal, commonly called hydrogen blistering. Cracks can occur from one blister to the next. The cracking between blisters can take place without externally applied stress, known as Hydrogen Induced Cracking (HIC), or with an applied stress, known as Stress Oriented Hydrogen Induced Cracking (SOHIC)

HIC, SOHIC and SSC hydrogen damage can occur throughout the refinery process units wherever there is an aqueous H_2S environment. For more information see process unit descriptions in chapter 4. The fractionator towers, fractionator's overhead drums, absorber column, stripper column, separators and knockout drums and connected heat exchangers are all prone to Wet H_2S cracking. Sour water stripper overhead systems are especially prone to Wet H_2S corrosion. Generally, the susceptibility of Wet H_2S corrosion will increase if cyanides are also present. Amine regenerator's overhead systems are also prone to Wet H_2S cracking. In hydroprocessing units increasing concentration of ammonium bisulphide increases the potential for blistering and HIC. Acid gas rich amine flash drum is also vulnerable for severe hydrogen blistering [11]. The main parameters affecting the hydrogen flux are pH, temperature and other contaminants such as cyanides, ammonium or chlorides.

3.5.2.1 Sulphide stress cracking (SSC)

Sulphide stress cracking is a type of cracking due to hydrogen embrittlement caused by penetration of atomic hydrogen. Atomic hydrogen atoms are small enough to penetrate the metal lattice and position themselves interstitially between metal atoms which restricts dislocation movement and lattice mobility; causing embrittlement. SSC is most likely to occur in high strength steels or in weld deposits or hard heat affected zones of welds in lower strength materials. SSC is typically intergranular with little branching [9, 10].

The susceptibility to SSC depends on the amount of atomic hydrogen penetrating the material, which is equivalent to the hydrogen flux from the cathodic reaction R3. The hydrogen flux is consequently related to the wet H_2S corrosion rate. The corrosion rate will increase both as the pH increases and as the pH decreases from this near neutral range, as mentioned in chapter 3.2.3. A very low pH will increase the amount of dissolved H_2S in the water while a very high pH will favor bisulphide (HS^-) in dissociation. Both an increase in H_2S concentration or bisulphide concentration will increase wet H_2S corrosion rates and thusly the possibility of SSC. Higher temperature will increase corrosion rates by increasing diffusion and reaction rates. Generally, the lowest rates in steels typically results from corrosion in near natural pH solutions (pH 5.5-7.5) [11].

3.5.2.2 Blistering and Hydrogen Induced Cracking (HIC) or Stress Oriented HIC (SOHIC)

Hydrogen blisters are subsurface planar cavities that from inside a metal. The blisters are the outcome of excessive internal pressure created as the atomic hydrogen (H°) formed in the cathodic reaction of wet H_2S corrosion (R3) combine into molecular hydrogen (H_2). The Blisters are located near the surface in low- strength metals and can produce visible surface bulges.

Hydrogen blistering can occur when atomic hydrogen (H˚) enters an alloy. Similar to hydrogen embrittlement the source of atomic hydrogen is the reduction reaction on a metal, i.e. the cathode side of a corrosion reaction, or by dissociative chemical adsorption of H_2 as shown in figure 5 (left). The hydrogen evolution occurs on the metal surface that is exposed to the acidic electrolyte or gaseous H_2 [2, 3]. Atomic hydrogen is small enough to diffuse through the metal lattice, and if the corrosion rate is sufficient some of the produced atomic hydrogen will migrate into the metal. The atomic hydrogen diffuses through the metal until they meet with another atomic hydrogen atom, usually at inclusions or voids in the alloy, to form molecular hydrogen gas (H_2). Hydrogen molecules, unlike atomic hydrogen atoms (H˚), are typically too big to migrate and become trapped within the metal, creating a hydrogen blister. As shown in figure 6 (right).

Figure 5. *Effect of molecule size on metal migration*

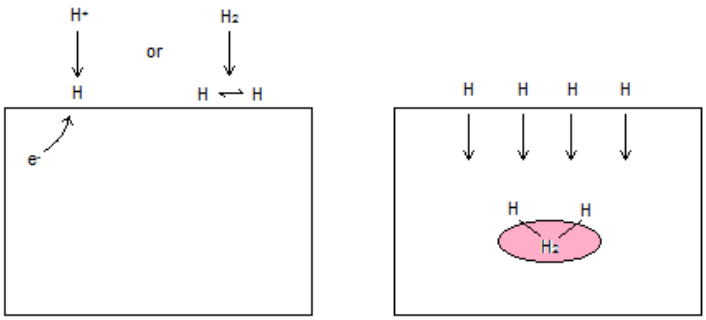

The accumulation of molecular hydrogen inside the metal voids will lead to build-up of internal pressure, which will produce high local stresses at the blister circumference. When the circumference stresses get high enough cracks will initiate from the blister wall. Hydrogen blistering is controlled by the source of hydrogen by reducing hydrogen supply or minimizing acidic environments that leads to corrosion. Since atomic hydrogen combine around inclusions and defects, hydrogen blistering is generally not a problem in high-quality steels that have low impurity and inclusion levels. Blistering is most prevalent in low-strength steels, where the blisters may even appear as visible surface bulges [3, 1].

Hydrogen Induced Cracking (HIC) is defined as stepwise internal cracking that connects adjacent hydrogen blisters. No externally applied stress is needed for the formation of HIC. Areas of high localized stress form around the blisters caused by the blisters high internal pressure. Interactions between the high stress areas causes cracks to develop between blisters. In steel the cracks are usually stepwise and parallel to the surface [10]. Stress Oriented Hydrogen Induced Cracking (SOHIC) is stepwise linking of blisters initiated by an applied external stress. In the presence of external stress the crack can propagate across the thickness of the steel and generally causes transgranular cracks. HIC nor SOHIC will occur without the presence of water. In carbon steels, if the partial pressure of H2S > 3.5mbar the risk of HIC should be considered. [11]

4. Coupon degradation mechanisms

An oil refinery is an advanced industrial process plant where crude oil is processed into more valuable petroleum products. In reality the process flow is very complex with extensive piping running throughout and between different process units. Extensive explanation of the process flow and all the process units from crude to product falls beyond the scope of this report. However a schematic description can be found in chapter *4.1*.

A detailed account of individual positions and the explicit environment surrounding each of the 22 coupons can be found chapters *4.2.1* to *4.2.5*. To convert the retrieved data from the coupons into information more useful for a large refinery each coupon has been allocated to a corrosion loop. The concept of corrosion loops is described in chapter *2.3*. For every corrosion loop a hypothesis regarding degradation mode is presented. The validity of the proposed hypothesis will be evaluated in the results of this report, chapter *6*.

4.1 General process description

Figure 6 is a schematic simplification of the process flow from crude oil to product at Preem Refinery Gothenburg. Figure 8 focuses on the process flow of the middle distillates since it involve the process units where the sampled coupons are located. As mentioned above the process units concerned in this study are ARU (9), Synsat (15), GHT (16), Common (17) and SRU (27-29). The boxes representing these units are highlighted red. The final products are characterized as blue boxes with blue text; this signifies the final product that is eventually created downstream the process flow.

Figure 6. *General process description*

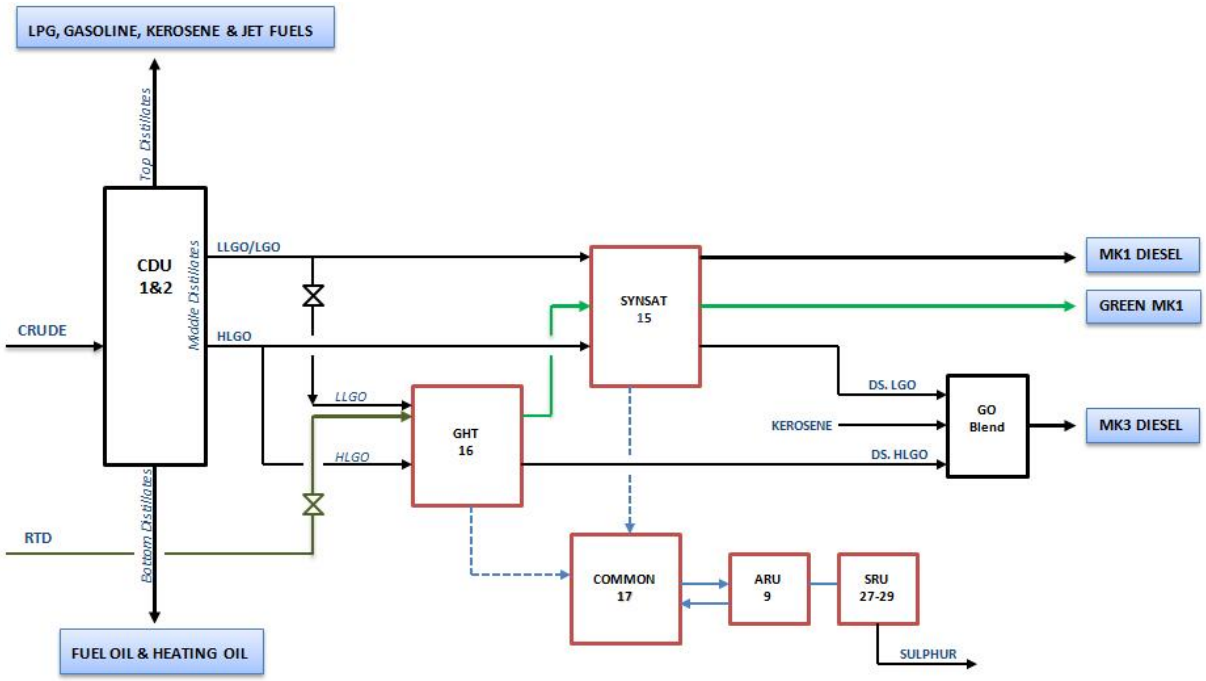

Desalted and preheated crude oil is fed to the Crude Distillation Units (CDU). The CDU's principal function is to separate the hydrocarbons through fractional distillation. The crude is heated to boiling

and the vapour is sent through the CDU fractionation columns where it is separated into different fractions depending on boiling range. The heavier fractions are condensed on the lower trays of the fractionation columns while the lighter fractions are condensed higher up.

The lower boiling point hydrocarbons stream is labelled Top Distillates and have a hydrocarbon length of about C_1 to C_{12} with an approximate boiling point below 220°C (at atmospheric pressure). The stream also includes the low molecular weight non-hydrocarbons within the same boiling range. The top distillates will progress through a series of process steps to eventually produce a range of products, primarily liquefied petroleum gas (LPG), gasoline and kerosene.

The bottom distillates are hydrocarbons longer than C_{18} and with an approximate boiling point above 300°C. The bottom distillates together with heavier fractions recovered downstream the process will mainly be used to produce fuel oil and heating oil.

The middle distillates in contain hydrocarbons with carbon chain lengths roughly between C_{12} to C_{18} with an approximate boiling point range between 200°C to 365°C. The middle distillate can be divided into two cuts: A straight Light Gasoil cut (LGO) or a light- and heavy cut of the light gas oil (LLGO and HLGO respectively).

The straight Light Gasoil (LGO) cut contains hydrocarbons that cover the entire boiling point range of the middle distillates. The light cut of LGO (LLGO) is retrieved higher up in the fractionation column than straight LGO and can be described as the light end of a straight LGO cut plus the heavy end of the kerosene cut. The heavy cut of LGO (HLGO) contains a mixture of the higher boiling point hydrocarbons of the middle distillates. HLGO is retrieved further down in the fractionation columns and has a higher amount of long hydrocarbons compared to straight LGO.

The choice of cut is made batch-wise and is determined by the quantity and quality of the product you want to produce. The middle distillates are mainly used to produce three types of diesels: Swedish environmental class 1 (MK1), Euro diesel (MK3) and the Green environmental class 1 (Green MK1) containing processed Raw Tall Diesel (RTD).

To produce MK1 diesel LLGO is fed from the CDU straight to the Synsat unit which function is primarily to convert unsaturated hydrocarbons, reduce aromatics and remove sulphur through hydrogenation. The resulting product is a diesel with MK1 quality.

In Green mode: LLGO is mixed with Raw Tall Diesel (RTD), approximately 70% LLGO with 30% RTD, and fed to the GHT unit. More details on RTD can be found under the GHT unit description *4.2.3*. The GHT has essentially two functions. To convert the fatty acids and resin acid from the RTD into hydrocarbons and to remove sulphur, nitrogen and oxygen. The resulting GHT-downstream product is fed to the Synsat unit to produce the final product Green MK1.

To produce MK3 diesel several options are available, HLGO can be fed straight through Synsat to produce a desulphurized HLGO (DS. HLGO). Similarly a straight LGO cut can be fed to the Synsat unit to produce a desulphurized LGO (DS. LGO). Another option is to feed HLGO to the GHT unit to produce a lighter desulphurized product (DS. HLGO). The downstream products are then blended with kerosene and other components to produce a product with Euro diesel quality.

For simplicity the processing of the middle distillates can be divided into three separate operations: Separation of fractions (CDU), quality improvement of distillates (Synsat and GHT) and purging of generated residual gas/liquid stream (Common, ARU and SRU).

Fractions of the gaseous streams generated in the Synsat and GHT unit need purging before being redistributed. The Common unit remove primarily dissolved ammonia (NH_3) and hydrogen sulphide (H_2S) from the generated sour water. The ARU remove H_2S, CO_2, CO_S, mercaptans and other organic sulphur compounds from gases and light hydrocarbon liquids. The SRU is used to recover sulphur from the acidic gases generated in the ARU and Common unit. Recovery of sulphur is achieved by converting H_2S to elemental sulphur.

As previously mentioned the sampled weight loss coupons can be found on five different process units ARU (9), Synsat (15), GHT (16), Common (17) and SRU (27). The process unit descriptions contains: a simple explanation of unit function, the position of coupon marked in a unit schematic, the colour coded corrosion loops marked in the same unit schematic and a table of relevant stream properties approximated at coupon position. The stream properties are estimated from: results from previously performed simulations, reclaimed analysis results from previous samples taken adjacent to the position and personal approximations of probable properties at the site. Further explanation of simulations, sample results and approximations used to compile the stream properties tables can be found in Appendix B.

The precise values of some constituents presented in the stream estimation tables are unknown. These are estimated by the level of effect they have on the potential degradation of material. If an amount of a constituent in the table is denoted as Very high, the amount is such that the effect it has on the probable degradation rate and degradation mode is assessed as very high. The levels are Very high, High, Moderate, Low and Very low. Further, in many condensed streams the pH level is unknown. The pH is assessed from the stream table data and is represented by how much it deviates from neutral pH.

For every coupon position a set of proposed corrosion mechanisms is presented. These are deduced from the prevailing refining corrosion mechanisms (Chapter 3) and the tabled stream properties for each corrosion loop.

4.2 ARU - Amine regeneration unit (9)

The function of an ARU is to remove mainly H_2S, CO_2 but also COS, mercaptans and other organic sulphur compounds from gases and light hydrocarbon liquids. This is achieved through absorption of H_2S, CO_2 rich gas (i.e. acid gas) in methyldiethanolamine (MDEA) in an absorber column. The treated gas passes over top while the bottom H_2S, CO_2 rich amine solvent is passed to a regenerator, which is essentially a column with trays. In the regenerator MDEA is recovered while the H_2S, CO_2 rich gas is sent to the Sulphur recovery unit (SRU). The ARU has only one coupon installed, 9CC-1, located in the regenerator overhead.

4.2.1 ARU regenerator

The acid rich amine enters the regenerator at the top. The acid gas is heated by an up-flowing current of steam and stripped of the MDEA. The stripped MDEA is retrieved at the bottom of the

regenerator column and circulated back to the absorbers. The overhead vapour is sent through an air-cooled condenser to an overhead reflux drum. The condensed water is sent back to the regenerator while the acid gas is sent to the SRU for further treatment. Figure 7 is a part of a unit schematic demonstrating the regenerator and overhead system described above.

Figure 7. *ARU Regenerator*

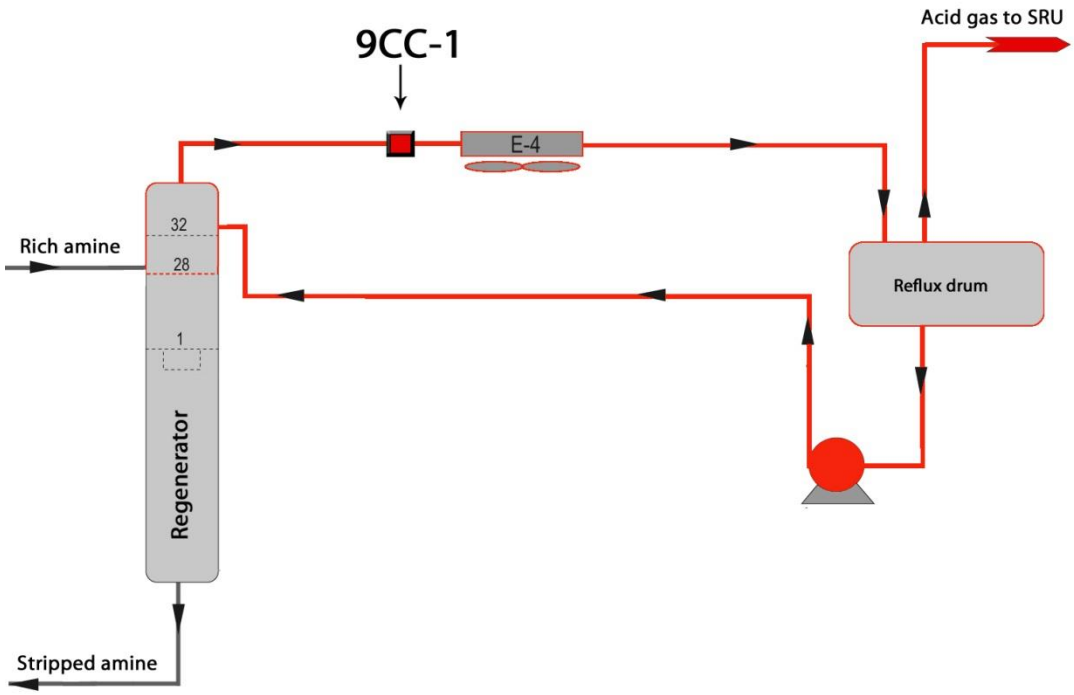

The ARU has one coupon 9CC-1 positioned in the top vapour stream prior to the overhead condenser E-4. The unit has only one corrosion loop, marked red in Figure 7, stretching from the top part of the regenerator past the condenser and reflux drum and downstream to the SRU.

4.2.1.1 Coupon 9CC-1

The top generated vapour from the regenerator column consists of acid gases, water, saturated steam and residual hydrocarbons. The precise composition of the overhead stream passing 9CC-1 is not known since there is no possibility of taking a regular sample at the position due to the toxicity of the gases. The vapour composition was therefore estimated from simulations, old sampling and gauges available at the site. The estimated conditions in the 9CC-1 stream are presented below in Table 3. The remarks presented in Table 3 are explained in Appendix B.

Table 3. *Process conditions coupon 9CC-1*

Stream properties	Estimated value	Remarks
Rate [kg/h]	11525	Design rate from simulation 1996 around a point in regenerator overhead stream
Phase	Vapour	Almost exclusively water and acid gas (H_2S + CO_2)
Temperature [°C]	120	Temperature gauge on regenerator outlet
Pressure [barg]	0.2	Pressure gauge on regenerator outlet
Water [wt]	59.2%	Estimated from amine regenerator design
H_2S [wt]	22.9%	Composition calculated from single sample taken on top outlet stream from reflux drum in 2010. Assumed 100% water in bottom stream from reflux drum. Rate known from simulation 2010, amount of water calculated backwards using material balance.
Ammonia [wt]	None	
Chlorides [wt]	Low	
CO_2 / CO [wt]	17.0% / < 1.0%	
pH	Fairly low	Assumed. Referring to the first condensed water. Assuming pK_a, of H_2S(aq) is approximately 7 then pH should be around pH≈4.

4.2.1.2 Proposed dominating corrosion mechanisms for coupon 9CC-1

The proposed dominating corrosion mechanisms are assumed to be similar throughout the corrosion loop marked in red in Figure 7 above.

- ✓ Wet H_2S corrosion
- ✓ Wet H_2S cracking including: Sulphide stress cracking (SSC), Hydrogen blistering and Hydrogen-induced cracking (HIC)/Stress-oriented hydrogen-induced cracking (SOHIC)
- ✓ Amine stress corrosion cracking (ASCC)
- ✓ CO_2 corrosion

4.3 Synsat unit (15)

The Synsat unit operates in two modes; to produce ultra-low sulphur and low aromatics MK1 and to produce low sulphur Euro diesel. The unit is characterized by two main reactors; a hydrodesulphurisation reactor (HDS) to remove sulphur as H_2S. Besides hydrodesulphurisation, hydrogenation of nitrogen and trace oxygen compounds also occurs in the HDS. The second reactor is a hydrodearomatization reactor (HDA) for removal of aromatics which saturates unsaturated hydrocarbons. Both reactors, HDS and HDA, use a reaction with hydrogen on catalyst at high temperature and pressure. Following the HDS and HDA reactors is a series of separation steps operating at different temperature and pressure that removes gases from the product stream. A diesel stripper strips the last dissolved gases and light hydrocarbons from the diesel before it's dried to final product. For simplicity the Synsat unit will be split into two parts; the initial part involving

reactors and effluent separation *4.4.1* and the final part involving the diesel stripper *4.4.2*. The Synsat unit has a total of four coupons installed in two different positions 15CC-2 A&B and 15CC-9 A&B.

4.3.1 HDS & HDA reactors and effluent separation

The schematic Figure 8 describes the initial part of the Synsat unit which contains coupons 15CC-2 A&B and the corrosion loops surrounding them. The feedstock to the HDS comes either from crude distiller, upstream units or storage. The feedstock is combined with hydrogen and fed to the HDS reactor. The gaseous (rich in H_2S & NH_3) is stripped from the liquid HDS reactor outlet stream (low in sulphur). One part of the stripped effluent is sent to the HDA reactor while the rest of the liquid stream is sent downstream to the diesel stripper. Both the HDS and the HDA reactor use hydrogenation to fulfil their function which requires a hydrogen supply. If the Synsat unit operates under MK3-mode, all liquid is sent downstream without entering the HDA reactor. If the Synsat unit operates under MK1-mode, the bottom product from the HDA reactor is sent downstream to a diesel stripper while the top effluent is mixed with the gaseous stream from middle stripper and sent to a hot high pressure separator (HHPS). The bottom stream from the HHP is sent downstream to a diesel stripper. The top stream from the HHPS is usually over the dew point at normal operations, to avoid salt deposition wash water is injected prior to entering the air cooler E-9. The hydrogen-rich gas from HHPS is separated from the liquids in the cold high pressure separator (CHPS) and sent to an amine absorber unit for hydrogen recovery and H_2S removal. The hydrocarbon liquid from CHPS is sent together with the liquids from stripper, HDA and HHPS downstream to the diesel stripper. The water, identified as sour water, is sent to the Common unit.

Figure 8. *HDS&HDA reactors and effluent separation*

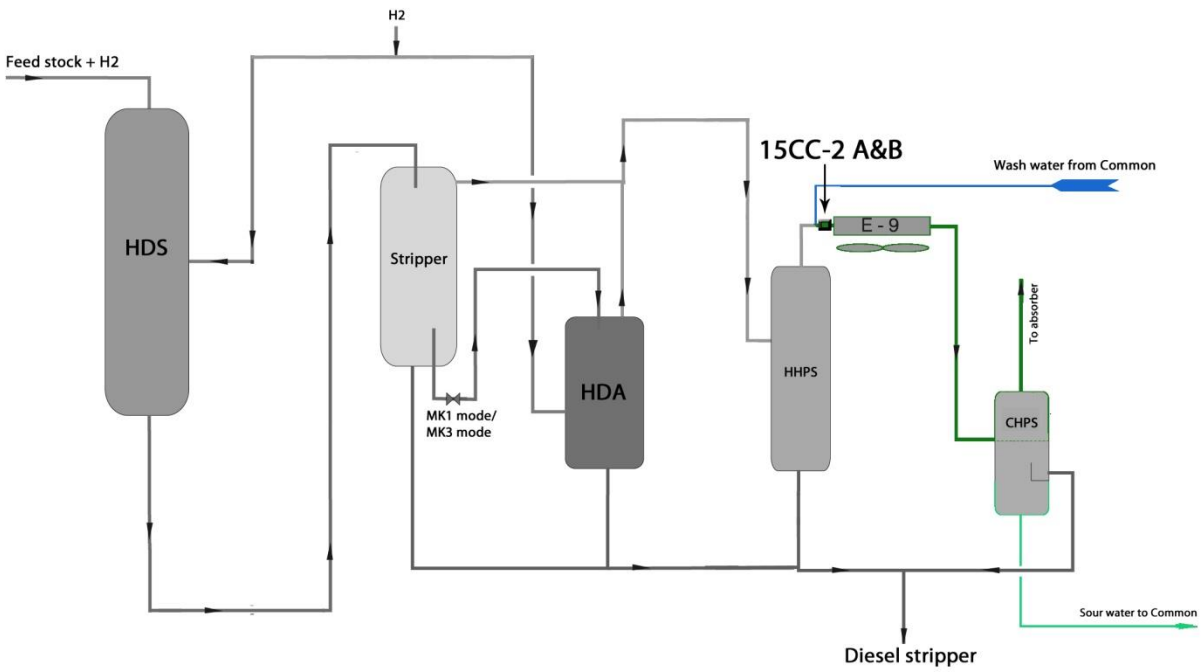

Figure 8 incorporates three corrosion loops: One blue entering from the Common unit, one turquoise leaving to the Common unit and one green. The green corrosion loop contains coupon sample 15CC-2 A&B which stretches from the wash water injection point before the tube condenser E-9 to the top part of the cold high pressure separator.

4.3.1.1 Coupons 15CC-2 A&B

Coupons 15CC-2 A & B are located in the overhead stream from the HHPS, after the water injection point. From the HHPS reactor top stream is expected to contain H_2, H_2S, NH_3, HCl, water and light saturated hydrocarbons from the reactions with hydrogen in the HDA and HDS. Wash water is continuously injected ahead of the tube condensers to force the water dew point, scrub chlorides out of the effluent hydrocarbon liquid/vapour stream, and dilute the salts and ammonium bisulphide plugging in the resulting condensate water. The tube condenser cools the reactor effluent well below dew point before it is sent to the cold high pressure separator. Most of the NH_3 entering CHPS is expected to have been removed from the gas phase with the sour water. The precise composition of the overhead stream passing 15CC-2 A&B is not known since there is no possibility of taking a regular sample at the position. Therefore the composition was estimated from a simulation made in 1994, available gauges and assumptions presented in Appendix B. The difference between compositions when operating in MK1-mode/MK3-mode is small. The HDA reactor produces an increased amount of light hydrocarbons in MK1-mode mode, but the produced hydrocarbons are considered irrelevant in a degradation rate and/or degradation mode perspective. All streams downstream the water injection point before 15CC-8 A&B will only be considered in Euro diesel-mode. The estimated conditions, when Synsat is in Euro diesel-mode, at 15CC-2 A&B positions are presented below in table 4.

Table 4. *Process conditions coupons 15CC-2 A&B*

Stream properties	**Estimated value**	**Remarks**
Rate [kg/h]	20948	Total rate, Inlet E-9. Calculated from simulation 1994
Phase	Mixed	After approx 100 m^3/day cold wash water feed
Temperature [°C]	107	Calculated from simulation 1994
Pressure [barg]	57	Pressure gauge outlet HHP
Water [wt]	31.2%	Calculated from simulation 1994
H_2S [wt]	12.3%	Calculated from simulation 1994
Ammonia [wt]	0.2%	Calculated from simulation 1994
Chlorides [wt]	Moderate amount	Assumed. Most water and HCl is passed over top from HHPS
CO_2 / CO [wt]	Low	CO_2 & CO passes over top from HHPS
pH	Unknown	CO_2 & H_2S content high but also high amount of NH_3 The amount of NH_3 may be enough to neutralize HCl with the result that very low pH is avoided in aqueous phase

4.3.1.2 Proposed dominating corrosion mechanisms for coupons 15CC-2 A&B

The proposed dominating corrosion mechanisms are assumed to be similar throughout the corrosion loop marked in green in Figure 8 above.

- ✓ Wet H_2S corrosion
- ✓ Wet H_2S cracking including; Hydrogen blistering, HIC, SOHIC and SSC
- ✓ NH_4Cl corrosion
- ✓ HCl corrosion

4.3.2 Diesel stripper

Figure 9 below describes the diesel stripper mentioned above, which incorporates coupons 15CC-9 A&B and the corrosion loops surrounding them. The liquid from Synsat reactor area is depressurised before it's fed to the diesel stripper. The lower pressure and steam stripping flashes out most of the remaining light end components, such as LPG, together with virtually all of the H_2S, NH_3, HCl, and water. The lower pressure condensate is sent downstream to end up as final MK1 or Euro diesel/MK3 product. The overhead vapours are condensed in an air cooled condenser E-12 prior to entering the overhead drum (O/H Drum). Wash water is injected before the condenser E-12. The O/H drum separates liquid hydrocarbons, sour water and non-condensable vapours. The sour water and non-condensable vapours are sent to the Common unit while the liquid hydrocarbons are passed back to the diesel stripper.

Figure 9. *Diesel stripper*

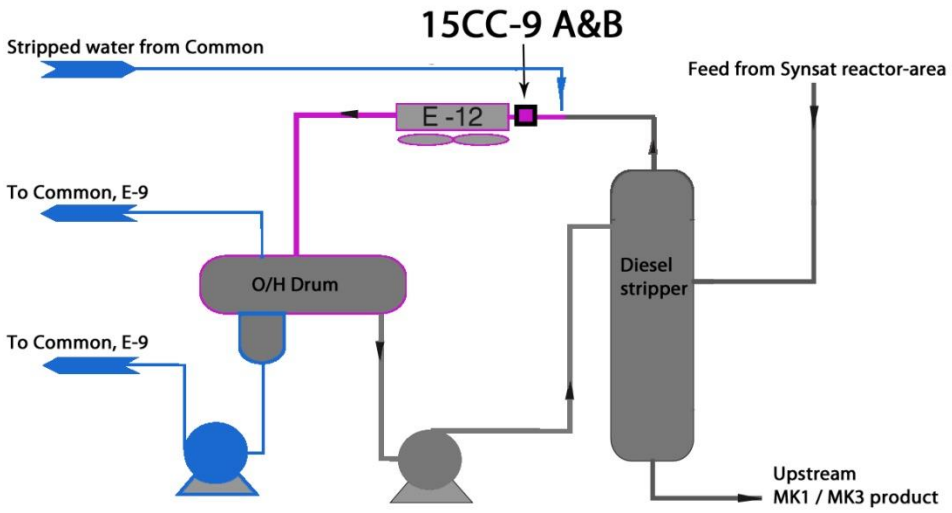

Figure 9 incorporates two corrosion loops: One blue leaving to the Common unit from the O/H drum and entering from Common unit and one purple. The purple corrosion loop have coupon 15CC-2 A&B in it and stretches from the wash water injection point before the tube condenser E-12 to the top part of overhead drum (O/H drum).

4.3.2.1 Coupons 15CC-9 A&B

Coupons 15CC-9 A & B are located in the top stream from the diesel stripper, after the water injection point. The diesel stripper top stream is expected to contain light hydrocarbons, H_2S, NH_3, HCl, and large amounts of water. A small amount of additional wash water is injected before the

condenser E-12 to avoid salt deposition as discussed before in this chapter. As before the precise composition of the overhead stream at sample 15CC-9 A&B is not known since there is no possibility of taking a sample at the position. The composition was therefore estimated from a simulation made in connection with the construction of the unit 1994 and assumptions explained in Appendix B. The estimated conditions at 15CC-9 A&B positions are presented below in Table 5. As mentioned in *4.3.1.1* the difference between compositions when operating in MK1-mode/MK3-mode is small and assumed the same. The conditions presented in Table 5 are when Synsat is in MK3-mode.

Table 5. *Process condition coupons 15CC-9 A&B*

Stream properties	Estimated value	Remarks
Rate [kg/h]	21750	Total rate, Inlet 15E-12. Calculated from simulation 1994
Phase	Mixed	After approx. 25 m^3/day cold water feed
Temperature [°C]	107	Estimating a 5% drop in temperature after 25 m^3/day cold water feed
Pressure [barg]	57	Pressure gauge top of diesel stripper
Water [wt]	33.9%	After approx. 25 m3/day cold water feed (approx. 1042 kg/h)
H_2S [wt]	2.2%	From simulation 1994
Ammonia [wt]	300ppm	From simulation 1994
Chlorides [wt]	Low	Assuming most CO_2, CO removed from product flow in HHPS. Less than 2 mg/l chlorides added with water injection.
CO_2 / CO [wt]	Low	
pH	Moderately low	Assumed based on H2S, CO_2 and Chloride content with low amount of NH_3

4.3.2.2 Proposed dominating corrosion mechanisms for coupon 15CC-9 A&B

The proposed dominating corrosion mechanisms are assumed to be similar in throughout the corrosion loop marked in purple in Figure 9 above.

- ✓ Wet H_2S corrosion
- ✓ Hydrogen blistering including; HIC, SOHIC and SSC
- ✓ NH_4Cl corrosion
- ✓ HCl corrosion

4.4 GHT - Green hydrotreating unit (16)

In 2010 Preem refinery Gothenburg converted their Mild Hydrocracker unit (MHC) into a Green hydrotreater unit (GHT). Traditionally the MHC was used to hydrotreat a feed of Heavy-Light GasOil

(HLGO). The revamp to GHT was done to be able to hydrotreat two different feeds. One feed consisting of conventional HLGO and another consisting of Light-Light GasOil (LLGO) and Raw Tall Diesel (RTD). The purpose of using RTD is to produce a final product with the same amount of energy that has lower net emissions than most other green diesel blends. The environmental advantage of RTD is explained further in *4.4.1* below. When LLGO + RTD feed is hydrotreated in the GHT unit the main objective is to remove sulphur, oxygen, nitrogen and produce a GHT-product with low TAN number. The GHT-product is then sent to Synsat unit for dearomatization to produce Green MK1. When a HLGO feed is hydrotreated in the GHT unit the main objective is to remove sulphur, oxygen, nitrogen and produce a lighter higher converted downstream HLGO. The downstream HLGO is used as a component in MK3 diesels. For more detailed explanation of the hydrotreating process see *4.5.2*. The GHT has thus two modes depending on feed to the reactor; "Green mode" when RTD + LLGO + H_2 feed is used and "Fossil mode" when HLGO + H_2 feed is used.

The feedstock, LLGO or HLGO, is mixed with hydrogen rich gas and heated under high pressure. If in Green mode the RTD is mixed with the feedstock/gas blend. The hot oil/gas mixture is fed to the reactor, where through a series of active beds of catalyst, the sulphur and oxygen containing components are converted. After the reactor the effluent is cooled and sent to the separation system. In the separation system the gas is removed from the diesel in a series of separators and a steam stripper. For simplicity the GHT unit description will be split in two parts, GHT reactor *4.4.2* and Separation and steam stripper *4.4.3*.

4.4.1 Raw Tall Diesel

The paper and pulp industry produces some 2% of a waste product called raw tall oil (RTO). The RTO is processed to Raw Tall Diesel (RTD) at Sunpine, a factory part owned by Preem and located at Piteå. The Raw Tall Diesel (RTD) produced at Sunpine consist of fatty acids (predominantly oleic and linoleic acids), resin acids and FAME. RTD is a product from the forest industry it is considered a renewable source of energy. By using a renewable source the net total of CO_2 emissions can be reduced.

RTD has a high concentration of straight chain C16-C20 molecules, which makes it ideal as for production of diesel. However, oxygen and sulphur has to be removed before it can be used as standard diesel. The RTD is therefore transported to the Gothenburg refinery, where it is further treated in the GHT unit.

Most recent studies suggest that the FAME decomposes at the high pressure and high temperature present in the GHT reaction [23]. This is extra relevant since the reactor can be run in "Green mode" with other oxygen-containing imported feeds than RTD, for example tallow methyl esters (TME). TME and other products produced by transesterification of animalistic oils contain almost exclusively FAME.

4.4.2 GHT reactor

The GHT reactor is a 60 meter high vessel with four beds of solid catalyst, illustrated in Figure 10. The GHT reactor has six coupons, 16CC-10 A through F, installed in the top reactor inlet. The GHT reactor uses the function of hydrogenation to remove oxygen, sulphur and to reduce the amount of unsaturated hydrocarbons. The hydrogenation is done by using hydrogen gas. The chemical reactions occurring in the reactor are exothermic. Consequently the temperature will increase down through

the reactor. Uncontrolled temperature profile can cause increased catalyst deactivation rate by coking, fouling and other types of deactivation. Thus it's important to control the outlet temperature between each bed in the reactor, especially in reactions with RTD since they release large amounts of energy. As mentioned in the introduction the reactor can be run in two different modes; "Green mode" and "Fossil mode". The reactor effluent from both modes is sent downstream for gas separation and steam stripping.

In "Green mode" LLGO mixed with hydrogen rich gas is heated before sent towards the reactor, as illustrated in Figure 10 (feedstock + H_2). The hot LLGO/gas mix is blended with RTD prior to entering the GHT reactor. The RTD feed is split in two; half the RTD is mixed with the LLGO/gas feed and sent into top of reactor while the other half is mixed with hydrogen and used as quench between bed 1 and 2. The second RTD injection between bed 1 and 2 cools down the oil leaving bed 1 and spreads out the heat release over two beds instead of one. Note that the second RTD inlet further down in the reactor is not mixed with LLGO prior to entering the reactor. The reason for adding RTD separately is to control the temperature profile and avoid corrosion problems in the top inlet, furnace and piping upstream the reactor. In other words more RTD can be fed to reactor if the feed is split as this will result in less corrosion and operative problems. As mentioned the GHT reactor has primarily three functions; remove oxygen, remove sulphur and reduce the amount of unsaturated hydrocarbons. The removal of oxygen in the RTD is very fast, thus all the RTD entering the reactor will primarily be converted in beds 1 and 2. As mentioned above RTD contains large amounts of oxygen in the form of fatty acids, resin acids and FAME. In this report it will be assumed that all FAME present will decompose to fatty acids due to high pressure and temperature. The preheated feed/gas mixture enters the reactor and reacts with hydrogen over the catalyst bed, the oxygen containing compounds (fatty acid and resin acid) react according to the unbalanced proposed reactions R1 to R4 below.

$$Unsaturated\ fatty\ acid + Hydrogen \xrightarrow{hydrodeoxygenation} Paraffins + H_2O \qquad \text{(R20)}$$

$$Unsaturated\ fatty\ acid + Hydrogen \xrightarrow{decarboxylation} Paraffins + CO_2 \qquad \text{(R21)}$$

$$Resin\ acid + Hydrogen \xrightarrow{hydrodeoxygenation} Unsaturated\ hydrocarbon + H_2O \qquad \text{(R22)}$$

$$Resin\ acid + Hydrogen \xrightarrow{decarboxylation} Unsaturated\ hydrocarbon + CO_2 \qquad \text{(R23)}$$

As proposed by reaction R1 to R4 larger amounts, than normal for the HDS unit, of CO_2 and water can be expected downstream bed 1 and 2 due to the oxygen-containing compounds in the RTD feed. The reactions that remove sulphur, nitrogen, chlorides and saturates hydrocarbons occurs in beds all beds. Similar to the Synsat unit sulphur, nitrogen and chlorides will be removed by hydrotreating to produce NH_3, H_2S, HCl and hydrocarbons. Some saturation of hydrocarbons also occurs on the expense of hydrogen. As illustrated in Figure 10 the hydrogen to the reactor is provided as quench gas between the remaining catalyst beds below bed 1 and 2, to control the temperature profile.

When the reactor operates in "Fossil mode" the feedstock is HLGO and no RTD is mixed into the reactor feed. Schematically, the three point valve in is closed. Hydrotreating HLGO works in a similar fashion; the reactor reduces the amount of unsaturated hydrocarbons and removes sulphur, nitrogen and chlorides. The difference between "Green mode" and "Fossil mode" is that HLGO enters

the reactor as primarily hydrocarbons and thus contains way less oxygen-compounds. Consequently one can expect very low oxygen-compound conversion and therefore almost no CO, CO_2 and water in the reactor effluent. Notice also that in “Fossil mode” only the top injection point to the reactor is in use.

Figure 10. GHT Reactor

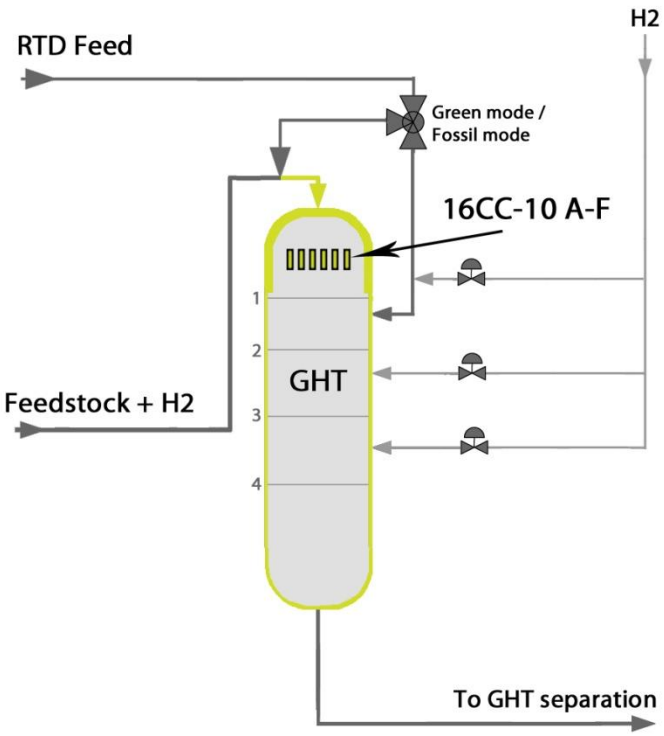

In the top part of the RTD reactor there are a total of six coupons installed, 16CC-10 A to F, in one corrosion loop. The corrosion loop incorporates the entire reactor, from the RTD/LLGO mixing point to the reactor outlet.

4.4.2.1 Coupons 16CC-10 A to F

The six coupons 16CC-10 A, B, C, D, F are located in the top inlet to the GHT reactor, illustrated as thin yellow rectangles with a black edge in Figure 10. The coupons are oriented in a circular fashion, mounted by brackets, on the inside of the reactor top inlet pipe. As mentioned above the reactor can be run in two different modes: "Green mode" and "Fossil mode". Depending on mode the coupons will experience different environments.

In “Green mode” different amounts of RTD can be mixed into the LLGO in the top mixing point. Due to final product specifications the maximum reactor top inlet feed consists of 30% RTD. By assuming that the material degradation rate inside the reactor will increases with increased supply of RTD, “Green mode” will be studied at a 30% wt. RTD supply. To make it easier for future work and to be able to estimate RTD impact on total reactor top feed, an estimated composition of LLGO+H2 and RTD feeds are presented in Appendix B. The LLGO+H2 feed composition was estimated from a simulation made in 2010 and the RTD feed composition was estimated from a typical import specification from 2011.

In “Green mode” 30% wt. RTD is mixed into the LLGO+H2 and fed to the top inlet. The top inlet can be expected to contain hydrocarbons, H_2, fatty acids, resin acid and some water vapour with trace amounts of chlorides. No H_2S, CO, CO_2, and NH_3 can be expected in the top inlet. Note that HCl, H_2S, CO, CO_2, and NH_3 will be present further down in the reactor however that will not affect the coupons. There is no possibility of taking a sample at the position, so the composition was calculated from data given in Appendix B, around the top mixing point using 30% RTD. The estimated properties surrounding coupons 16CC-10 A to F, when the reactor operates in “Green mode”, are presented in Table 6 below.

In "Fossil mode" the reactor top inlet stream is likely to contain HLGO, H_2 and some water vapour with trace amounts of Chlorides. No H_2S, CO, CO_2, and NH_3 can be expected in the top inlet. There is no possibility of taking a sample at the position, so the composition was estimated from a simulation made in 2009. The degradation rate of the reactor material will be due to high-temperature degradation modes. Using the assumption that no H_2S, CO, CO_2, and NH_3 is present; only rate, temperature, pressure, hydrogen content, water content and chloride content of the reactor top inlet feed are presented in Table 6 below. The ground for Table 6 is presented in appendix B.

Table 6. *Process condition coupons 16CC-10 A-F*

Stream properties	**Fossil mode**	**Green Mode (30% RTD)**
Rate [kg/h]	54900	*
Phase	Mixed	*
Temperature [°C]	326	*
Pressure [barg]	64	*
Water [wt]	300ppm	*
H_2 [wt]	0.2%	*
Chlorides [wt]	traces	*
Fatty acids [wt]	-	*
Resin acid [wt]	-	*

**Considered classified and will not be published in this report*

4.4.2.2 Proposed dominating corrosion mechanisms for coupon 16CC-10 A-F

The proposed dominating corrosion mechanisms are assumed to be similar in throughout the corrosion loop marked in yellow in Figure 10 above.

- ✓ Fatty acid corrosion (at high temperature and pressure)
- ✓ Hydrogen embrittlement
- ✓ High Temperature Hydrogen Attack (HTHA)
- ✓ PTA-SCC of austenitic stainless steel components during shutdowns
- ✓ Cl-SCC of austenitic stainless steels during start-up

4.4.3 Separation and diesel stripper

Figure 11 below describes the separation of gas and contaminants in the GHT reactor effluent from the diesel. The separation and diesel stripper incorporates coupons 16CC-2 A&B and 16CC-8 A&B. The reactor effluent from the GHT reactor is sent to a hot high pressure separator (HHPS). The top stream from the HHPS is usually over the dew point at normal operations and the gaseous phase is sent over top, including water and light hydrocarbons. To force the dew point prior to entering the air cooler E-4 wash water is injected. The air condenser cools the reactor effluent to below dew point before it is sent to the CHPS. The gaseous phase from CHPS is sent to an absorber unit for hydrogen recovery. The hydrogen-rich gas will be passed through an absorber unit for mainly removal of H_2S and CO_2 created in the GHT reactor before being distributed back as hydrogen feed. The bottom product from the CHPS, identified as sour water, is sent to the Common unit. Most of the NH_3 entering the CHPS can be expected to be removed with the sour water. The hydrocarbon liquid from the CHPS is sent together with the liquids from the HHPS downstream a hot low pressure separator (HLPS). The low pressure flashes condenses additional diesel before entering the diesel stripper. The diesel stripper uses up-flowing steam that strips light hydrocarbons and dissolved gases from the down-flowing diesel. Light end components, such as LPG, together with virtually all of the H_2S, NH_3, HCl, and water are removed in the diesel stripper. The top product from the diesel stripper is combined with the gaseous fraction from the HLPS. The lower pressure condensate is sent downstream as Green GHT product for Synsat or downstream HLGO. The overhead vapours are condensed in an air cooled condenser E-9 prior to entering the overhead drum (O/H drum). Wash water is injected before the condenser E-9. The O/H drum separates liquid hydrocarbons, sour water and non-condensable vapours. Sour water and non-condensable vapours are sent to the Common unit while the liquid hydrocarbons are circulated back to the stripper.

Figure 11. *Separation and diesel stripper*

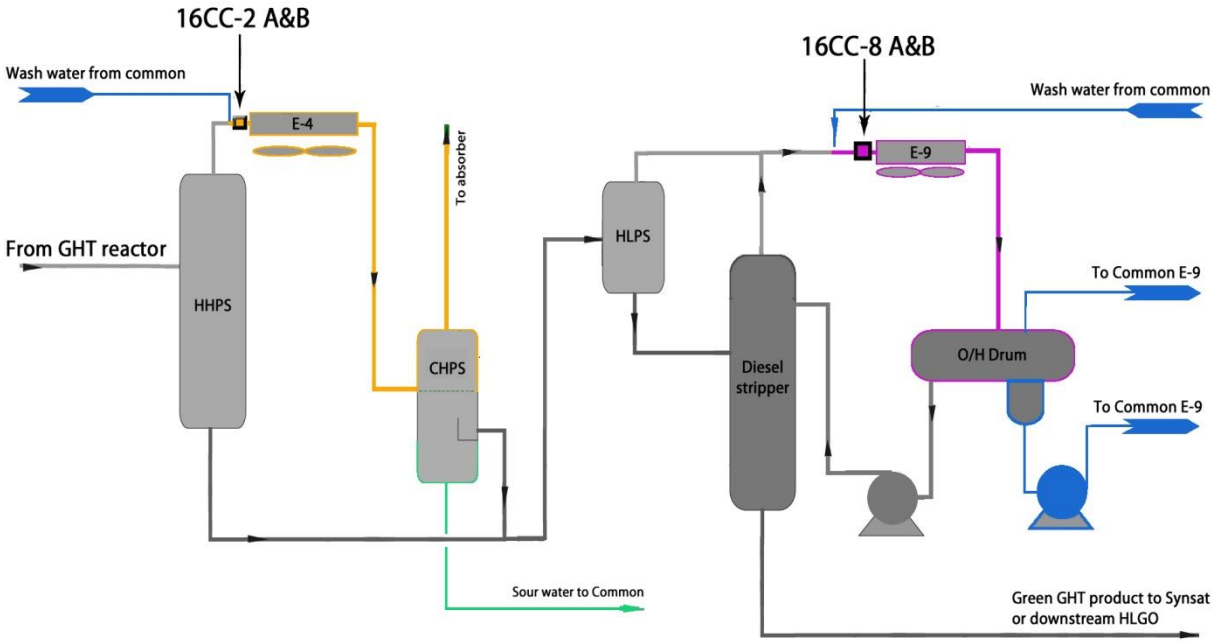

Figure 11 incorporates three corrosion loops; one blue, one orange and one purple. The blue leaving the Common unit from the O/H drum and entering from Common unit as wash water. The orange stretching from the wash water injection point on the HHPS overhead to the downstream absorber.

The purple extend from the wash water injection point prior to air cooler E-9 into the O/H drum, covering the top part of the drum. The orange corrosion loop contains coupons 16CC-2 A&B while the purple contains 16CC-8 A&B.

4.4.3.1 Coupons 16CC-2 A&B

Coupons 16CC-2 A & B are located in the overhead stream from the HHPS, after the water injection point. The top stream from the HHPS is usually over the dew point and is expected to contain H_2, H_2S, NH_3, HCl, CO, CO_2 and water from the reactions with hydrogen upstream in the GHT reactor. RTD contains large amounts of oxygen in the form of fatty acids and resin acids. When operating in green mode larger amounts of CO_2 and water can be expected downstream the reactor compared to fossil mode due to the oxygen-containing compounds in the RTD feed, as proposed by reaction R20 to R24 in chapter *4.4.2*. In both modes a fair amount of NH_3, H_2S and HCl is expected from the reactions that remove sulphur, nitrogen and chlorides. The estimated composition in green mode with 30% RTD and fossil mode at the 16CC-2 positions is presented individually in Appendix B. The current precise composition is not known since there is no possibility of taking a regular sample at the position. Therefore the composition was estimated from simulations made in 2010. The estimated acting conditions at 16CC-2 A&B, for both modes, are presented below in Table 7. Green mode represent a 30% RTD, 70% LLGO blend mixed with H_2 and fed to the GHT reactor.

Table 7. *Process conditions coupons 16CC-2 A&B*

Stream properties	**Fossil mode**	**Green Mode (30% RTD)**
Rate [kg/h]	7824	18549
Phase	Mixed	Mixed
Temperature [°C]	145	170
Pressure [bar]	56	53
Water [kg/h]	35.0%	22.3%
H_2S [wt]	1.2%	0.2%
H_2 [wt]	16.8%	9.7%
Ammonia [wt]	0.2%	*
Chlorides [wt]	High	High
CO_2 / CO [wt]	None / None	*
pH	Fairly low	Low

**Considered classified and will not be published in this report*

4.4.3.2 Proposed dominating corrosion mechanisms for coupons 16CC-2 A&B

The proposed dominating corrosion mechanisms are assumed to be similar in throughout the corrosion loop marked in orange in Figure 11 above.

- ✓ Wet H_2S corrosion
- ✓ Wet H_2S cracking including; Hydrogen blistering, HIC, SOHIC and SSC
- ✓ NH_4Cl corrosion
- ✓ HCl corrosion
- ✓ CO_2 corrosion (Green mode only)
- ✓ CL-SCC

4.4.3.3 Coupons 16CC-8 A&B

Coupons 16CC-8 A and B are located after the overhead stream from the diesel stripper, after the water injection point. The top stream from the diesel stripper and HLPS is expected to contain light hydrocarbons, H_2S, NH_3, HCl, and large amounts of water. A small amount of additional wash water is injected before the condenser E-9 to avoid salt deposition. As before the precise composition of the overhead stream at sample 16CC-8 A&B is not known since there is no possibility of taking a sample at the position. The composition was therefore estimated from simulations made in 2009. If the simulated 16CC-8 A&B composition in green mode and fossil mode is compared, the mass flow rate (kg/h) of H_2S, NH_3 and water is similar. The mass flow rate of light hydrocarbons is slightly higher due to reactor inlet rate in green mode but considered irrelevant in a degradation rate and/or degradation mode perspective. All streams downstream the water injection point prior to 16CC-8 A&B will only be considered in fossil mode. The estimated acting conditions at 16CC-8 A&B positions, in fossil mode, are presented below in Table 8. The pressure was estimated from pressure gauge at the location.

Table 8. *Process conditions coupons 16CC-8 A&B*

Stream properties	**Estimated value**	**Remarks**
Rate [kg/h]	1626	Total rate, Inlet E-9. From simulation 2009
Phase	Vapour	Prior to wash water injection. Injection < 10 m^3/d.
Temperature [°C]	204	From simulation 2009
Pressure [barg]	5	Pressure gauge diesel stripper
Water [kg/h]	39.9%	From simulation 2009
H_2S [wt]	0.4%	
Ammonia [wt]	300ppm	
Chlorides [wt]	Moderate amount	Assumed. Chlorides carried with water out from top of diesel stripper.
CO_2 / CO [wt]	Traces / traces	All CO2 / CO removed in CHPS
pH	Fairly low	Assumed based on H2S and Chloride content with low amount of NH_3

4.4.3.4 Proposed dominating corrosion mechanisms for coupons 16CC-8 A&B

The proposed dominating corrosion mechanisms are assumed to be similar in the corrosion loop marked in purple in Figure 11 above. The corrosion mechanisms are identical to those for 15CC-9 A&B.

- ✓ Wet H_2S corrosion
- ✓ Wet H_2S cracking including; Hydrogen blistering, HIC, SOHIC and SSC
- ✓ NH_4Cl corrosion
- ✓ HCl corrosion

4.5 Common (17)

The Synsat and GHT unit generate liquid streams that need treatment before being redistributed. The Common unit remove primarily dissolved H_2S and NH_3 from the generated contaminated water. A simplified version of the Common unit consists of three types of separators preceding a sour water stripper. The first separator works as a collective drum where wash water and sour water from different parts of the process is collected and skimmed from light hydrocarbons. The second separator collects sour water and separates it from slightly heavier hydrocarbons. The third vacuum separator operates at low pressure and is used to flash out any residual hydrocarbon from the sour water. The sour water is fed to the Sour Water Stripper (SWS) where H_2S, NH_3 and other contaminates are stripped from the water. For simplicity the Common unit description will be split into two parts; the initial Collective O/H *4.5.1* and the following Sour water stripper *4.5.2*. In total 6 coupons are installed in the Common unit, at 5 different positions. Each position will be dealt with below. It is, as previously explained, assumed that the estimated conditions for the coupons installed in the Common unit are unaffected by operating mode of the Synsat and the GHT unit.

4.5.1 Collective O/H

Figure 12 show the initial separator labelled collective O/H which incorporates coupons 17CC-1 A&B, 17CC-2, 17CC-6 and their corrosion loops. The sour water from Synsat and GHT enters the collective O/H directly while the wash water passes through an air cooler E-9 prior to the O/H Drum. A small amount of the stripped water from the SWS is sent into the collective O/H and the rest is sent to GHT and Synsat. The collective O/H works as a skimmer which separately removes light hydrocarbons from the wash- and sour water. Separation occurs in two compartments, one where sour water is the only intake (middle compartment), one for the wash water and stripped water (left compartment). The light hydrocarbons are skimmed and end up in the right compartment. The non-condensable vapours are sent over top to an amine absorber. The skimmed sour water is fed to the sour water stripper (SWS) while the wash water is circulated back to GHT and Synsat.

Figure 12. *Collective OH*

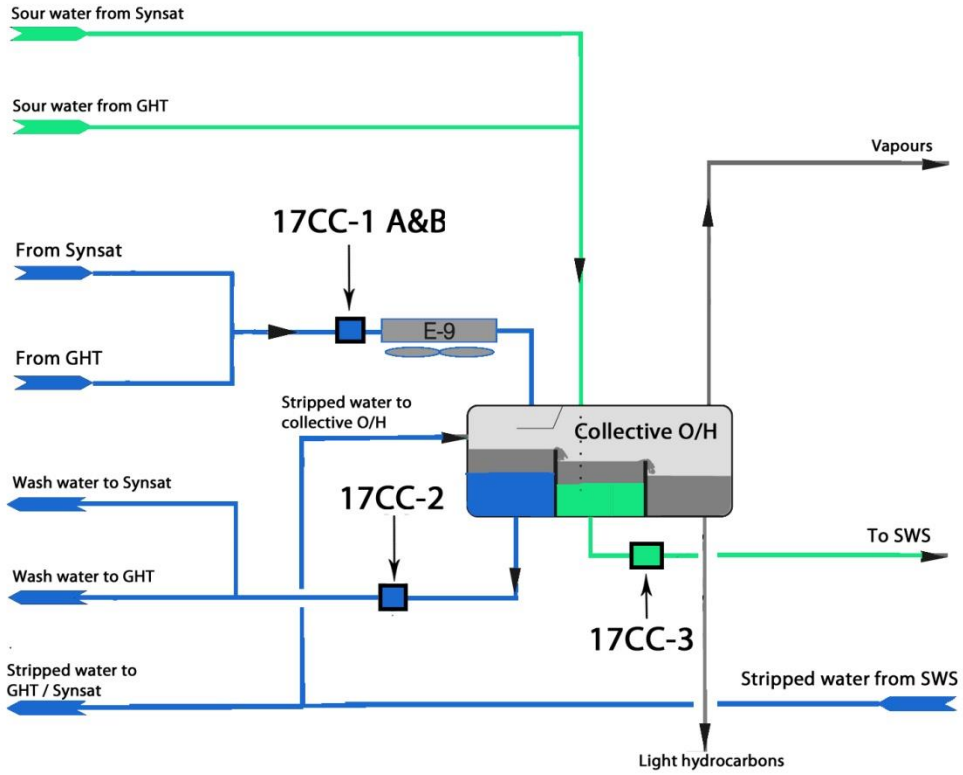

Figure 12 incorporates two corrosion loops; one blue and one turquoise. The blue corrosion loop enters from the Synsat and GHT unit, passes through air cooler E-9 and the collective O/H, and then returns back to Synsat and GHT as wash water. In the blue loop three samples, 17CC-1 A&B and 17CC-2 are present at two different positions. Each of the two positions in the blue loop will be dealt with separately. The turquoise loop enters from Synsat and GHT, passes through the collective O/H and is sent to SWS. From the SWS the turquoise loop returns and is sent to GHT/Synsat or it enters the collective O/H again.

4.5.1.1 Coupons 17CC-1 A&B

Coupon 17CC-1 A&B is located on the inlet to air cooler E-9. The majority of the feed into the blue corrosion loop comes from the diesel stripper O/H drum in the Synsat and GHT units. By backtracking to the two O/H drums the stream can be expected to contain light hydrocarbons , H_2S, NH_3, HCl, and large amounts of water before entering the air cooler E-9. As before there is no possibility of taking a sample at the position, so the composition was estimated from a simulation made in 1994 and the reasons presented in Appendix B. The estimated conditions at 17CC-1 A&B positions are presented below in Table 9. The basis for the composition is presented in Appendix B.

Table 9. *Process condition coupons 17CC-1 A&B*

Stream properties	Estimated value	Remarks
Rate [kg/h]	26480	Total rate, Inlet 17E-9, from simulation 1994
Phase	Mixed	
Temperature [°C]	110	
Pressure [barg]	5	Values from simulation 1994
Water [wt]	31.2%	
H_2S [wt]	2.5%	
Ammonia [wt]	340ppm	
Chlorides [wt]	Moderate amount	Assumed from extrapolating backwards. Mean flow rate of CO_2 / CO and chlorides from 15CC-9 and 16CC-8 position, assuming all CO_2 / CO and chlorides come from Diesel stripper O/H drum
CO_2 / CO [wt]	Low	
pH	Moderately low	Assumed based on H_2S, CO_2, NH_3 and Chloride content

4.5.1.2 Coupon 17CC-2

The 17CC-2 coupon is located on the wash water outlet from the O/H drum. The wash water stream is expected to contain almost exclusively water since most of the hydrocarbons are removed in the collective O/H drum. One can expect more or less same composition as 17CC-1 position without hydrocarbons and lower temperature. Nevertheless, some of the H_2S, NH_3, CO_2 and CO will be dissolved in the water. Also there will most likely be chlorides present. The values presented in Table 10 are estimated from simulations and the reasons presented in Appendix B.

Table 10. *Process conditions for coupon 17CC-2*

Stream properties	Estimated value	Remarks
Rate [kg/h]	11700	Total rate, wash water outlet collective O/H, from simulation 1994
Phase	Liquid	Wash water
Temperature [°C]	40	From simulation 1994
Pressure [barg]	5	From simulation 1994
Water [kg/h]	11700	Assumed 100% water
H_2S [wt]	400ppm	Calculated with Henrys law at simulated temperature and pressure (see Appendix B)
Ammonia [wt]	500ppm	
Chlorides [wt]	Moderate amount	Assuming that most chlorides will be soluble in water and follow condensed water from 17CC-1.
CO_2 / CO [wt]	Very low	Assuming most CO2 and CO should have been flashed out by this point
pH	More or less neutral	Assumed based on H2S, CO_2, NH_3 and Chloride content

4.5.1.3 Proposed dominating corrosion mechanisms for 17CC-1 A&B and 17CC-2

The proposed dominating corrosion mechanisms are assumed to be similar in throughout the corrosion loop marked in blue in Figure 12 above.

- ✓ Wet H_2S corrosion
- ✓ Wet H_2S cracking including; Hydrogen blistering, HIC, SOHIC and SSC
- ✓ NH_4Cl corrosion
- ✓ HCl corrosion

4.5.1.4 Coupon 17CC-3

The 17CC-3 coupon is located on the sour water outlet from the O/H drum. The water comes from the two CHPS in the GHT and Synsat unit and enters middle compartment of the collective O/H. The incoming sour water is separated from light hydrocarbons and sent to the SWS. The skimmed sour water passing position 17CC-3 can be expected to contain fairly large amounts of NH_3, H_2S and Chlorides. The estimated composition is presented in Table 11, the basis for the composition is presented in Appendix B. Table 11 are estimated from simulations, available gauges and assumptions presented in Appendix B.

Table 11. *Process conditions coupon 17CC-3*

Stream properties	Estimated value	Remarks
Rate [kg/h]	11960	Total rate, sour water outlet collective O/H, from simulation 1994
Phase	Liquid	Sour water
Temperature [°C]	40	Temperature gauge inlet collective O/H
Pressure [barg]	5	Pressure gauge collective O/H
Water [kg/h]	11690 (98%)	From simulation 1994 (essentially 100% water)
H_2S [wt]	1.7%	From simulation 1994
Ammonia [wt]	0.5%	From simulation 1994
Chlorides [wt]	Fairly high	HCl from CHPS in GHT and Synsat unit
CO_2 / CO [wt]	Low / low	Solved CO2 / CO from CHPS in GHT and Synsat unit. Maximum CO2 content when GHT reactor operates in "Green mode".
pH	Unknown	High chloride content with moderate amount of H_2S, but also high ammonia content

4.5.1.5 Proposed corrosion mechanisms for coupon 17CC-3

The proposed dominating corrosion mechanisms are assumed to be similar in throughout the corrosion loop marked in turquoise in Figure 12 above. The corrosion mechanisms are identical to those for 17CC-6 and 17CC-10 (turquoise corrosion loop).

- ✓ Wet H_2S corrosion
- ✓ Wet H_2S cracking including; Hydrogen blistering, HIC, SOHIC and SSC
- ✓ NH_4Cl corrosion
- ✓ HCl corrosion
- ✓ NH_4HS corrosion

4.5.2 Sour water stripper

As mentioned the Common unit consist of three types of separators (simplified) preceding a sour water stripper. Figure 12 deals with the initial separator, while Figure 13 deals with the subsequent SWS feed drum, Vacuum separator and the Sour Water Stripper (SWS). The sour water from the collective O/H drum enters the SWS feed drum, where the heavier hydrocarbons are skimmed from the water. The heavier hydrocarbons are fed to a Vacuum separator where, due to pressure decrease, additional hydrocarbons are flashed out and separated from the water. The sour water from the Vacuum separator is circulated back to the SWS feed drum. The sour water from SWS feed drum is fed to the SWS where, after preheating in heat exchangers, the hot feed enters the stripping tower where H_2S and NH_3 are separated overhead by steam stripping. Besides H_2S and NH_3 there are

other dissolved gases, such as carbon dioxide, hydrocarbons, corrosion products and solids in sour water that also end up in the sour water stripper unit. The H_2S and NH_3 rich gas is recovered in the SWS overhead drum (SWS O/H) and sent to the SRU. The stripped or treated water is cooled and sent back to Collective O/H drum or the GHT and Synsat units.

Figure 13. *Sour water stripper*

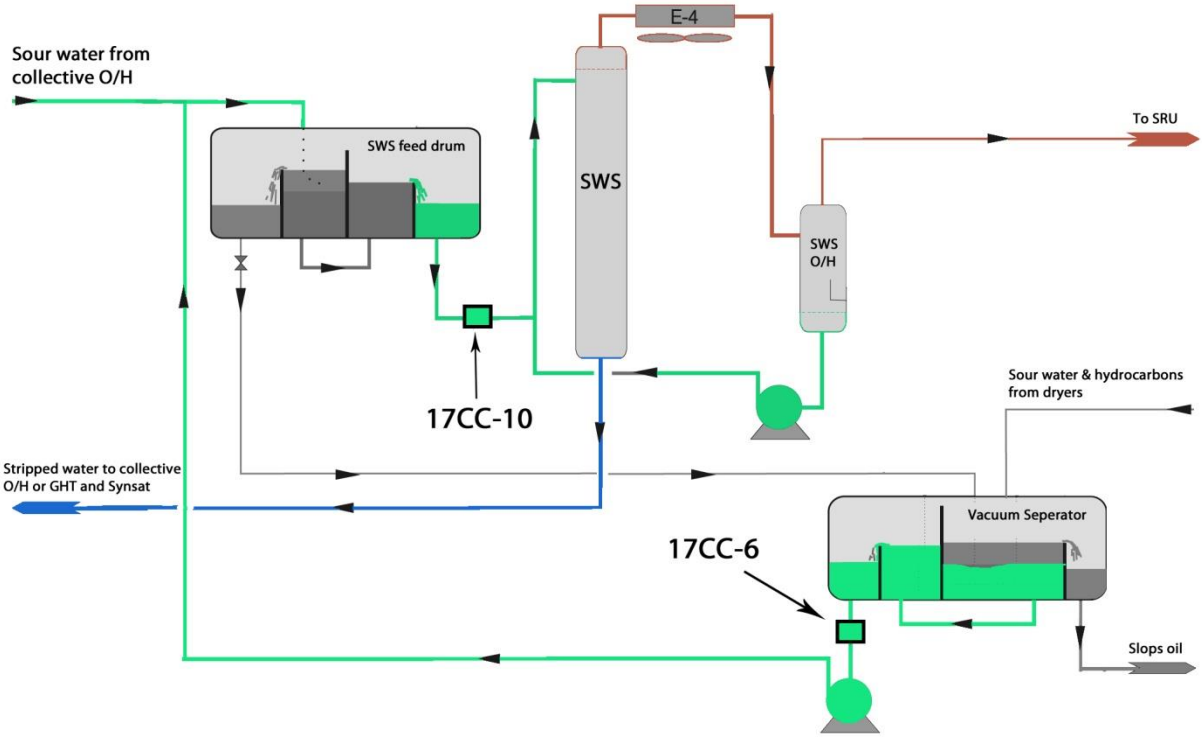

Figure 13 incorporates two corrosion loops one blue and one turquoise. The blue corrosion loop leaves to the collective O/H or the Synsat and GHT unit. The turquoise loop enters from the collective O/H, passes through the SWS feed drum and Vacuum separator, and is sent to Sour water stripper (SWS). From the SWS O/H the turquoise loop returns to the SWS. In the turquoise corrosion loop there are two samples, 17CC-6 and 17CC-10 that are present at two different positions. Each of the two positions in the blue loop will be dealt with separately.

4.5.2.1 Coupon 17CC-6

Coupon 17CC-6 is located on the outlet to the Vacuum separator. The majority of the feed into the Vacuum separator comes from the SWS feed drum and upstream product dryers. The inlet feed, by backtracking, can be expected to contain heavier hydrocarbons, H_2S, NH_3 and large amounts of water. The outgoing feed at the 17CC-6 position, due to lower pressure, can be expected to contain lower amounts of dissolved H_2S, NH_3 in water. As before the there is no possibility of taking a sample at the position. Therefore the composition was estimated from a simulation made in 1994, nearby gauges and the assumption that more H_2S, NH_3, HCl, CO, CO_2 and hydrocarbons have been flashed out in the Vacuum separator. The estimated conditions at 17CC-6 positions are presented below in Table 12.

Table 12. *Process conditions coupon 17CC-6*

Stream properties	Estimated value	Remarks
Rate [kg/h]	1190	Total rate, sour water outlet Vacuum separator, from simulation 1994
Phase	Liquid	Sour water
Temperature [°C]	30	Temperature gauge inlet Vacuum separator
Pressure [bar]	0.1	Pressure gauge Vacuum separator
Water [kg/h]	1190	Assumed 100% water
H_2S [wt]	<1%	Assumed less than 17CC-10
Ammonia [wt]	< 0.5%	Assumed less than 17CC-10
Chlorides [wt]	Moderate amount	Assumed less than 17CC-10
CO_2 / CO [wt]	Very Low	Assumed less than 17CC-10
pH	Estimated to be pH≈9	Assumed similar to 17CC-10

4.5.2.2 Coupon 17CC-10

The 17CC-10 coupon is located on the SWS feed drum outlet that feeds the Sour water stripper (SWS). The water comes from SWS feed drum, where the heavier hydrocarbons have been skimmed from the sour water. The outgoing sour water passing position 17CC-10 can be expected to contain fairly large amounts of NH_3, H_2S and Chlorides dissolved in water. A sample taken on the SWS inlet in 2008 will be used to estimate the NH_3, H_2S and pH at the 17CC-10 position. Table 13 is estimated from simulations, available gauges, sample 2008 and assumptions presented in Appendix B .The estimated composition is presented in Table 13; the basis for the composition is presented in Appendix B.

Table 13. *Process conditions coupon 17CC-10*

Stream properties	Estimated value	Remarks
Rate [kg/h]	13300	Total rate sour water from rate gauge on outlet SWS feed drum
Phase	Liquid	Sour water
Temperature [°C]	40	From simulation 1994
Pressure [barg]	5	Pressure gauge outlet SWS feed drum
Water [kg/h]	12880 (98%)	from simulation 1994
H_2S [wt]	1.0%	From sample 2008
Ammonia [wt]	0.5%	From sample 2008
Chlorides [wt]	Fairly high	Assumed, same amount of chloride as 17CC-3 dissolved in sour water
CO_2 / CO [wt]	Low	Same amount of solved CO2 / CO as 17CC-3 dissolved in sour water
pH	9	From sample 2008

4.5.1.5 Proposed corrosion mechanisms for coupon 17CC-6 and 17CC-10

The proposed dominating corrosion mechanisms are assumed to be similar in throughout the corrosion loop marked in turquoise in Figure 13 above. The corrosion mechanisms are identical to those for 17CC-3 (turquoise corrosion loop).

- ✓ Wet H_2S corrosion
- ✓ Wet H_2S cracking including; Hydrogen blistering, HIC, SOHIC and SSC
- ✓ NH_4Cl corrosion
- ✓ HCl corrosion
- ✓ NH_4HS corrosion

4.6 SRU - Sulphur recovery unit (27-29)

The Sulphur recovery unit (SRU) is used to recover sulphur from acid gases produced from amine recovery unit (ARU) and the Common unit Sour Water Stripper (SWS). In the reactor area of the SRU sulphur recovery is achieved via the Claus process, which converts H_2S to elemental sulphur that is condensed to a liquid state for handling and transportation. The small amount of sulphur remaining in the stream is burned in the incinerator before being released to the atmosphere.

4.6.1 SRU Knockout

The SRU only has one coupon installed 27CC-2 which is located in the initial knockout part of the unit, thus only this part will be included in this chapter. Figure 14 is a schematic of the initial knockout part of the SRU. Overhead gases from the Sour Water Stripper (Figure 13) are sent to the SWS knockout drum (SWS K.O.) where the H_2S rich gases are separated from residual sour water. In a similar way the acid gas from the Amine Regeneration Unit (Figure 7) is mixed with other gases and fed to the ARU knockout drum (ARU K.O.).

Figure 14. *SRU Knockout*

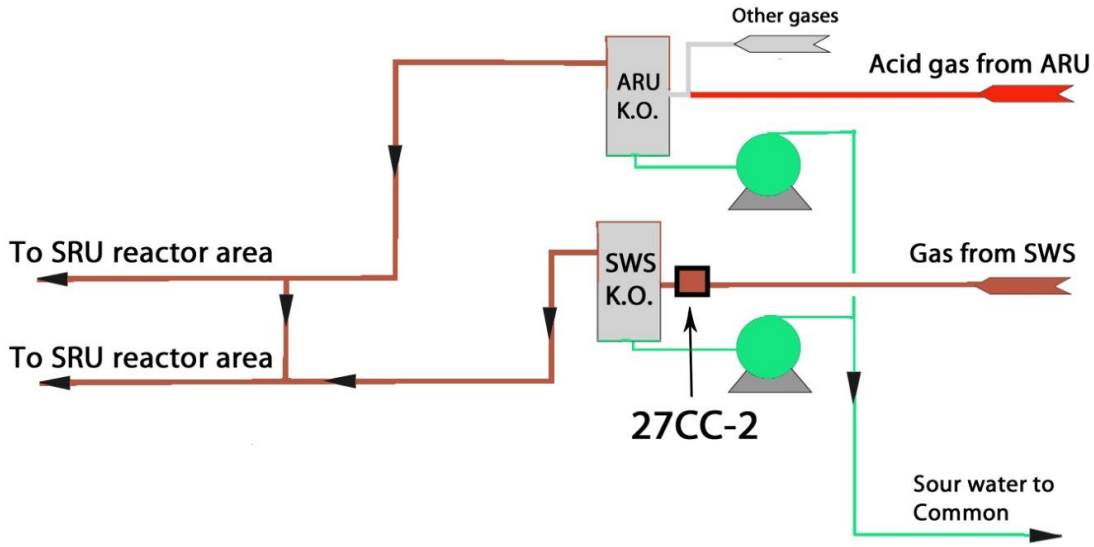

Figure 14 incorporates three corrosion loops one turquoise, one red and one brown. The turquoise corrosion loop leaves from ARU- and SWS knockout drum to the collective O/H drum in the Common unit. The red loop enters from the ARU and ends when it gets mixed with other gases. The brown corrosion loop enters from the SWS O/H drum in the Common unit, passes through the SWS K.O., and leaves to the SRU reactor area. The outlet from ARU K.O. is considered to exhibit similar conditions and is therefore also included in the brown corrosion loop. In the brown corrosion loop there is one sample, 27CC-2.

4.6.1.1 Coupon 27CC-2

Coupon 27CC-2 is located in the inlet to the air SWS knockout drum (SWS K.O.). The feed comes from the SWS overhead drum (SWS O.H, Figure 13). The inlet gas feed, by backtracking, can be expected to contain large amounts of H_2S, NH_3 and water. Also a small amount of CO, CO_2 and chlorides can be expected since most dissolved contaminants end up in the SWS overhead. In a study made in 2010 a sample was taken on the SWS K.O. inlet in 2010 and a material balance was calculated. The sample data will be used to estimate the NH_3, H_2S, CO and CO_2 at the 27CC-2 position. The material balance will be used to estimate temperature, pressure and flow rate. The amount of chlorides will be assumed. The grounds for the estimated conditions are presented in Appendix B. The estimated conditions at 17CC-6 positions are presented below in Table 14.

Table 14. *Process conditions coupon 27CC-2*

Stream properties	Estimated value	Remarks
Rate [kg/h]	105	Total rate acid gas inlet SWS K.O. drum, from material balance 2010
Phase	Vapour	Acid gas
Temperature [°C]	98	From material balance 2010
Pressure [bar]	0.7	From material balance 2010
Water	30.0%	From sample 2010
H_2S [wt]	51.3%	From sample 2010
Ammonia [wt]	14%	From sample 2010
Chlorides [wt]	High	Assumed. Large amount of chlorides will be carried over top from SWS
CO_2 / CO [wt]	3.6% / <0.1%	From sample 2010

4.6.1.2 Proposed corrosion mechanisms for coupon 27CC-2

The proposed dominating corrosion mechanisms are assumed to be similar in throughout the corrosion loop marked in brown in Figure 14 above.

- ✓ Wet H_2S corrosion
- ✓ Wet H_2S cracking including; Hydrogen blistering, HIC, SOHIC and SSC
- ✓ NH_4HS corrosion

5 Measurements and observations

A refinery is configured with most units in series and in continuous operation. During an inspection shutdown the whole refinery has to be down in order to do the mandated inspections. An inspection shutdown is a major undertaking for the refinery. All pressurised equipment, such as heaters, exchangers, distillation towers, have to be emptied, dismantled and cleaned in order to enable the inspection. The operation requires large extra manpower and heavy machinery. This increased risk for accidents leads to a great deal of safety regulation and demand for planning. Therefore the early part of this study was spent planning the removal of the corrosion coupons. This means: finding out when equipment will be depressurized, dismantled and cleaned in order to enable the removal safely. Attain the correct authorization documents for the opening and removal of equipment. Getting help from competent personnel with gear suitable for the operation. This gear may include gas meters, fresh air masks, fire fighting equipment, fall protection etc. Besides attaining or ordering replacement parts and tools necessary for the removal and re-installation of the coupons, extra mechanics are needed since working alone is not allowed. Close contact with the appropriate work supervisor and knowledge of the safety risks where necessary in order to complete the practical on-site part of this study. An inspection shutdown is done every fourth year and is now adjusted to occur again in six years. The shutdown is carried in a very tight widow of time due to the cost of lost production. As can be imagined rigorous planning is necessary due to the fixed time table.

5.1 Preliminary investigation

To practically execute the weight loss analysis and optical inspection, presented in chapter *2.2.2* and *2.2.3*, a preliminary investigation was performed. The intention of the preliminary investigation was to determine:

- Method of cleaning the coupons from organic products after exposure
- Means of removing the corrosion products from the coupon

In order to examine the corrosion products on the exposed coupons the organic substances should be removed. By using organic solvents the organic compounds should be removed from the non-organic corrosion product. It was decided to use a three-step cleaning process; toluene, GUM (½ toluene ½ acetone) and acetone in an ultrasound bath followed by drying. Each cleaning step would be repeated until no visual divergence from pure solvent could recognized, subsequently all organic oily contaminant on the corrosion product was considered to be dissolved by the solvent. Two old unclean corroded coupons, one disc- and one strip coupon, was exposed to the three-step cleaning over a period of time. Each cleaning cycle was timed to 3 minutes and after each cleaning cycle was completed the process was repeated. The removal of organic products from coupons will be referred to as *degreasing*. The results of the preliminary investigation into degreasing method can be viewed in appendix D. After 2 cycles or 6 minutes the mass loss was less than 1mg which is less than the repeatability of the used scale. Thus it was decided that the method for removing organic substances from the coupons was to be a three step cleaning cycle with toluene, GUM and acetone in an ultrasound bath for a total time of minimum 6 minutes. After the cycle is completed the coupon sample are dried in compressed air at low pressure.

In order to perform the metal loss analysis the corrosion products must be removed from the coupons. The least time consuming way of removing corrosion products is by blasting. Available at Preem was a Norclean sand blaster 0.1kW. Sand was used as blasting agent to make the method of removal less forceful. To be able to establish the correct mass loss it is important to remove all corrosion products while minimizing material loss of the coupon base metal. To investigate the mass loss over time; three old corroded coupons (two disc and one strip coupon) was exposed to blasting at different blasting pressures over time. The samples was blasted for a period of time, then cleaned with acetone and dried before weighed to four decimal places. Between each blasting period the coupons where investigated visually and with microscope (5 times magnification) to see if any residual corrosion products could be observed. The mass loss versus time was plotted and the time when the coupons were considered to be clean from corrosion products was noted. The results of the preliminary investigation of removal of corrosion products can be viewed in appendix D.

At a blasting pressure less than 2.5 bar the corrosion products could not be removed effectively, at 4 bar the mass loss over time were considered to be too high. It was determined that a blasting pressure of 2.5 bar should be used and that each blasting session should be timed. As can be observed in the time/mass curve there is no clear decline in mass loss corresponding to when all the corrosion products have been removed. This implies that the erosion rate is approximately the same for the corrosion product as for the metal substrate. This means that the method will depend on continuously observing the coupon surface and that some loss of uncorroded metal is inevitable. A blasting session is deemed complete when no corrosion products can be observed visually after which the coupons should be investigated optically. If residual corrosion products are found optically, the coupon should be blasted for additionally 30-60 seconds and the total blasting time should be noted. This process will be repeated until the coupon is considered clean from corrosion products.

5.2 Measurement execution

In this study only 10 coupons could be replaced by new coupons due to retailer issues and the unique features of some coupons. The GHT-coupons and the coupons installed at 16CC-2 A&B position could not be replaced. The 10 new coupons were in most cases used to replace one coupon in locations where the position had an A and a B fitting. The coupons that could not be replaced were after weight loss analysis, optical inspection and photographic documentation reinstalled at the same position. The practical execution is summarised below:

i. Removal of coupon. Coupon and holder placed sealed plastic bag and transported to laboratory.
ii. Coupon removed from coupon holder and flushed with toluene. Coupon placed in toluene container together with screws and nylon insulators. Coupon holder placed in steam washer at 80°C for 20 minutes.
iii. Oily coupon degreased in three steps using toluene, GUM and acetone in ultrasound bath. Oily products considered removed when solvent appearance and coupon weight remains unchanged.
iv. Front and back of coupon photographed with stamped serial number upwards. Followed by weighing of sample.
v. Non-organic corrosion products present on coupon visually and optically inspected. The corrosion product produced on the surface is deemed uniform or non-uniform and areas of

interest are photographed through microscope (5x magnification only). Colour, structure and location of product formation are noted.

vi. On the GHT-coupons, 16CC-2 A&B and the 10 saved coupons the corrosion products are removed by scraping. The products are transported to Chalmers for X-Ray diffraction (XRD) analysis.

vii. All coupons are blasted at 2.5 bar blasting pressure until corrosion products are visually considered removed. The coupons are then examined optically at 5x magnification to confirm removal. If corrosion products are found the coupons will be blasted again for 30-60 seconds. The total blasting time will be noted.

viii. After blasting the coupons are cleaned from residual blasting agents by flushing with acetone. The samples are then dried with compressed air at low pressure and weighed to four decimal places. The GHT-coupons will go through the same procedure but weighed to an accuracy of one decimal place due to the accuracy of the scale available.

ix. The surface is investigated visually for local corrosion attacks and the corrosion is deemed uniform and/or localized. The density of pits will be estimated throughout the surface.

x. The maximum pit depth on the surface is then determined optically. The maximum corrosion depth on the surface is measured by the focus dial of the microscope. Focus is put on the lip of the pit then on the deepest point in the pit. The difference in height is measured by how many units the focus dial is turned. One complete rotation of the focus dial equals 0.4 mm in vertically. This was confirmed through measurements of objects of known height. Repeatability of 0.01 mm has been reported using this method of measuring pit depth, but since the quality of the calibration is unknown and the experience level is low the accuracy is considered to be to 0.05 mm of depth. The coupon is scanned for the three pits that are considered the deepest. The mean depth of these pits are considered the maximum pit depth. It should be noted that a combination of general corrosion and pitting corrosion is expected which means that the pit-border is not uncorroded. This may underestimate the total amount of metal lost in the pit.

xi. The localized corrosion attacks on the surface of the coupon is then optically investigated. The shape of the attack is assessed as being narrow, elliptical to shallow. Areas of interest are photographed.

xii. Installation weight, dimensions and stamped serial numbers are noted on the six coupons that are to be re-installed. Newly installed coupons are weighed to four decimal places to confirm installation weight. The coupons are then mounted on holders with clean insulators and transported out to the process area for fitting.

The weight acquired (step viii) was subtracted from the installation weight to give the weight loss. The weight loss together with the exposure time, exposed area and the alloy density reported in chapter 2.2.1 was used in the weight loss analysis equation 1 [eq.1] in chapter 2.2.2 to calculate the average corrosion rate, $v_{average}$ [mm/y]. The weight loss was also used in equation 2 [eq.2] to calculate the average penetration depth [mm].

The maximum penetration depth (step x) was divided with the exposure time according to equation 4 [eq.4] chapter 2.2.3 to calculate the corrosion rate due to pitting, $v_{pitting}$ [mm/y]. The maximum corrosion depth was also divided with the average penetration depth in equation 5 [eq.5] to calculate the pitting factor.

The results from the XRD analysis (step vi) of the corrosion products together with the observations and background study will be used to determine the dominating degradation modes. The observations being the visual investigation of the corrosion product (step v) together with the size (step xi) and density (step x) of localized attacks on the coupon base material. The pitting factor may aid the investigation. The estimated dominating degradation modes at the coupon position will be considered the same throughout the entire corrosion loop. The degradation modes will entail all equipment in the loop with the same material. For the equipment with non-coupon material or modes undetectable by the method used then the degradation mode estimated in chapter 4 will be used.

6 Results

6.1 Analyses of results excluding GHT Reactor

The methodology (*Chapter 2*) and the measurements (*Chapter 5*) have been used to calculate the results given in Table 15 below. The corrosion rate and pitting rate severity used is given in Table 16 in accordance with ASTM G46 - 1994 "Standard Guide for Examination and Evaluation of Pitting Corrosion". The results of the XRD analysis presented in Table 15 are visualized in *Appendix D*. The data used in the calculated values of table 15 are presented in table 23 in *Appendix D*.

Table 15. *Calculated coupon corrosion effects (excluding GHT reactor)*

Coupon Tag No.	Coupon Material	$v_{average}$ [mm/year]	$v_{pitting}$ [mm/year]	Pitting Factor	XRD
9 CC-1	C1018	0,0220	0,0229	1,04	Amorphous
15 CC-2A	C1018	0,0116	0,0457	3,94	Amorphous
15 CC-2B	C1018	0,0059	-	-	-
15 CC-9A	C1018	0,0116	-	-	-
15 CC-9B	C1018	0,0113	0,0228	2,01	Amorphous
16 CC-2A	SS*	0,0015	< 0,0360	1,00	FeS
16 CC-2B	SS*	0,0013	< 0,0360	1,00	FeS
16 CC-8A	C1018	0,0161	-	-	-
16 CC-8B	C1018	0,0327	0,0457	1,40	Amorphous
17 CC-1A	C1018	0,0105	-	-	-
17 CC-1B	C1018	0,0132	< 0,0114	1,00	Amorphous
17 CC-2	C1018	0,0258	0,0457	1,77	Amorphous
17 CC-3	C1018	0,0016	< 0,0114	1,00	Amorphous
17 CC-6	C1018	0,0340	0,0342	1,01	Amorphous
17 CC-10	C1018	0,0151	0,0227	1,50	Amorphous
27 CC-2	C1018	0,0112	0,0114	1,02	FeS

**Grade considered classified*

Table 16. *Corrosion/Pitting rate severity*

Corrosion/Pitting rate	mm/year
low	0,025
moderate	0.025-0.124
severe	0.125-0.25
very severe	>0.25

6.2 Analyses of results GHT reactor

Results of the GHT-coupons will not be published in this report.

7 Discussion

This chapter will discuss the results presented in Chapter 6, future recommendations and the study scope.

7.1 Analyses of results (excluding GHT Reactor)

7.1.1 Coupon 9CC-1 – Red corrosion loop

Fairly uniform corrosion at low to moderate rate, probably due to wet H_2S/CO_2 corrosion at relatively low pH. The ratio of CO_2 to H_2S partial pressure is below 100 which suggest that the corrosion is H_2S dominated, with a corrosion product dominated by FeS. The lack of evidence for crystalline FeS may be due to contaminates or the acting conditions at the position, creating non-favourable environment for creating FeS with long range order. MDEA has low aggressiveness and should have small effect on the overall corrosion attack. A photograph of coupon 9CC-1 is available in figure A1, Appendix A.

7.1.2 Coupons 15CC-2 A&B – Green corrosion loop

Low uniform corrosion rate, moderate pitting rate with high pitting factor. The pitting is probably caused by local NH_4Cl/HCl attacks at moderate chloride levels and high amount of ammonia. At this position the uniform corrosion rate is low which might be deceptive. External inspection methods, such as ultrasonic thickness gauges, might fail to detect the severity of the local attacks. To evaluate the severity of local attacks a more comprehensive internal inspection of the equipment is suggested. A photograph of coupon 15CC-2A is available in figure A2, Appendix A.

7.1.3 Coupons 15CC-9 A&B and 16CC-8 A&B – Purple corrosion loop

Coupons 15CC-9 A&B and 16CC-8 A have low uniform corrosion rates, with limited pitting. Coupon 16CC-8 B have moderate, predominantly even, corrosion rate. No reasons for the identified difference in corrosion rates between 16CC-8 A and 16CC-8 B have been identified. However, it is suggested that it might be due to differences in flow profiles. A photograph of coupon 16CC-8B is presented in figure A3, Appendix A.

Figure A12, Appendix A, shows a magnified photograph (10 times magnification) of the corrosion product present on coupon 16CC-2B. A red-brown and a blue coloured product can been seen. The red-brow product can be hydrous ferrous oxide, $Fe(OH)_3$ (regular rust). Hydrated magnetite in the presence of organic complexants (such as paraffin hydrocarbons) can appear to have a blue colour. Also, partially oxidized $Fe(OH)_2$ (ferrous hydroxide or “green rust”) can be formed when the oxygen supply is insufficient to form $Fe(OH)_3$. It can also be formed if $Fe(OH)_2$ briefly exposed to air in the presence of moisture, for example when the samples were taken out. The corrosion products mentioned above all require oxygen to be able to form. If this is the case; oxygen has entered during the stop. It should be noted that no crystalline evidence for the mentioned corrosion product could be found in the XRD analysis.

7.1.4 Coupons 16CC-2 A&B – Orange corrosion loop

Low corrosion rate without local attacks. This is the only coupon here made of stainless steel. The identification of FeS by XRD indicates that H_2S induced corrosion is occurring, but no other degradation method providing long-range crystalline products could be identified. A photograph of coupon 16CC-2B is available in figure A4, Appendix A.

Indications of localized attacks on the protective layer have been identified in figure A13, Appendix A. No degradation to the base metal could be recognized. In this study the Stainless steel (grade classified) has shown good resistance considering the high chloride environment.

7.1.5 Coupons 17CC-1 A&B and 17CC-2 – Blue corrosion loop

17CC-1 A&B have low corrosion rate. 17CC-2 exhibits predominantly general corrosion and a moderate corrosion rate, predominantly even, corrosion rate. The corrosion is probably caused by wet H_2S. A photograph of coupon 17CC-2 is available in figure A4, Appendix A.

The difference in measured corrosion rate between 17CC-1 A&B and 17CC-2 could be explained by coupon appearance. 17CC-1 A&B are disc coupons while 17CC-2 is a strip coupon. Strip coupons will be slightly less accurate at imitating the process interface but they are larger than the disc coupons, thus provides a larger area on which corrosion can develop and be readily observed.

7.1.6 Coupons 17CC-3, 17CC-6 and 17CC-10 – Turquoise corrosion loop

17CC-3 and 17CC-10 shows low corrosion rates. 17CC-6 has moderate corrosion rate and moderate pitting rate i.e. local attacks in combination with relatively rapid loss of material. The corrosion of 17CC-10 is probably caused by a combination of wet H_2S corrosion and HCl corrosion.

It is not clear why 17CC-6 has higher corrosion rate than 17CC-10. Both are located in sour water and contaminants are higher at the 17 CC-10 location. Further examination of 17CC-6 position is suggested to determine cause of effects. A photograph of coupon 17CC-6 is available in figure A5, Appendix A.

An observation worth mentioning is that during the handling/cleaning of coupon 17CC-6 the corrosion product appeared to have poor adherence to the base metal. Figure A14, Appendix A, show minor discoloration below the black outer corrosion layer. One could speculate that some contaminant or stream property affect the build-up of ferrous sulphide, making it porous. The porous layer may break off revealing fresh base metal leading to an increase in corrosion rate.

7.1.7 Coupon 27CC-2 – Brown corrosion loop

Coupon 27CC-2 has mostly uniform corrosion at a low corrosion rate. The corrosion is most likely caused by wet H_2S corrosion by condensed liquid on the surface of the coupon. Narrow localised pitting can be observed, might be the cause of NH_4HS corrosion. A photograph of coupon 27CC-2 is available in figure A6, Appendix A.

7.2 Analyses of results GHT reactor

Discussion regarding the GHT-coupons will not be published in this report.

7.3 Recommendations

The existing inspections intervals should be evaluated with regard to the findings in this study, especially in locations where the measured coupon corrosion rates are relatively high. Inspection measurements should also be compared to data in this study.

Recommendations regarding the GHT-coupons will not be published in this report.

7.4 Study scope

The setup of this thesis was, in retrospect, too broad and general. The refinery is extremely complex from technical, material and corrosion perspectives. The corrosion coupons are located at 11 different locations under 11 different process and corrosion conditions. By definition the coupons are located where the corrosion is suspected to be severe and where the corrosion rate is related to a number of interacting corrosion mechanisms. The setup of the thesis resulted in a lot of work related to practical handling and background which limits the theoretical depth of the thesis.

The coupons were removed and reinstalled during the major turnaround. Due to the safety regulations the work to remove/reinstall the coupons at every location had to have a separate work permit. The work had to be done by dedicated mechanics. The work had to be fit in the overall turnaround, with over 1000 contractors on site. In practice this meant that the removal/reinstallation of the coupons had to be "slotted in" on short notice. The "slot in" process, involving a number of planning and supervision people within the organisation, had to be managed. This means that the removal/reinstallation of coupons takes a large amount of time.

The starting point of the data collection is to put the corrosion coupon locations in a context of process conditions. The data available are too detailed to be useful in this study. Adapted process diagrams and descriptions had therefore to be made.

The process conditions at 11 locations had to be derived from a combination of existing simulations, measurements and estimates. Generally there are very few possibilities to measure composition or other stream data. Within the time frame available it was not possible to set up specific simulations for this thesis.

7.4.1 Study achievements

The main purpose of the thesis was to establish corrosion rates and to evaluate probable corrosion mechanisms for each coupon. This is described in Chapter 6. A more general view of possible corrosion mechanisms for each location is given in Chapter 4.

The thesis should suggest improvements on the methodology regarding corrosion coupons. Actually, it turned out that no such documented methodology existed. As part of this master thesis work, a method has been designed, as described in Chapter 5. This will enable the refinery to systematically follow the corrosion of the corrosion coupons.

7.4.2 Study scope reduction/recommended future work

The time needed for practical handling, method development and information gathering made it necessary to limit the scope. The scope of the thesis has been reduced in order to fit into the available time frame. The reasons are given below and can be seen as suggestions for future work.

7.4.2.1 Evaluate the method of using corrosion coupons in relation to other corrosion control methods

A refinery is a very complex operation. This means that almost all available inspections methods are used. It would take considerable time and effort only to describe and evaluate all these methods and the evaluation would lack academic interest. One of the purposes of this thesis was to compare the results from the corrosion coupons with inspection data. This means that a system has to be set up that enables the corrosion coupon results, in one location, to be compared to inspection data, in other locations. The comparison with other methods/results did not fit within the timeframe of this thesis, and will be left to refinery experts. However, the results from this study could be used by refinery expertise as a foundation for evaluation.

7.4.2.2 Estimate lifetime for associated piping and equipment based on measured corrosion rates.

It takes expertise and experience to evaluate the results from the existing corrosion control methods. The measurements are made in one location at one single time. For each of the locations there are a number of possible corrosion mechanisms. Regarding economic and safety liabilities it is not my place to draw conclusions regarding lifetime of surrounding piping and equipment. However, the results from this study highlight areas where existing data should be evaluated by the refinery experts.

Another aim of this thesis was to highlight locations with increased risks due to the prolonged inspection interval from four to six years. Here the same point could be made as the paragraph above; existing data should be evaluated by the refinery experts.

References

[1] R. XueChong, Z. QingJun, C. WuYang. 2007; *The mechanism of nucleation of hydrogen blister in metals*. Chinese Science Bulletin July 2007, Volume 52, Issue 14, pp 2000-2005.

[2] ASTM G4-1995; *Standard Guide for Conducting Corrosion Coupon Tests in Field Applications*.

[3]; J. Ćwiek, 2010. *Prevention methods against hydrogen degradation of steel*. Journal of Achievements in Materials and Manufacturing Engineering. Volume 43, issue 1 November 2010.

[4] Alexandre Bleuze et al, 2006; *On-stream Inspection for High Temperature Hydrogen Attack.* European Conference on NDT (*ECNDT*) 2006.

[5] Different Types of Corrosion - Recognition, Mechanisms & Prevention*; High-temperature Hydrogen Attack (Decarburization)*. WebCorr - Corrosion consulting services, Singapore 1995-2012. *http://www.corrosionclinic.com/types_of_corrosion/hightemperature%20hydrogen%20attack_decarburization.htm* (retrieved 2011-12-20)

[6] Koji Kawano 2004; *Recent activities on high temperature hydrogen attack*. Idemitsu Engineering Company, Ltd. Chiba, Japan.

[7] Einar Bardal. 2004; *Corrosion and Protection.* Brian Derby (red.) Engineering Materials and Processes ISSN 1619-0181, Springer-Verlag London Berlin Heidelberg.

[8] Winston Revie, 2011. *Uhlig's Corrosion Handbook*. Third edition, John Wiley & Sons Inc. Hoboken New Jersey.

[9] Shell Global corrosion manuals for the refining industry, www.shell.com (retrieved 2011-12)

[10] Linda Garverick. 1994; *Corrosion in the Petrochemical Industry,*ASM International.

[11] DP Ghosh. 2007; *Wet H_2S cracking problem in oil refinery processes – Material selection and operation control issues*, Haldia Refinery, Indian Oil Corporation Limited.

[12] Environmentally Induced Cracking, ASM Handbook, Vol. 13: Corrosion, 9th Edition, ASM International, 1987, pp. 145-189

[13] Richard J Horvath. 2007; *Prediction of and Assessment of Ammonium Bisulfide Corrosion under Refinery Sour Water Conditions*. http://events.nace.org/conferences/c2011/images_author/SamplePaper.pdf (retrieved 2012-11-01)

[14] Adan Sun and Deyuan Fan. 2010; *Prediction,montoring and control of ammonium chloride corrosion in refining processes.* Conference Paper CORROSION 2010, March 14 - 18, 2010 , San Antonio.

[15] September 2010 API Recommended Practice 571 *Damage Mechanisms Affecting Fixed Equipment in the Refining and Petrochemical Industries,* Section 5

[16] Chen Wang. February 2011; *High temperature naphthenic acid corrosion of typical steels.* Canadian Journal on Mechanical Sciences and Engineering Vol. 2, No. 2.

[17] Juan A Melero et al, 2010; *Stability and corrosion studies of Triglyceride-based Biomass and Petrol Mixtures in standard refinery units*. Hydrocarbon world Vol. 5 Issue 2.

[18] AvBruce D. Craig. 1995; *Handbook of Corrosion Data*. 2nd edition, ASM International.

[19] H.S. Khatak,B Raj. 14 okt 2002; *Corrosion of Austenitic Stainless Steel: Mechanism, Mitigation and Monitoring.* Woodhead Publishing, England.

[20] T. Charng, F. Lansing. 1982; *Review of corrosion causes and corrosion control in a technical facility*. DNS Engineering Section, TDA Progress report.

[21] ASTM G 46 – 1994 (Reapproved 2005); *Standard Guide for Examination and Evaluation of Pitting Corrosion*

[22] FranCois Ropital. 2010; *CORROSION AND DEGRADATION OF METALLIC MATERIALS*: *Understanding of phenomena and applications in the petroleum and process industries.* Editions Technip Paris.

[23] *Corrosion resistance to nickel-containing alloys in organic acids and related compounds*. Nickel institute, http://www.nickelinstitute.org/en/TechnicalLiterature/INCO%20Series/1285_CorrosionResistanceofNickel_ContainingAlloysinOrganicAcidsandRelatedCompounds.aspx (retrieved 2012-12).

[25] C. M. Scjillmoller. 1992; *Selection and use of stainless steels and nickel-bearing alloys in organic acids*. Nickel institute, http://www.stainless-steel-world.net/pdf/10063.pdf, (retriever 2012-11).

[26] A.J. Invernizzi, E. Sivieri, S.P. Trasatti. *Corrosion behaviour of Duplex stainless steels in organic acid aqueous solutions*. Materials Science and Engineering: A, Volume 485, Issues 1–2, 25 June 2008, Pages 234–242, June 2008.

[27] Joaquín Quesada-Medina, Pilar Olivares-Carrillo. *Evidence of thermal decomposition of fatty acid methyl esters during the synthesis of biodiesel with supercritical methanol.* The Journal of Supercritical Fluids, Volume 56, Issue 1, February 2011, Pages 56–63.

Appendix A

This appendix contains blasted sample coupon pictures referred to in the chapter 7.1 and 7.2. It also contains enlarged photographs (10x) from the visual investigation.

Figure 15. *Photographs A1 to A7 of sampled coupons after blasting, referred to in chapter 7.1*

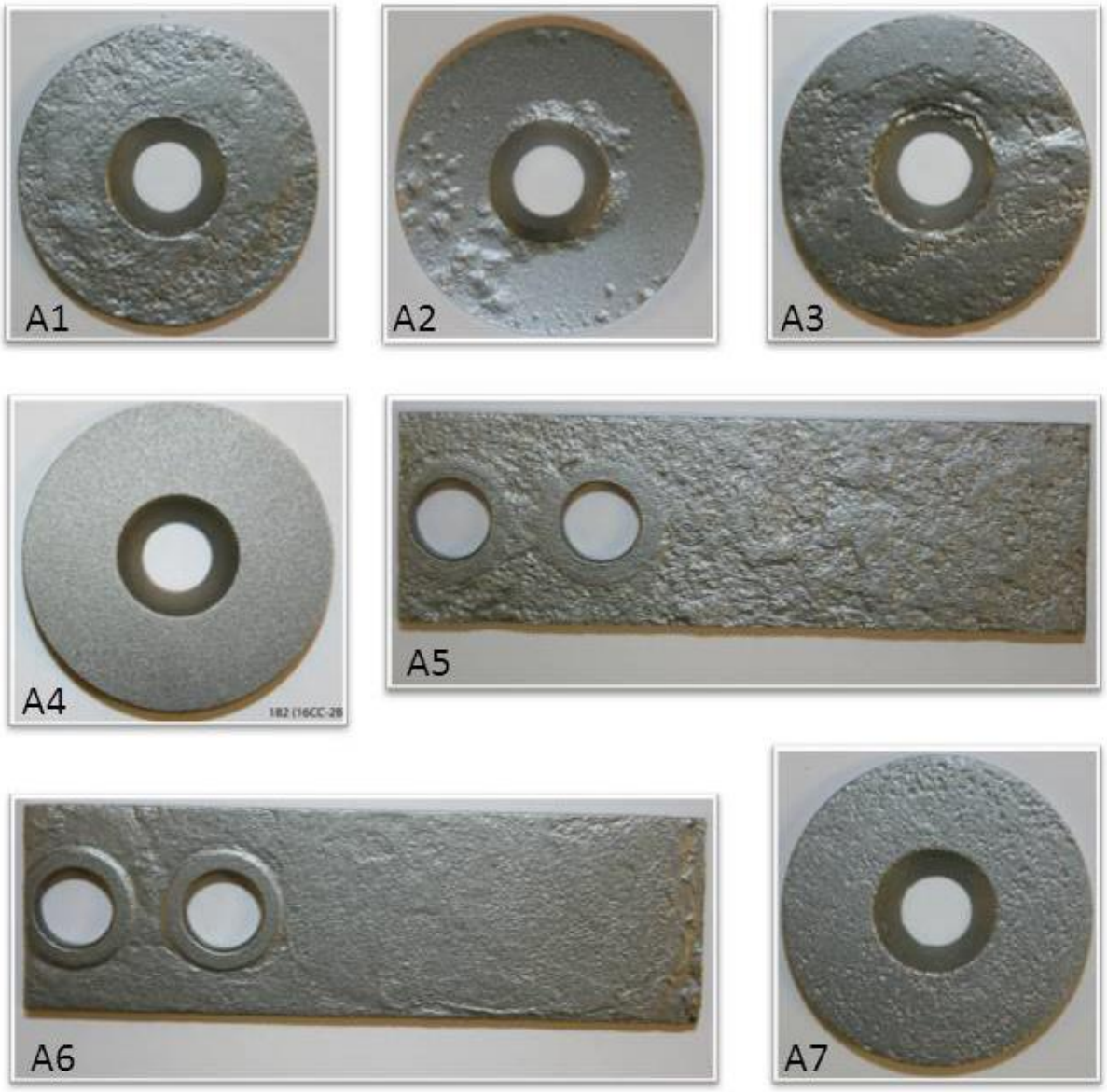

Figure 16. *Photographs A8 to A11 of sampled coupons after blasting, referred to in chapter 7.2*

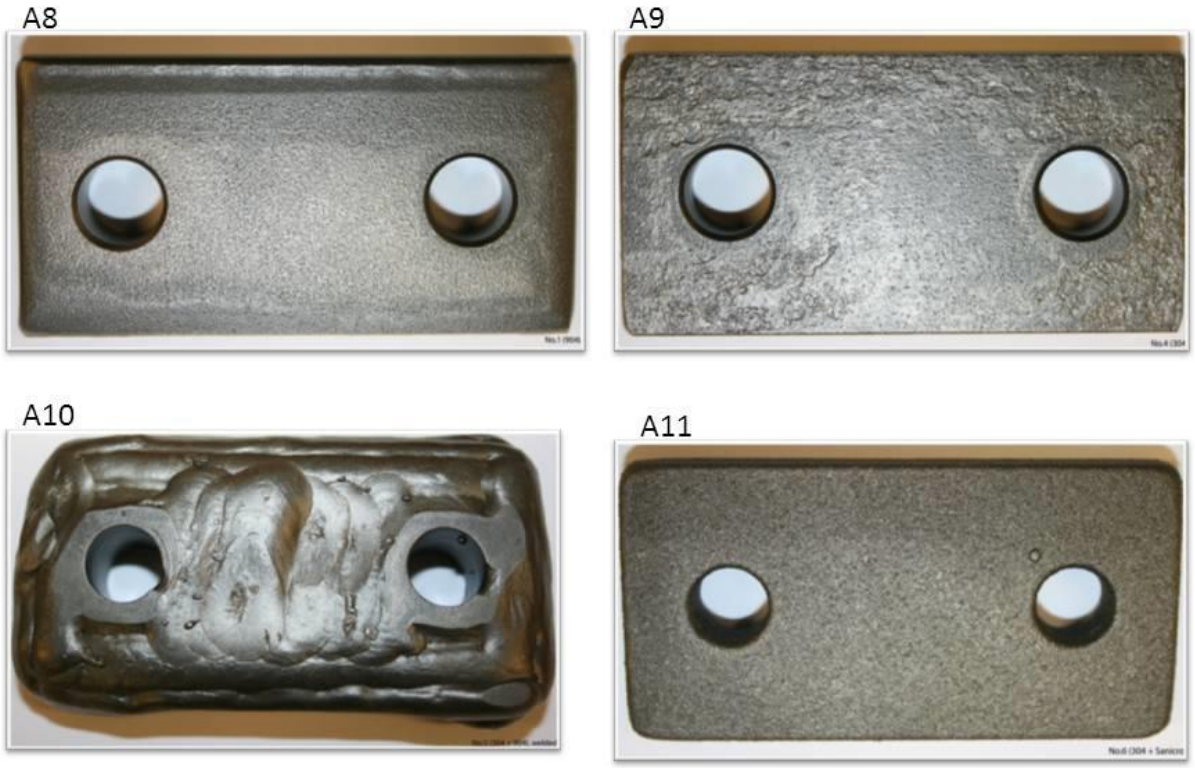

Figure 17. *A12 through A14* contains enlarged photographs (10x) from the visual investigation*, referred to in chapter 7.1. A15 is blasted coupon referred to in 7.2.*

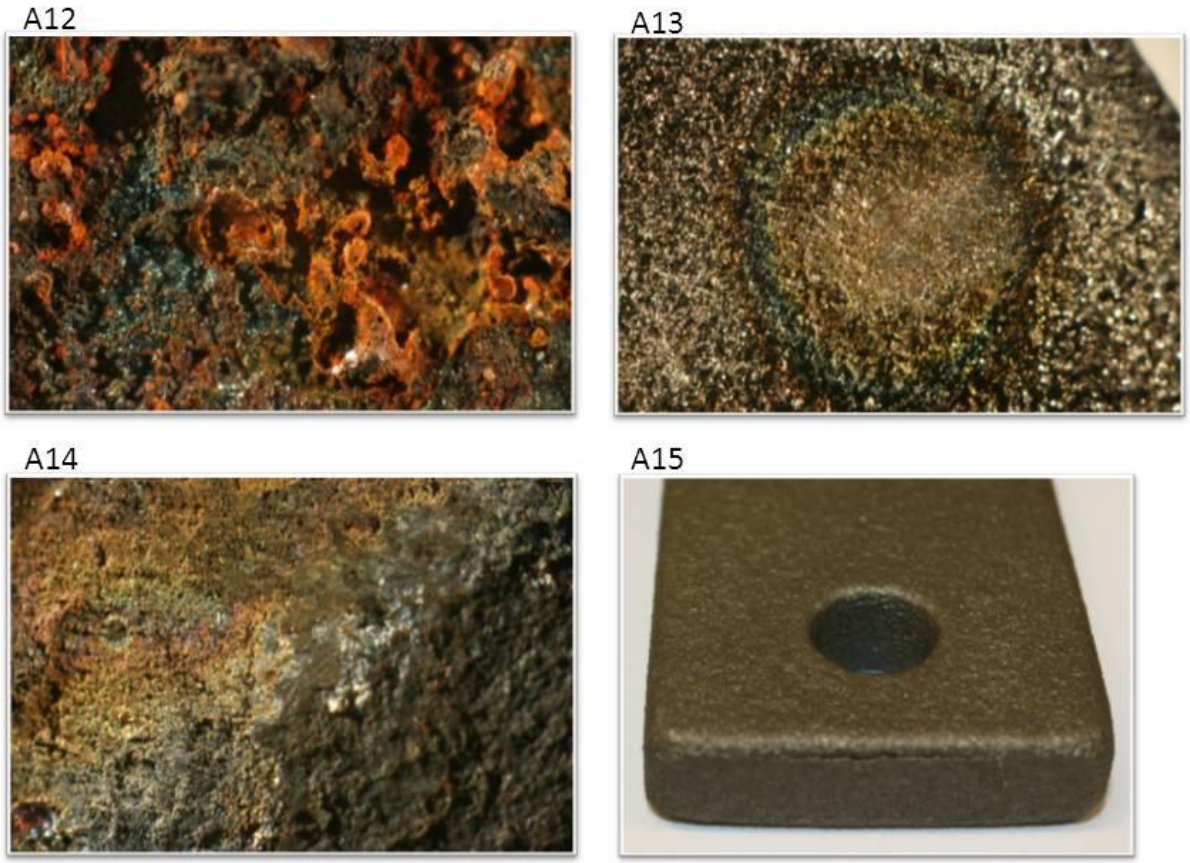

Appendix B

The properties surrounding the coupons are estimated through simulations, sample analysis, assumptions and reasoning around each coupon. The quality of the simulations, the sample data, the assumptions and the table remarks are motivated in this appendix. Detailed explanations and calculations will not be offered in this chapter, the values presented in the tables below should be seen as approximations and nothing more.

B1. Coupon 9CC-1

Flow rate was estimated from simulation around a point on the condenser inlet, made in connection with the construction of the unit 1996, i.e. design values.

Temperature and pressure was taken from temperature- and pressure gauges on the regenerator outlet.

H_2S, NH_3, CO_2, CO and hydrocarbon content was taken from a sample taken on the reflux drum outlet 2010. The residual part of the total rate was assumed to be water, with 100% water from reflux drum back to regenerator. By using material balance, since the water content in top outlet stream is known from the same simulation, the amount of water can be calculated.

The amounts of chlorides are assumed on the basis that the water carries dissolved chlorides from adjacent units connected to the ARU. Since the ARU inlet is gases and light hydrocarbons are above the dew point one can assume that a fairly small amount of chlorides will be entering the ARU. But since all chlorides will end up in the regenerator and carried with the steam over top, one can assume that all chlorides entering the ARU will be present in the stream passing coupon 9CC-1.

If water is condensed in some areas or on the coupon, pH can be estimated to be high. Large amounts of acidic gases will cause the first condensed water to have a pH well below neutral.

B2. Coupons 15CC-2 A&B

By using a simulation from 1994 it was estimated that the water injection stream prior to 15CC-2 A&B positions was approximately 100m^3/day. The water content was added to the total flow rate and the mass flow rate of water presented in table 3. The same simulation from 1994 was used to estimate temperature, phase, H_2S content and NH_3 content. The pressure is taken from a pressure gauge on the HHPS outlet.

More or less all CO_2 and CO produced in the HDS and HDA reactor will pass over top from the HHPS and end up in the HHPS overhead stream where 15CC-2 A&B are positioned. All the CO and CO_2 produced in the reactors, when oxygen-containing compounds are removed, ends up in the 15CC-2 stream. The HLGO, LLGO or GHT-product fed to the Synsat unit has fairly low oxygen-containing compounds, but to be on the safe side a moderate amount can be assumed.

The Synsat reactors remove a fair amount of chlorides from the diesel in the form of HCl. Since the HHPS operates over the dew point, these will be carried over top. So it can be safe to assume that a moderate amount of chlorides will be present in the HHPS overhead stream. Since the amount of

chlorides and CO_2 is unknown and a fair amount of NH_3 is present the pH will be deemed as unknown.

B3. Coupons 15CC-9 A&B

By using a simulation from 1994 it was estimated that the water injection stream prior to 15CC-9 A&B positions was approximately 25m^3/day. The water content was added to the total flow rate and the mass flow rate of water presented in table 4. The temperature of the wash water injection is approximately 40°C, resulting in an estimated temperature drop of 5%. With the diesel stripper outlet temperature know from the simulation, the temperature and phase at the 15CC-9 position could be calculated. The pressure is taken from a pressure gauge on the diesel stripper outlet. The same simulation from 1994 was used to estimate temperature, phase, H_2S content and NH_3 content

The amount of Chlorides, CO_2 and CO is estimated by extrapolating backwards. Assuming that most CO_2 and CO is removed upstream in the HHPS a small amount will still be dissolved in the downstream product. The chloride content at 15CC-9 is estimated to be moderate since the temperature and pressure drop will flash out additional HCl into the diesel stripper overhead. A low amount of NH3 and a fairly high H_2S and HCl content will probably result in a low pH in the condensed phase.

B4. Coupons 16CC-10 A to F

In the planning stage of the reconstruction of the MHC into a GHT unit several simulations where made, including one in 2009. By knowing the simulated values of the LLGO+H_2 temperature and pressure and assuming no temperature and pressure drop, the same values where used. Estimating a maximum mix of 30% RTD a maximum rate was calculated from the simulated LLGO+H_2 flow rate.

Three import specifications between 2011-05-07 and 2011-07-10 were used to calculate the mean value of water, chlorides, FAME, Fatty acids and Resin acids.

The temperature and pressure present in the top inlet will cause FAME to decompose. Most likely the FAME will decompose to fatty acids and hydrocarbons since there is no additional oxygen present. But to be on the safe side, in a corrosion rate perspective, the total mass flow of FAME in the feed will decompose into the same mass flow of fatty acids. I.e. 52 kg/h FAME decompose into 52kg/h Fatty acids. Note that the FAME should decompose into fatty acids with lower mass, thus the approximation is a slight overestimation of the fatty acids mass flow. I will offer no speculation regarding molar rate or TAN, nor will I explain the stated fatty acid mass flow further in this report. The values presented in table 4 should be seen as rough estimations and nothing more. A typical RTD composition is presented below in table 17.

Table 17. *A typical RTD composition*

Stream properties	**Estimated value**	**Remarks**
Rate [kg/h]	*	Rate prior to RTD mixing point, from simulation 2009
Phase	Mixed	
Temperature [°C]	*	From simulation 2009

Pressure [barg]	*	From simulation 2009
Water [wt]	*	Mean value from import specifications 2011-05-07 to 2011-07-10.
Chlorides [wt]	*	Mean value from import specifications 2011-05-07 to 2011-07-10.
H_2 [wt]	*	
FAME [wt]	*	Mean value from import specifications 2011-05-07 to 2011-07-10. The FAME will decompose to approximately 52 kg/h fatty acid when mixed with LLGO.
Fatty acids [wt]	*	Mean value from import specifications 2011-05-07 to 2011-07-10.
Resin Acid [wt]	*	Mean value from import specifications 2011-05-07 to 2011-07-10.

**Considered classified and will not be published in this report*

The same simulation from 2009 was used to compile a composition of the LLGO/gas mix in table 18 below. The simulation was made around a point after the preheating but before the RTD injection point. The simulation showed no H_2S, CO, CO_2 or NH_3 present and is thus disregarded in table 18. A trace of chlorides carried from LLGO produced in the CDU is assumed.

Table 18. *A typical a composition of the LLGO/gas mix*

Stream properties	Estimated value	Remarks
Rate [kg/h]	40172	Rate prior to RTD mixing point, from simulation 2010
Phase	Mixed	LLGO+H2
Temperature [°C]	320	From simulation 2009
Pressure [barg]	65	From simulation 2009
Water [wt]	700ppm	From simulation 2009
Chlorides [wt]	traces	Assumed. Chlorides carried from CDU.
H_2 [wt]	5%	From simulation 2009

The same simulation from 2009 had data if the GHT-reactor was operating in Fossil mode. That data was used to compile table 19 of the HLGO/gas feed prior to entering the reactor. The simulation

showed no H_2S, CO, CO_2 or NH_3 present and is thus disregarded in table 19. A trace of chlorides carried from HLGO produced in the CDU is assumed

Table 19. *Typical HLGO/gas feed prior to entering the reactor*

Stream properties	Estimated value	Remarks
Rate [kg/h]	54900	Total rate, top inlet reactor, from simulation 2010
Phase	Mixed	Predominantly HLGO+H_2
Temperature [°C]	326	From simulation 2009
Pressure [barg]	64	From simulation 2009
Water [wt]	300ppm	From simulation 2009
Chlorides [wt]	traces	Assumed. Chlorides carried from crude.
H_2 [wt]	2%	From simulation 2009

B5. Coupons 16CC-2 A & B

A simulation of GHT-reactor operating in "Fossil mode" with approximately 30% RTD mix from 2009 was available. The simulation was around a point on the inlet to E-4 after the wash water injection, just like coupons 16CC-2 A&B. Hence rate, temperature, pressure, water, H_2S, H_2, NH_3, CO_2 and CO was estimated. The GHT reactors remove chlorides from the diesel in the form of HCl. Since the HHPS operates over the dew point, these will be carried over top. So it can be safe to assume that a moderate amount of chlorides will be present in the HHPS overhead stream. With high amount of chlorides and H_2S the pH is assumed to be low. Note that a fair amount of NH3 is present so the pH is probably not terribly low. The estimated conditions for 16CC-2 in Fossil mode are presented in table 20 below:

Table 20. *Estimated conditions for 16CC-2 in Fossil mode*

Stream properties	Estimated value	Remarks
Rate [kg/h]	7824 kg/h	Total rate, Inlet E-4. From simulation 2009
Phase	Mixed	After cold water feed
Temperature [°C]	145	From simulation 2009
Pressure [bar]	56	From simulation 2009
Water [kg/h]	35.0%	From simulation 2009
H_2S [wt]	1.2%	From simulation 2009
H_2 [wt]	16.8%	From simulation 2009

Ammonia [wt]	0.2%	From simulation 2009
Chlorides [wt]	High	Assumed
CO_2 / CO [wt]	None / None	From simulation 2009
pH	Fairly low	Assumed. Based on CO2, H2S and chloride content

By using a simulation of GHT-reactor operating in "Green mode" with approximately 30% RTD mix from 2009 was available. Rate, temperature, pressure, water, H_2S, H_2, NH_3, CO_2 and CO was estimated from this simulation. Since the HHPS operates over the dew point HCl, CO_2 and CO will be carried over top. Since the RTD contains a high amount of oxygen-compounds a higher amount of CO_2 and CO is anticipated, as table B4 shows. It can be safe to assume that a moderate amount of chlorides will be present in the HHPS overhead stream. With high amount of chlorides, CO_2 and H_2S the pH is assumed to be very low. The estimated composition at 16CC-2 A&B when operating in "Green mode" with 30% RTD mix is presented below in table 21.

Table 21. *The estimated composition at 16CC-2 A&B when operating in "Green mode" with 30% RTD mix*

Stream properties	Estimated value	Remarks
Rate [kg/h]	18549 kg/h	Total rate, Inlet E-4. From simulation 2009
Phase	Mixed	After cold water feed
Temperature [°C]	170	From simulation 2009
Pressure [bar]	53	From simulation 2009
Water [kg/h]	*	From simulation 2009
H_2S [wt]	*	From simulation 2009
H_2 [wt]	*	From simulation 2009
Ammonia [wt]	100ppm	From simulation 2009
Chlorides [wt]	High	Assumed
CO_2 / CO [wt]	*	From simulation 2009
pH	Very Low	Assumed. Based on CO2, H2S and cloride content

**Considered classified and will not be published in this report*

B6. Coupons 17CC-1 A&B

The total rate is calculated from a nearby flow rate gauges prior to air condenser E-9. A simulation from 1994 was used to estimate the values of temperature, pressure, phase, water content, H_2S content and NH_3 content.

The CO, CO_2 and Chloride content was estimated by extrapolating backwards in the process flow to coupon 15CC-9 A&B and 16CC-8 A&B which is present upstream. Assuming that no CO, CO_2 or chlorides are lost on the way, the estimated mean flow rate of CO, CO_2 and chlorides from 15CC-9 A&B and 16CC-8 A&B is used; resulting in Very low content CO_2 / CO and a Moderate amount of chlorides.

B7. Coupon 17CC-2

A simulation from 1994 is available which includes values for flow rate, temperature and pressure. The simulation assumes 100% water content at the 17CC-2 position, no values for H_2S and NH3 was available. To somewhat estimate the composition of H_2S and NH_3 a few assumptions had to be made. First it is assumed that the collective O/H drum removes exclusively all liquid hydrocarbons from the water. Then, liquid-vapour phase equilibrium is assumed. Since the composition of outlet vapours from the O/H drum is known from the same simulation 1994, it can be used as approximation of the gas phase composition in the collective O/H drum. By assuming liquid-vapour phase equilibrium and using H_2S, NH_3 as solute solved in pure water, the amounts solved in water phase can be calculated with Henrys law. The solubility will be calculated using Henrys constants at the simulated temperature and pressure, with partial pressures of components in the gas phase (i.e. vapours stream) in accordance with Henrys law. Noted that this will only be a rough estimation since acting conditions in the collective O/H will be far from gas-liquid phase equilibrium. Henrys law is presented below in eq. 5:

$$c_i = k_{H,i} \cdot y_i \cdot P \qquad \text{(eq. 5)}$$

Where c is the concentration solute in aqueous form [mol_{aq}/dm^3_{aq}], k_H is the Henrys constant at 40˚C [mol/(atm*dm^3)] in pure water solvent, y is the molar fraction and P [atm] is the total pressure.

According to simulation 1994, the gas phase in collective O/H has the following properties: T=40˚C (313.15K), P=4.9atm, y_{H2S}=0.033, y_{NH3}=8*10^{-4}. The Henry's constant at 298.15K ($k_{H,i}^{\Theta}$) is retrieved $k_{H,H2S}^{\Theta}$= 0.1 mol/(atm*dm^3) and $k_{H,NH3}^{\Theta}$= 10 mol/(atm*dm^3). The Henry's constant at T=40˚C is estimated with eq. 6 below.

$$k_{H,i}(T) = k_{H,i}^{\theta} \cdot \exp\left(\frac{-\Delta_{Soln}H}{R} \cdot \left(\frac{1}{T} - \frac{1}{T^{\theta}}\right)\right) \qquad \text{(eq. 6)}$$

Where $\frac{-\Delta_{Soln}H}{R}$ is the temperature dependence, which equals: for H_2S: 2100 and for NH_3: 1500. Using the data presented above in eq. B2 gives: $k_{H,H2S}$=0.07 and $k_{H,NH3}$=7.86 [mol/(atm*dm^3)].

Using the Henrys constants with given molar fraction and pressure in eq. B1 gives: c_{H2S}=0.011 and c_{NH3}=0.031 [mol_{aq}/dm^3_{aq}]. The concentration of solute in aqueous form is recalculated to weight fraction by using eq. 7.

$$x_i = \frac{M_i \cdot c_i}{\rho_{H2O}} \qquad \text{(eq. 7)}$$

Where ρ_{H2O} is the density of water and M is the molar weight. The density of water at T=40˚C is approximately ρ_{H2O}=0.992 kg/dm^3, the molar weight is M_{H2S}=34.07*10^{-3} kg/mol and M_{NH3}=17.03*10^{-3} kg/mol. Inserting these values into eq. 3 gives approximately x_{H2S}=400ppm and x_{NH3}=500ppm.

The pH and chloride content of the incoming stripped water from SWS to the left compartment are known from regular analysis from samples on the SWS outlet. Approximate values from a sample on incoming stripped water made in 2008 reveal pH: 9.7 and Total chloride content: 2ppm.

Assuming that all hydrocarbons are removed in the O/H drum; the pH can be expected to be more or less neutral at 17CC-2 since the incoming wash water is expected to be acidic and the incoming stripped water is basic. The incoming wash water is expected to have a moderate amount of chlorides while the stripped water has very low chloride content. To be on the safe side a moderate amount of chlorides is assumed.

B8. Coupon 17CC-3

At the 17CC-2 position a simulation from 1994 is available which includes values for flow rate, water content, H_2S content and NH_3 content.

By backtracking to the individual CHPS of the GHT and Synsat units; the inlet to the CHPS can be represented by 15CC-2 and 16CC-2 positions at lower temperature. In the CHPS most of the gas is sent over top while the sour water is taken out and sent to the middle compartment of the Collective O/H, where 17CC-3 is positioned on the outlet. Assuming the a large amount of chlorides stay dissolved during the pressure drop from CHPS to Collective O/H the amount of Chlorides is expected to be fairly high. Assuming that almost all the CO_2 and CO is removed in the CHPS and that the pressure drop flashed out even more, the CO_2 and CO content can be expected to be low. The pH at 17CC-3 must be considered to be unknown since the estimated data is too vague.

B9. Coupon 17CC-6

Temperature was taken from temperature gauge on the Vacuum separator inlet, pressure taken from Vacuum separator drum. A simulation from 1994 is available which only include value for flow rate. The simulation assumes 100% water content at the 17CC-6 position but no values of H_2S, NH_3, chloride, CO_2 or CO content.

To estimate the remaining components a two assumption where made. One, the inlet feed flow rate from the dryers is negligible compared to the feed from the SWS feed drum. Two, all hydrocarbons are removed in the Vacuum separator. Then by backtracking to the SWS feed drum where coupon 17CC-10 is positioned on the middle outlet; then asserting that the pressure drop from the SWS feed drum to the Vacuum separator will decrease solubility of the components, thus removing them in the outlet gas feed. If the above stated is true, then mass flow of aqueous H_2S, NH_3, chloride, CO_2 and CO should be less or equal to that at 17CC-10. By using the worst case scenario the same amount of compound is presented (the fraction of compound will differ due to the difference in flow rate).

B10. Coupon 17CC-10

Flow rate was taken from gauge on the SWS feed drum outlet, pressure taken from gauge in SWS feed drum. At the 17CC-10 stream there is a location where samples can be taken, by using a sample taken in 2008 values of pH, H_2S and NH_3 is estimated. A simulation from 1994 is available which include values for temperature and water content.

Assuming that the chlorides follows the sour water, the chloride content is estimated to be the same as for 17CC-3; fairly high. Using the same logic: the amount of dissolved CO_2 / CO in 17CC-10 should be the same as in 17CC-3; very low.

B11. Coupon 27CC-2

In 2010 a study concerning the efficiency of the SWS was done. In this study a material balance was constructed from samples taken on site. This material balance was used to compile values of rate, temperature, pressure and the content of water, NH_3, H_2S, CO_2 and CO in the knockout drum inlet. Then by assuming that a fair amount of chlorides will be carried from the SWS overhead to the SWS the chloride content was estimated to be high.

Appendix C

This appendix contains sample set-up pictures referred to in the chapter 2.2.1 and results from the preliminary investigation chapter 5.1.

C1. Sample set-up: Holders, coupons and on-scene photos

Figure 18. *GHT coupon set-up pictures. Mounted holders (left) and close-up of coupon+ holder (right)*

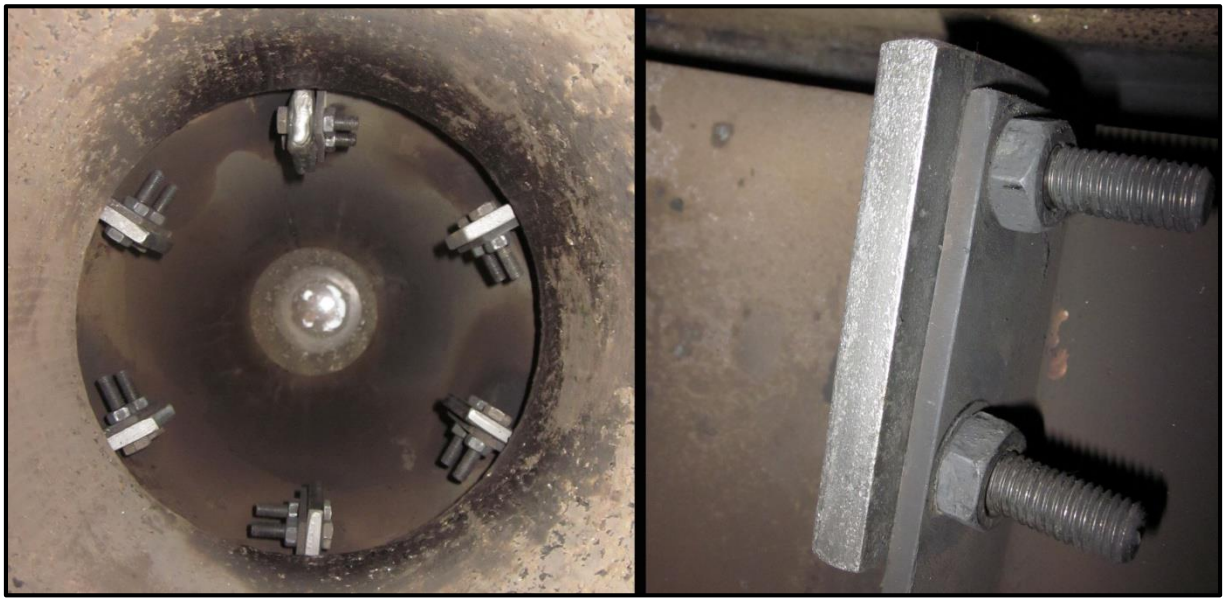

Figure 19. *Disc coupon set-up pictures. Holders (left) and on-scene photo of position (right)*

Figure 20. *Strip coupon set-up pictures. Holders (left) and on-scene photo of position (right)*

Figure 21. *Stainless steel disc coupon set-up pictures. Holders (left) and on-scene photo of position (right)*

Appendix D

This chapter includes all the measured data and subsequent calculations.

D1. Preliminary investigation: Degreasing- and blasting tests

Figure 22. *Result of degreasing preliminary investigation. Illustrating mass loss over time*

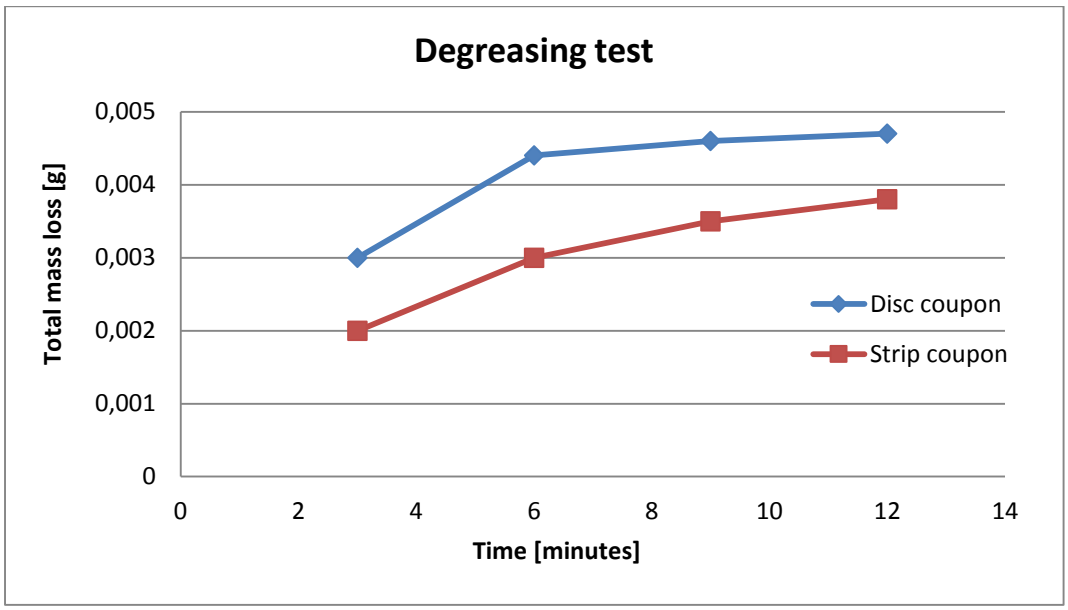

Figure 23. *Result of blasting preliminary investigation. Illustrating mass loss over time*

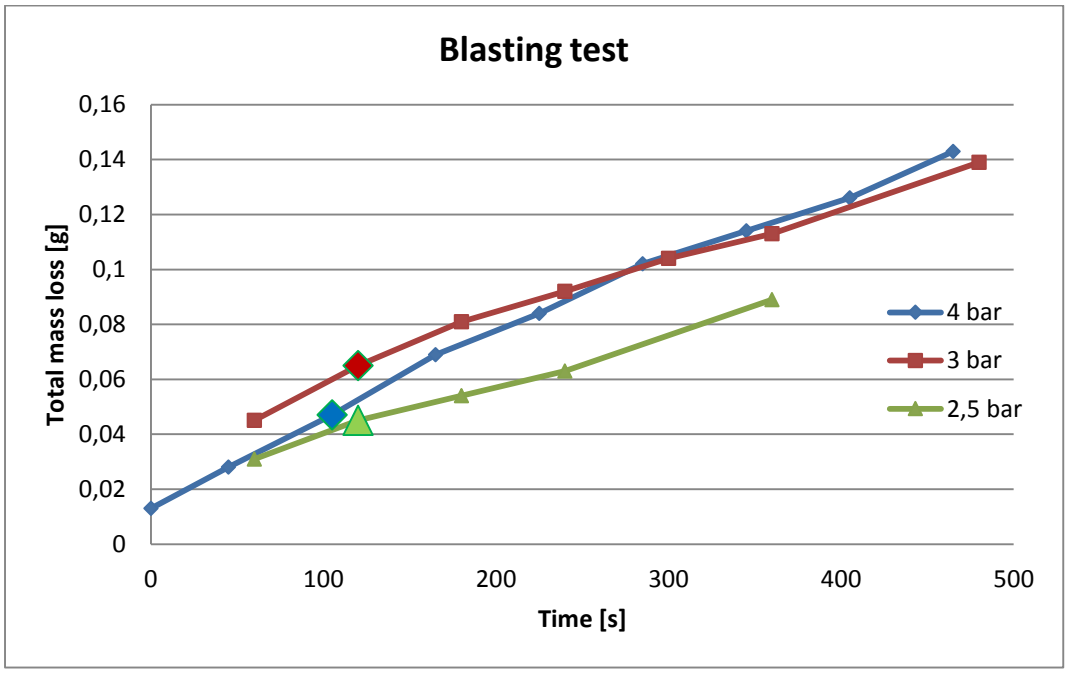

D2. XRD analysis results

Figure 24. *XRD analysis of GHT coupons; Black: 16CC-10F, red: 16CC-10C&D, blue: 16CC-10A&B, green: 16CC-10E*

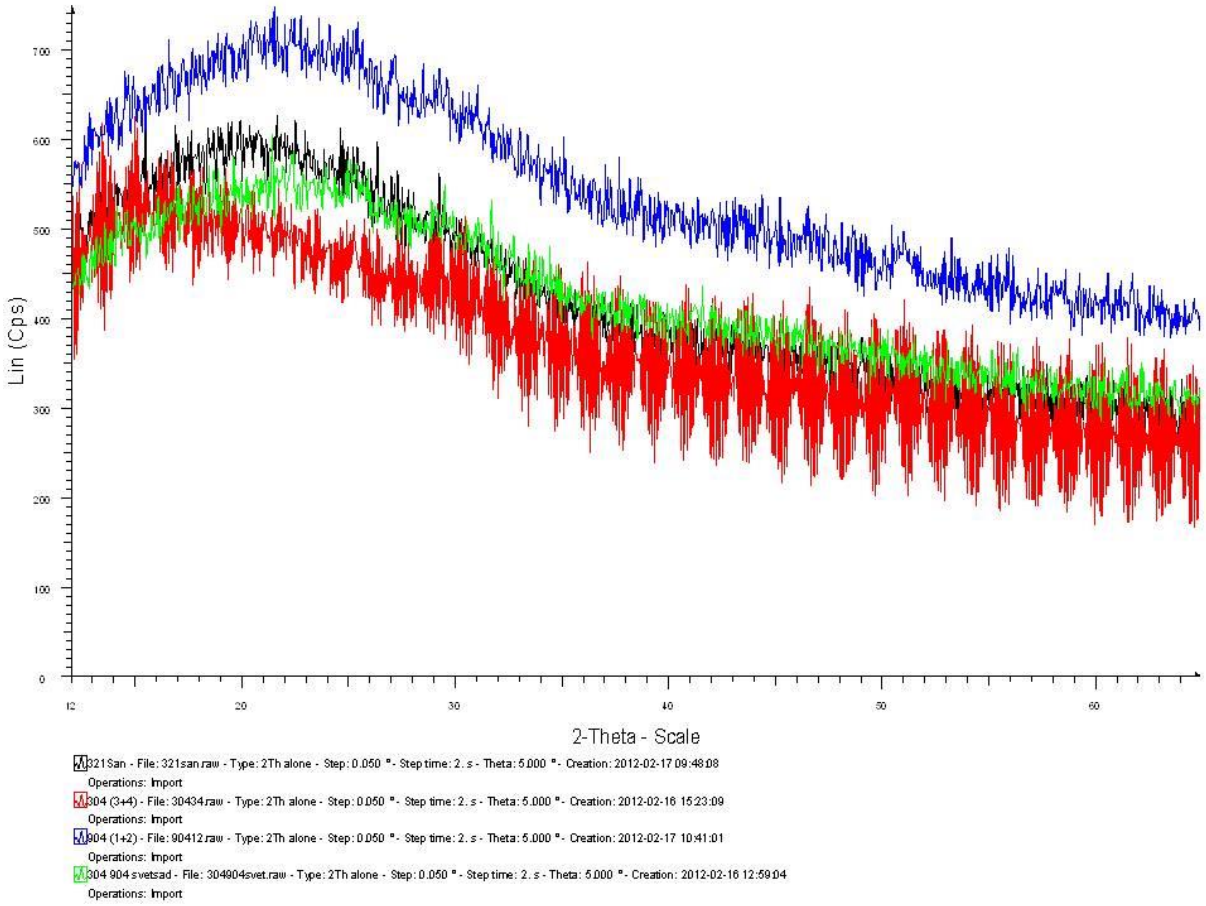

Figure 25. *XRD analysis of two carbon steel coupons; Black: 17CC-10, red: 17CC-6*

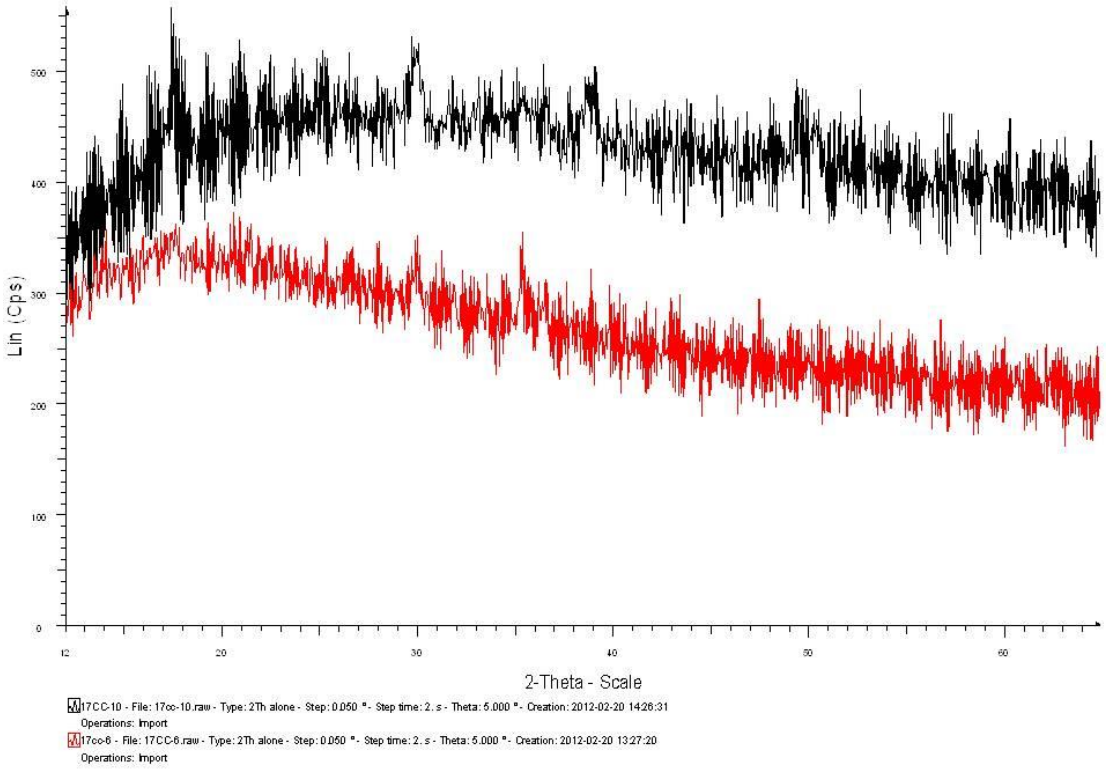

Figure 26. *XRD analysis of stainless steel coupon16CC-2B, indicating trolite formation*

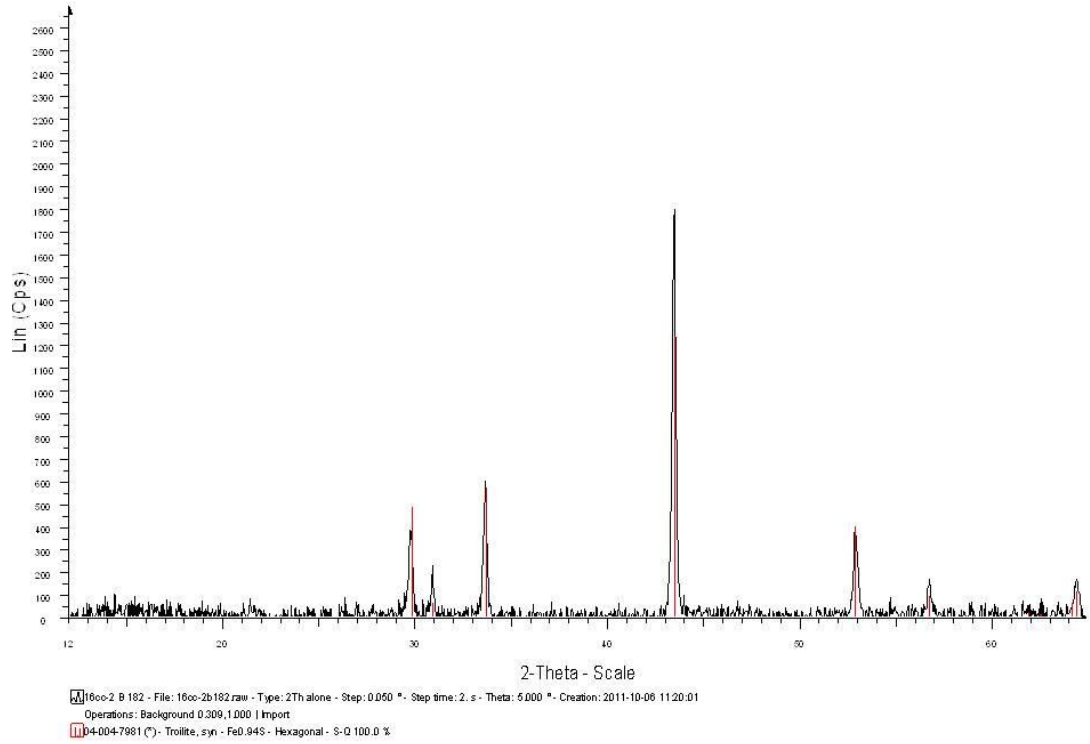

D3. Weight loss analysis (excluding GHT-coupons)

Table 22. *Weight loss analysis data and calculations*

Coupon Tag No.	9 CC-1	15 CC-2A	15 CC-2B	15 CC-9A	15 CC-9B	16 CC-2A	16 CC-2B	16 CC-8A	16 CC-8B	17 CC-1A	17 CC-1B	17 CC-2	17 CC-3	17 CC-6	17 CC-10	27 CC-2
Installation Weight [g]	17,7952	17,5906	17,5680	17,7510	17,6127	18,2040	18,2840	17,8073	17,5689	17,6920	17,8236	36,9854	37,6833	37,0406	37,4718	17,6797
Actual Weight [g] (after blasting)	16,6032	16,9625	17,2472	17,1241	16,9985	18,1774	18,2610	16,9345	15,7998	17,1241	17,1094	34,1279	37,5001	33,2739	35,7892	17,0741
Time Installed to Removal [days]	1596	1597	1597	1598	1598	507	507	1598	1598	1598	1598	1599	1605	1599	1605	1598
Mass Loss [g]	1,1920	0,6281	0,3208	0,6269	0,6142	0,0266	0,0230	0,8728	1,7691	0,5679	0,7142	2,8575	0,1832	3,7667	1,6826	0,6056
Avarage calc. penetration depth [mm]	0,0964	0,0508	0,0259	0,0507	0,0496	0,0022	0,0019	0,0706	0,1430	0,0459	0,0577	0,2310	0,0148	0,3045	0,1360	0,0490
Measured Max.Pitting depth [mm]	0,10	0,20	-	-	0,10	< 0,05	< 0,05	-	0,20	-	< 0,05	0,20	< 0,05	0,25	0,10	0,05

D4. Optical analysis results (Excluding GHT-coupons)

Table 23. *Results of the optical analysis*

No.	Corrosion product (Prior to blasting)	Localized attacks (After blasting)	Pit shape	Pit density	Types of attack
9 CC-1	Non-uniform. Uniform products in large patches with large areas of localized corrosion products	Yes	Narrow	Large	Large areas and indication of pitting
15 CC-2A	Uniform. Mostly uniform but indication of small dots of localized product structure	Yes.	Narrow to elliptical	Moderate	Deep pitting and galvanic
15 CC-2B	Uniform	Yes	-	-	-
15 CC-9A	Uniform (backside suffers from patches of localized corrosion)	Yes	-	-	-
15 CC-9B	Uniform. Does have small areas of localized product structure	Yes	Narrow	Low	Pitting
16 CC-2A	Uniform. Thin corrosion product layer with indication to initiation stages of localized corrosion. See microscope images of small pits in corrosion product layer	No	N/A	N/A	N/A
16 CC-2B		No	N/A	N/A	N/A
16 CC-8A	Non-uniform. Parts of heavy formation of localized corrosion products	Yes	-	-	-
16 CC-8B	Non-uniform. Parts of heavy formation of localized corrosion products	Yes	Narrow to elliptical	Moderate	Pitting and large areas of deep attack
17 CC-1A	Non-uniform. Mostly uniform but small patches of deviant product structure (backside more local)	Yes	-	-	-
17 CC-1B	Non-uniform. Large areas of uniform fromations of product but also localized formation (backside more local)	Yes	Very shallow	High	Almost unifrom, uneven corrosion or very shallow pits
17 CC-2	Non-uniform formation. Products less bonded to base metal partially.	Yes	Elliptical to shallow	High	Uneven corrosion. Indication of widespread pitting
17 CC-3	Uniform	No	N/A	N/A	N/A
17 CC-6	Non-unifrom. Areas of dis-colouration. Product poorly bonded to base metal.	Yes. Very localized	Shallow	Low	High penetration depth affecting specific areas
17 CC-10	Non-unifrom. Product poorly bonded to base metal.	Yes	Elliptical to shallow	Moderate	Locally uneven corrosion and shallow pitting
27 CC-2	Uniform	Yes	Narrow	High	Pitting

D5. Densities and exposed areas

The densities and calculated exposed areas used in the weight loss analysis are presented in table 24 below. *The density and exposed area of the GHT-coupons are considered classified, and will not be present in this report.*

Table 24. *Calculated exposed areas and densities (Excluding GHT-coupons)*

Area disc [cm^3]	15,86
Area strip [cm^3]	32,46
Density, carbon steel [g/cm^3]	7,80
Density, stainless steel [g/cm^3]	8,00